STRUCTURAL CONDITION MONITORING USING MULTISPECTRAL AND DIC BASED METHODS

Submitted in partial fulfilment of the requirements
for the award of the degree of

DOCTOR OF PHILOSOPHY
in
CIVIL ENGINEERING

by
KUMARAPU KUMAR
(Roll No: 701603)

Supervisors
Dr. M. Shashi
Prof. K. Venkata Reddy

DEPARTMENT OF CIVIL ENGINEERING
NATIONAL INSTITUTE OF TECHNOLOGY
WARANGAL, TELANGANA – 506004, INDIA
AUGUST – 2023

NATIONAL INSTITUTE OF TECHNOLOGY

WARANGAL

CERTIFICATE

This is to certify that the thesis entitled**"STRUCTURAL CONDITION MONITORING USINGMULTISPECTRAL AND DIC BASED METHODS"**being submitted by **Mr. KUMARAPU KUMAR** for the award of the degree of **DOCTOR OF PHILOSOPHY** in the Department of Civil Engineering, National Institute of Technology, Warangal, is a record of bonafide research work carried out by him under my supervision and it has not been submitted elsewhere for the award of any degree.

Dr. M. Shashi
Thesis Supervisor
Associate Professor
Department of Civil Engineering
National Institute of Technology
Warangal (T.S) – India

Prof. K. Venkata Reddy
Thesis Co-Supervisor
Professor
Department of Civil Engineering
National Institute of Technology
Warangal (T.S.) – INDIA

Dissertation Approval

This dissertation entitled **"STRUCTURAL CONDITION MONITORING USINGMULTISPECTRAL AND DIC BASED METHODS"** by **Mr.Kumarapu Kumar**is approved for the degree of **Doctor of Philosophy.**

Examiners

_____

_____

_____

Supervisor(s)

_____

_____

_____

Chairman

_____

Date: _____

Place: _____

DECLARATION

This is to certify that the work presented in the thesis entitled **"STRUCTURAL CONDITION MONITORING USINGMULTISPECTRAL AND DIC BASED METHODS"**is a bonafide work done by me under the supervision of **Dr. M. Shashi** and **Prof K. Venkata Reddy** and was not submitted elsewhere for the award of any degree. I declare that this written submission represents my ideas in my own words and where others' ideas or words have been included, I have adequately cited and referenced the original sources. I also declare that I have adhered to all principles of academic honesty and integrity and have not misrepresented or fabricated or falsified any idea /data / fact /source in my submission. I understand that any violation of the above will be a cause for disciplinary action by the Institute and can also evoke penal action from the sources which have thus not been properly cited or from whom proper permission has not been taken when needed.

_____

(Kumarapu Kumar)

(Roll No: **701603**)

Date: _____

Acknowledgement

With great pleasure and proud privilege, I manifest my heartiest thankfulness to my research supervisors, **Dr. M. Shashi**Associate Professor, Department of Civil Engineering and **Prof. K. Venkata Reddy,** Department of Civil Engineering, for their invaluable suggestions, sagacious guidance, scholarly advice and comprehensive critical remarks in bringing out this research work with artistry.

Kumarapu Kumar
Roll No: 701603

ABSTRACT

India's developing infrastructure necessitates effective urbanisation techniques, placing special emphasis on the need of construction site inspection. The time-consuming inspection and quality control procedures used in structural condition monitoring have compelled engineers to look for technologies that may partially automate the evaluation process. The successful in-contact Nondestructive real-time monitoring techniques require a lot of resources and can only collect data from a single installed spot. A quest for economical, reliable and rapid monitoring methods have facilitated in investigating the usage of remote sensing imagining monitoring methods. Considering that the abundant capabilities of imaging techniques are for analysing the entire jobsite in a single scan. In this study, imaging sensor applications for the visible and multispectral ranges are designed and developed in a lab for assessing ongoing construction sites and existing structures for serviceability assessments. UAV mounted optical camera digital image correlation method is used for investigating the deformation metrics during the vehicle passage on a bridge. UAV photogrammetry is used for assessing the dimensional accuracy of the concrete elements in a construction site and also mapping the progress of the work. Similarly, NIR imaging is used for concrete hydration monitoring and thermography is used for strength estimation studies of concrete. The remote sensing imaging methods have expressed its abilities in monitoring the structural condition easily without need the well-trained professionals for data acquisition. The remote sensing nondestructive (RSNDT) methods like thermography for strength estimation have opened a new paradigm in the area of concrete evaluation studies.

Keywords: SCM, NDT, Remote sensing, photogrammetry, thermography and hydration of concrete.

Table of Contents

List of Figures

List of Tables

Abbreviations

2D	: Two Dimensional
3D	: Three Dimensional
AE	: Acoustic Emission
AT	: Aerial Triangulation
C3A	: Tricalcium Aluminate
CCD	: Charged Coupled Device
CMM	: Concrete Maturity Method
CSH	: Calcium Silicate Hydrate
DGCA	: Director General of Civil Aviation
DIC	: Digital Image Correlation
DIP	: Digital Image Processing
DLT	: Direct Linear Transformation
DSLR	: Digital Single-Lens Reflex
EMI	: Electromagnetic Interference
EMR	: Electromagnetic Radiation
EMS	: Electromagnetic Spectrum
FHWA	: Federal Highway Administration
GCP	: Ground Control Points
GGO	: Guarantee Global Orientation
GNSS	: Global Navigation Satellite System
GPR	: Ground-Penetrating Radar
GPS	: Global positioning system
GSD	: Ground-sampling Distance
GUI	: Graphical User Interface
IR	: Infrared
IRT	: Infrared Thermography
ISO	: Indirect Sensor Orientation
LiDAR	: Light Detection and Ranging
NDE	: Non-Destructive Evaluation
NDT	: Non-Destructive Testing

NIR	: Near Infrared
NIRS	: Near Infrared Spectroscopy
RCC	: Reinforced Cement Concrete
RGB	: Red Green Blue
ROB	: Rail Over Bridge
ROI	: Regions of Interest
RSNDT	: Remote sensing NDT
SCM	: Structural Condition Monitoring
SHM	: Structural Health Monitoring
TPE	: Three-Parameter Equation
UAV	: Unmanned Aerial Vehicle
UAVIC	: Unmanned Aerial Vehicle Image Correlation
UPV	: Ultrasonic Pulse Velocity
UV	: Ultraviolet
UV-Vis	: Ultraviolet-Visible

Chapter 1

Introduction

India needs a lot of infrastructure because it is still developing and has many requirements. To implement the strategies for rapid urbanisation, construction site inspection is a crucial subject. These days, the construction industry demands extremely accurate planning and work scheduling. Effective project management also includes good specification, requirements, and inspections of the project, allowing for total time, cost, and resource efficiency. Therefore, in order to produce quality, it is essential to adopt an effective and efficient technique when monitoring development. However, many projects continue to use outdated methods for performing inspections and tracking progress. Poor documentation is just one of the drawbacks it has had on decision-making. The relevant data and information is not appropriately recorded for proper planning of further works and scheduling. Deadline on the engineers for speed up delivery without compromising product quality is rapidly increasing now. When compared to many other sectors, infrastructure industry falls behind in adopting cutting-edge technologies.

Numerous improvements in modern engineering could be very helpful to the infrastructure sector in adopting the innovative technologies at the key areas of construction operations. Due to the massive size of construction structures, it is unlikely to approach a few facades to check on their condition. Real-time monitoring of the construction operations is necessary to perform a preliminary assessment before moving forward with the project's design and execution. Real time monitoring is highly hectic and cumbersome for rapid analysis and decision making. The amount of money and labour required for monitoring could possibly exceed the project's estimated cost. The inspection methods could potentially impede the development of the construction projects. Professionals, specialists, and planners are looking for an economical, reliable, and real-time monitoring system that can report on the entire project site with a few staff.

Non-destructiveTesting (NDT) methods are useful for assessing the state of structures by evaluating concrete attributes indirectly. NDT is the process of looking for discontinuities or differences in characteristics in materials, components, or assemblies while maintaining the serviceability of the part or system.These methods have advanced significantly in recent years, and their most advantageous feature is their ability to evaluate concrete without causing any harm. NDTis used by various academics to assess the condition of concrete structures. Depending on their intended use, the approaches range from simple to sophisticated.

1.1 Motivation

Monitoring every aspect in the construction is crucial from early stages of concreting to finishing and eliminates the possible errors.Inspections also becomes crucial following catastrophic occurrences like storms, earthquakes, significant accidents, or sabotage. Routine inspections, however, are constrained by the professionally trained manual inspector’s also manifest human errors.The human errors can only eliminated with the help of sophisticated tools in this sector.The motivation for this research is to develop a simple and effective construction site-monitoring tool based on the remote sensing and photogrammetric concepts.Unmanned Aerial Vehicle(UAV) mounted imaging sensory system acts as a real-

time NDT method to monitor and document the dimensional accuracies, concrete hydration, and material characteristics like strength and strain related aspects of the structural elements as shown in Fig 1.1.UAV use has the potential to significantly affect and alter the operations of the construction sector. The study will examine the effects of drone use in terms of timesaving's, cost savings, reduced human error, and improved safety measures.

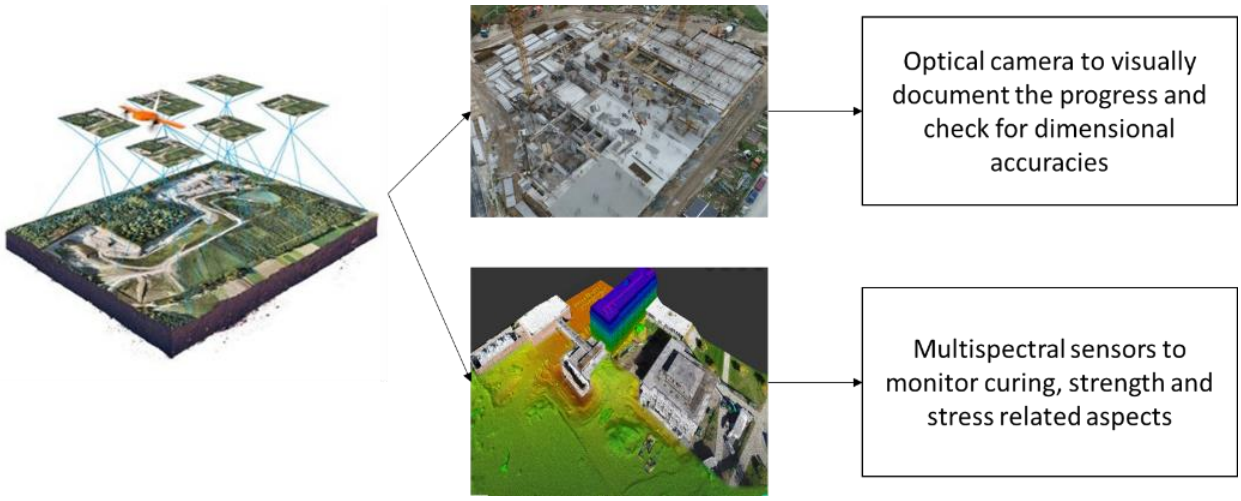

Fig 1.1 Motivation of the study

1.2 Structural condition monitoring(SCM)

In the field of engineering and construction, structural condition monitoring is a critical procedure that entails the ongoing assessment and evaluation of the health and integrity of various structures. This procedure is necessary to guarantee the longevity, dependability, and safety of dams, buildings, bridges, and other infrastructure elements. Monitoring the condition of structures primarily relies on non-destructive testing (NDT) techniques(Jensen *et al.* 2009, Rinaudo*et al.* 2012). These methods enable experts to examine a structure's internal and external features without risking damage or disruption. NDT techniques cover a range of methods, including magnetic particle testing, radiographic testing, and ultrasonic testing. Based on the unique characteristics and components of the structure being monitored, each method is chosen.

The primary goal of structural condition monitoring is to detect and identify any signs of deterioration, damage, or potential failure in a structure before they become serious problems. Engineers and experts can gain insights into the structural behaviour, performance, and overall health of a system over time by employing a variety of techniques and technologies. SCM entails the installation of sensors and monitoring systems to collect real-time data on variables such as vibrations, strains, temperatures, and load distribution. This information is analysed in order to provide insights into structural performance and potential deviations from expected behaviour(Palma *et al.* 2020,Kot*et al.* 2021, Zhao*et al.* 2021). Advanced sensors, techniques and data analytics, have significantly improved the capabilities of SCM systems.Engineers can ensure that structures remain in optimal condition, meet regulatory standards, and provide dependable service throughout their lifecycle by utilising NDT techniques and advanced monitoring systems.The SCM is carried out both during and after construction to assess whether the structural components design requirements are being met and to reduce the risk of structural failure or other problems. The research is broadly classified as concrete SCM during and after construction.

1.2.1 During construction

Due to urbanization, expansion of cities with smart city concepts are being encouraged. With the increased demand living space and limited area, the high-rise tower designs are adapted in the cities. Every aspect in the high-rise structure is crucial to monitor in the early stages of construction and eliminate the errors. During construction, the engineers need to approach the top floor for every required check and report the necessary points to be altered or rendered. The only traditional method of assessing the condition of structure is through manual visual inspection. This method of observation primarily offers crucial information about the structural deformation and any initial cracking and perhaps to the detachment of the topmost layers. The manual inspections techniques are also time consuming and not periodically followed (Hoang, 2018). The inspections also involves large equipment and arduous effort for inspection, when applied to large structures like dams, cooling towers or even basic multi-story buildings. Technological advancements have increased the pace and potential usage of various sensors in the construction industry.

Construction site monitoring

In the current construction industry, there is a growing demand for meticulous planning and efficient work scheduling. Effective project management requires well-defined specifications, thorough requirements, and comprehensive inspections, leading to optimized time, cost, and resource utilization. Monitoring progress plays a critical role in ensuring quality, necessitating an effective and efficient approach. Given the increasing pressure to shorten project completion times and the complexity of modern construction projects, enhancing productivity through real-time data has become essential. Indeed, leveraging technology, especially in communication and computing capabilities, can greatly aid the person in charge of a construction project. One crucial aspect is the ability to create visual documentation of the work progress. By utilizing advanced tools and techniques such as drones and mapping, it becomes easier to capture and record real-time data about the project's status (Anwar *et al.* 2018, Tkáčand Mésároš, 2019).Through these technological advancements, the industry can generate visual reports and documentation, which can be used for further planning and decision-making. These records provide valuable insights into the project's current state, allowing for better coordination, identification of potential issues, and adjustments to the project timeline if necessary.

Drones offer real-time visual documentation of construction progress (Ham et al. 2016, Mahajan 2021, Ngsdiman et al, 2021, Elghaish et al. 2021). Project managers can use them to monitor work activities, assess the completion of different phases, and compare the actual progress against the project schedule. This also helps in identify construction defects, assess the quality of workmanship, and ensure adherence to design specifications, resulting in improved overall construction quality.

Concrete hydration monitoring

In concreting works, curing is most essential part to develop hydro chemical reaction in concrete to ensure the maturity and strength gain of it. Curing need to be maintained for

every structural element to acquire the designed strength of concrete. Curing need to be monitored for round the clock for 28 days of casting an element to attain most of the strength. The manual inspection of works requires skilled labour and their efforts in a high-rise building which may varies from time to time and end up by compromising the compressive strength.

Early age concrete strength monitoring

Compressive strength of concrete is the crucial physical property to be monitored at initial stages of concreting. The standardised strength testing method is crushing the cube under gradual loading condition. There are alternative NDT like penetration method, rebound hammer, pull-out method, Ultrasonic Pulse Velocity (UPV) and Concrete Maturity Method (CMM) for strength estimation which are universally accepted and followed (Rashid and Waqas 2017, Moharana and Bhalla 2019). All the standardised methods are contact methods and confined to single point data acquisition samples and integrating to the entire structure. Except for CMM all other methods are performed to understand the strength of structure at any point of time, and also debris producing and time consuming. These methods also require a trained professional to perform and analysis the data obtained. The adaptability of technology by the constructors has been far from the reality due to the availability of the skilled labour for handling it.

1.2.2 In-service structure

The engineer's job is not just to construct the structure but also regularly check for the damages and maintenance them to increase the service life. The need for routine structural integrity examinations has increased due to the abundance of ageing structures in the construction sector, as well as the degradation of existing infrastructure elements including elevated structures like highways, bridges and high-rise structures. Because they are prone to structural flaws over time, maintaining old structures is a daunting undertaking. Particularly

elevated roadway constructions and railways systems are especially vulnerable to problems as they age. Further maintenance and building efforts are required due to the increased pressures that urban development and growth place on these structures. Even though the examination of these infrastructure parts are compulsory, assessments of them frequently show some degree of error due to the manual inspection techniques. Furthermore, human inspections tend to miss few details of the structure during the inspections due to inaccessibility and make these examinations less effective. By aiding human efforts, the use of robotic systems and technology for structural monitoring and inspection may successfully improve the effectiveness and accuracy of structural inspection assessments.

Deformation measurement

When exposed to heavy loads and ageing, structural concrete deteriorates, which causes failure. In order to assess the structural parameters and maintain them as they progress into serviceability, the SCM is essential. An essential component of determining the integrity and stability of concrete structures is the measurement of concrete structural displacement using NDT methods. This procedure entails precisely quantifying any displacement, deformation, or movement that a concrete element may experience as a result of a variety of conditions, including load, settlement, temperature changes, or external forces. NDT methods provide an unobtrusive way to measure these displacements without endangering the structure. There many established NDT methods to evaluate the deformation of the structure such as inclinometers, laser scanning, vibration monitoring, acoustic testing, fiber optics, deflectometers and Digital image correlation (DIC) method.

Crack morphological studies

The detailed examination and analysis of the physical traits, patterns, and behaviours of cracks that form in concrete structures constitutes concrete crack morphological studies. These studies are essential for comprehending the root causes of cracking, determining the

seriousness of the cracks, and developing effective maintenance and repair strategies. Engineers can learn a lot about the structural health and integrity of concrete elements by looking at the morphology (shape, size, distribution, and orientation) of cracks. Visual inspection, photography, microscopy, image analysis software, and various measurement tools are frequently used in crack morphological studies. Engineers can make educated decisions about repair techniques, retrofitting, and ongoing maintenance thanks to the information gathered from these studies about the nature of the cracking.

1.3 Sensory systems in SCM

The passive sensors and the active sensors are the two components of Structural Condition Monitoring (SCM) (Kong *et al.* 2017). To ascertain whether there are any fluctuations in the signal than the default is compared to test the integrity of the structure. Any difference in the periodic signal responses such as vibrations, movements, and loading conditions will alert the structural inspectors. The active reaction will monitor the signal in the interim and inform the system if it diverges from the natural signal. Fig 1.2 shows kinds of sensors used for monitoring the structural parameters. Due to the high equipment costs, centralised nature, and densification needed to gather enough data for system identification of contemporary complex buildings, the usage of contact-based sensors for gathering vibration data becomes uneconomical and time-consuming (Spencer *et al*. 2004, Lynch *et al.* 2007, Cho *et al.* 2008, Sony *et al.* 2019, Negi*et al.* 2023). Although, there are periodically enhancements in the technologies for monitoring the structures it has been not adopted and deployed by many on-site engineers. The adoptability of the non-destructive technologies is limited to very few projects as they are single use sensors. Due to the lack of faith in the system's resilience and robustness in actual field conditions and applications. Another major reason behind the lack of adaptability is sensor data acquisition at regular or particular points and integrating it to the entire structure is actually limiting the inspection to those peculiar locations.

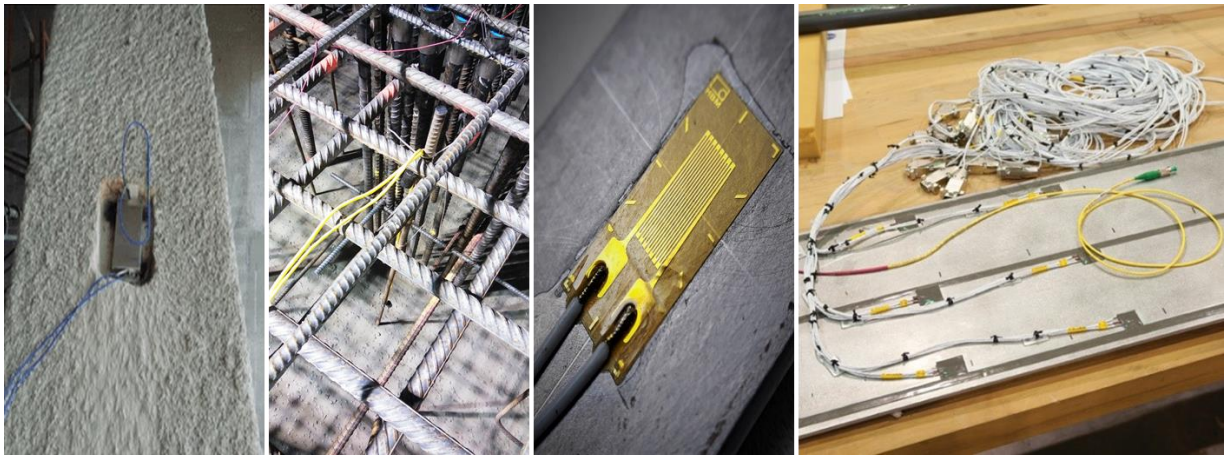

a) Accelerometer b) Thermocouple c) Strain gauge load cell d) Fibre optics sensor

Fig 1.2 Different kinds of sensors used for monitoring the structural parameters

The passive sensors and active sensors are used in SCM based on the monitoring requirements. Next-generation measuring technology for Structural Health Monitoring (SHM) is the consequence of the requirement to progress and create alternative techniques for effective sensing systems. Researchers have tried to address the issue by developing the imaging sensor technologies that can evaluate every structural element from single data acquisition platform.Different multispectral imaging sensors are available, and they are selected dependent on the monitoring application.Below is a discussion of the stages of the monitoring experimentsconducted in the thesis by utilising multispectral imaging sensors both during and after construction and aged structures.

Contact methods

There are different types of contact sensors available in building monitoring which are active and passive. Contact sensors are the most well-known and widely used sensors in construction industry. Most of the contact methods doesn’t need any skilled labour to manage as they directly transmit the signal to the engineers and automatically alert for abnormal situations. Some of the above-mentioned sensors in Fig 2.1 are contact sensors that diagnose the structural information by embedded on to the structure. Some of the other available sensors are piezoelectric sensors, humidity sensor, vibrating wire traducers, linear variable differential transformer, load cell, inclinometer and tilt meter. Every sensor have its own

significance in monitoring the structure there are many such sensors available in construction industry. The major draw back in contact sensors are they restricted to gather the information only at the point installed and cannot communicate with the other parts of the structure. The contact sensors are hectic to manage as there is a need of periodic maintenance and sensors once fixed cannot be removed and they undergo damage in work locations. There are many reported incidents that the signal transmission is lost due to the tampering of connecting cables. To avoid all such instances the non-contact methods are required in monitoring the structures

Non-contact methods

Non-contact methods are easy to maintain and manage such as photogrammetric, ultrasonic sensor, Humidity sensor, acoustics emission (AE) sensor, Near Infrared (NIR) sensor, Thermography and laser point cloud. Non-contact methods are rapid, risk free and cost effective methods for Obtaining the sensor information can be automated but processing the information need to be managed for extracting the structural information. The non-contact methods are one time investment methods, can be used at multiple locations in a single scan of the imaging sensors. The handling of non-contact methods are simple and does not require skilled labours in most of the situation for acquiring the information. The study of SCM in this thesis is conducted using the remote sensing based imaging methods; it is briefed in the subsequent sections.

1.3.1 Remote Sensing imaging methods

Due to urbanization, expansion of cities with smart city concepts are being encouraged. With the increased demand living space and limited area, the high-rise tower designs are adapted in the cities. Every aspect in the high-rise structure is crucial to monitor in the early stages of construction and eliminate the errors. The engineers need to approach the top floor for every required check and report the necessary points to be altered or rendered.

The only traditional method of assessing the condition of structure is through manual visual inspection. This method of observation primarily offers crucial information about the structural dimensions and any initial cracking and perhaps to the detachment of the topmost layers. The manual inspections techniques are also time consuming and not periodically followed. The inspections also involves large equipment and arduous effort for inspection, when applied to large structures like dams, cooling towers or even basic multi-story buildings. Technological advancements have increased the pace and potential usage of construction industry.

UAV equipped camera

Remote sensing and photogrammetric techniques has proven its efficiency in assessing the structural condition quickly, because it can cover wide region and image-based evaluations made more rapid than by sending out adequately trained surveyors to the ground. However, it has not yet widely adopted by the ground-based surveys, engineers and contractors. The spatial resolution of the sensors is only partially responsible for the limitations of image-based damage assessment. The main issue is that most operational sensors view the world from a vertical angle, which primarily restricts the information about buildings to their rooftops. The researchers and engineers have their solution to the issue by employing the different sensors at image acquisition at different angles of the specimens. The perpendicular image acquisition through drones have facilitated in monitoring the concrete cracks and deformation of structure to the true vertical. Computer vision techniques has potential in monitoring the construction site for visual inspection and documentation. These remote sensing methods are easy to apply and follow in the automated SHM process.

It is the need of hour for professionals to develop an automated sequences of visual inspection techniques and algorithm and test its capabilities in a construction site. The inaccessible components of structures require non-contact sensors such as unmanned aerial vehicles (UAVs) or so-called drones and mobile sensors to acquire structural data. In this context, UAV based construction site monitoring and inspection along with documentation

with visible and multispectral imaging sensor system is an effective solution for engineers to further plan the project.

Infrared Thermography (IRT)

SHM is the continuous, on-board monitoring of a structure during operation by integrated systems of sensors. The real time data is required to evaluate the structural condition and the ultra-sensitive sensors can only obtain it. Remote sensing NDT(RSNDT) methods as Infrared Thermography for evaluating the damage in structures also provides an instant view of the structure with temperature variation at the location of stress release (Bagavathiappan*et al.* 2013, Kylili*et al.* 2014, Gholozadeh 2016, Omar and Nehdi 2017). The term "thermography" refers to the act of acquiring, processing, and interpreting thermal images in order to record the specimen's temperature. Thermography is based on the emissivity of a material, which causes fluctuations in the specimen's surface temperature. The use of thermography concepts is expanding in the field of structural rehabilitation as thermal imaging sensor capabilities rise. Although, RSNDT methods in SHM are systematic, instantaneous and advantageous for evaluating the damage of structure, it is confined to the aged building restoration works. There are various other works, which need to be monitored continuously during the construction phase that need to be transformed from the traditional manual inspection technique. One such activity to be monitored continuously is curing monitoring and it does not have any other alternative than manual inspection and can be transformed to the automation techniques. Compressive strength evaluation of the concrete is also such activity that need to be monitored for every mix design followed and traditional methods of cube crushing produces enormous debris in the site.

There are alternative NDT methods that are used to evaluate the fresh concrete compressive strength of the concrete by incubating the thermocouple sensors inside it. The fresh concrete temperature investigation are recorded continuously at regular periods to estimate the strength with time-temperature effect is called as CMM. The sensors embedded in the concrete are costly and for one time use only, these embedded thermocouples tend to fail or deteriorate in the site conditions after the concrete getting hard. The sensory failure in

well-established CMM is limiting the investigators to evaluate the strength of concrete specimen. Temperature being the major parameter in this method there are alternative methods of recording it. There are remote sensing methods to record the temperature like thermal gun or thermal camera. There is a need of RSNDT for strength estimation method that can real-time monitor the entire structure at a time within the initial days of construction. The analysis of imaging data will significantly improve operational intelligence and enhances the preventative or predictive maintenance of construction.

1.3.2 Digital Image Correlation (DIC)

DIC is a full-field non-contact optical technique that measures displacements by correlating digital images that were taken over the course of the test (McCormickand Lord2010, Gencturk*et al.* 2014, Aparna*et al.* 2015, Quanjin*et al.* 2020). By periodically photographing a bridge and computing stresses and displacements from photos captured at various operating circumstances, DIC can be utilized for monitoring. This information can be used to trace the progression of a defect's degeneration and choose the best course of action. The present study uses an easy, affordable, and useful imaging-based technique to keep track of deformation. This method's fundamental premise is based on comparing digital photographs of an object's before- and after-deformation, as well as determining an object's displacement and strain field based on the image's position. The surface deformation of an item can be determined using DIC. In the field of monitoring structural health, portable DIC and non-interferometric techniques are frequently employed. The non-interferometric method, which typically has less exacting expectations for experimental results, calculates the surface distortion by analyzing the variations in the object's surface's gray intensity both before and after deformation. The DIC approach is widely recognized as an efficient and adaptable instrument for measuring surface distortion as a component of experimental solid mechanics.

A portable DICand photogrammetric data acquisition system using only digital cameras for SCM that is simple and robust enough to be used in the field without specialized training is proposed.The proposed device and procedure will enable the two dimensional (2D) DIC as well as out of plane measurements using photogrammetry, without sacrificing

accuracy and at a lower cost. This system will enable global as well as localized measurements of structural deformation and provide data for periodic maintenance. The flowchart showing the image processing technique in Fig 1.3.

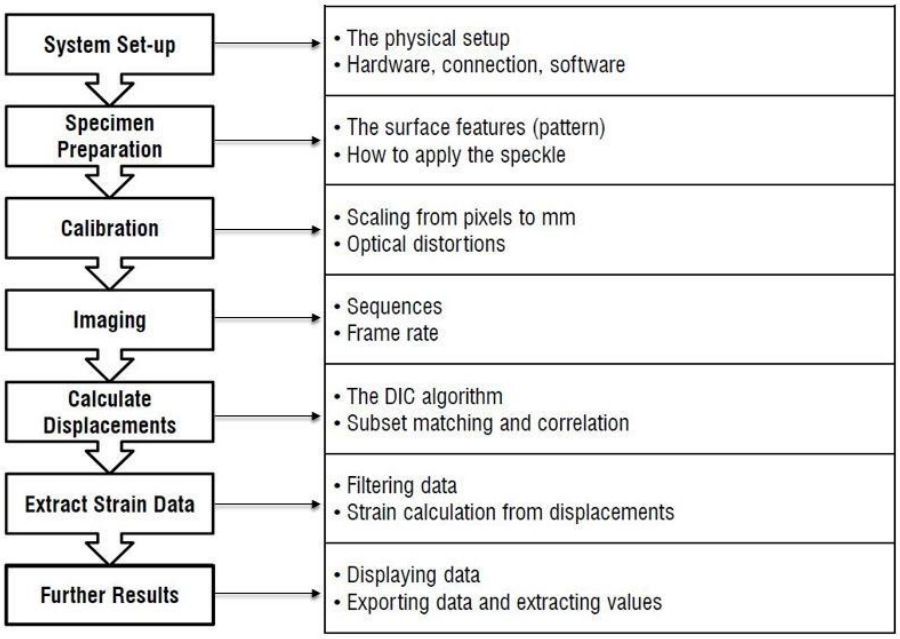

Fig 1.3 Flowchart showing the typical image processing procedure for DIC

DIC in high-rise structures

The majority of infrastructure failures were attributed to incorrectly identifying and maintaining the damage zone in a structure. High-rise structures made with reinforced cement concrete (RCC) are intended to last for designed life span. RCC structures tend to degrade under repeated loading and other environmental circumstances when they are in use. RCC constructions must be periodically monitored for damage and maintained for further commencement to service. Bridges built of RCC are crucial nodes in a transportation network because they serve as a key connecting link in highways and railroads. Bridges are monitored for vibrations and deformations upon loading conditions for accessing the life span and restricting the heavy freight on it. Ground-level structures are simple to examine for service life using the large variety of NDT techniques readily available. Structures higher than 5 metres above the ground are difficult to assess for serviceability since inspectors and

engineers are at risk due to the structure's height. Many engineering applications including SHM have become easier since the recent introduction of Digital Image Correlation (DIC). The remote sensing and photogrammetric DIC vision approach may detect an object's deformation by examining the prior and post-loading digital image. It has the capacity to visually record a large region in a rapid time without skipping any minute structural damage features.

1.4 The complete thesis is organized as follows:

i. **Chapter1,** of the thesis motivates the necessity of this study and discusses: a) The structural monitoring methods available in the current scenario b) the necessity of the remote sensing health monitoring methods in during and after construction c) DIC technique to study the structural health condition

ii. **Chapter2,** reviews the literature on UAV in construction site, DIC methods and models available, In-situ concrete strength estimation technique. The gaps in the literature are summarized.

iii. **Chapter 3,** details the scope of investigationand objectives.

iv. **Chapter4,** establishes UAV based DIC measurements of RCC beams and presents the validation on the in-situ bridge.

v. **Chapter 5,**UAV based construction site monitoring and dimensionalaccuracy assessment studies.

vi. **Chapter6,** develops the NIR based hydration monitoring method of concrete.

vii. **Chapter7,**develops the thermography based concrete strength estimation method.

viii. **Chapter8,**establishes a relation between concrete internal and external temperature using thermocouple and thermography.

ix. **Chapter9,** presents the conclusions, limitations and the scope for further study.

Chapter 2

Review of Literature

In the previous chapters, the need for remote sensing monitoring methods are discussed.The high-end computational efficiencies has compelled every sector to automation and self-diagnosis the problems that require prompt attention and treatment. The construction industry is seeking to explore and develop new techniques and approaches for monitoring material qualities in before and after construction. The inexpensive high-resolution imaging sensors have facilitated various opportunities of the exploration to develop applications based on the requirements(Liu et al. 2014, Hayat et al. 2016, Sivakumar and Malleswari 2021). To have comprehensive insight of the structure the optical imaging sensors aided with other multispectral sensors may potentially extract the structural properties. The detailed literature of studies conducted using UAV and multispectral sensors are discussed. The full potential of drone-based site monitoring by conducting ongoing research and development, establishing best practices, and incorporating technology improvements(Tenedorio et al. 2021, Estanqueiro et al. 2021,). These systematic techniques will make it possible to acquire,

analyze, and report data consistently and reliably, thus improving the effectiveness and efficiency of project site monitoring procedures.

2.1 Structural conditioning monitoring

At various points during a structure's lifespan, testing and quality assurance are crucial. Engineers need cutting-edge inspection techniques to maintain civil infrastructure effectively. It's imperative to develop new inspection techniques for ageing infrastructure. Compressive, flexural, and tensile strength tests are conducted on specimens simultaneously as part of the traditional method for evaluating the quality of concrete in civil structures. But there are several problems with these approaches. The concrete within specimens might not accurately represent the actual structure, and the strength properties of concrete specimens are influenced by their size and shape, making immediate prediction of results impractical. Numerous NDT techniques have been developed to overcome these restrictions.NDT techniques make use of the idea that certain physical and chemical characteristics of concrete are related to the durability and strength of structures. For more than 3 decades, these methods have been used to evaluate structural conditions. The term "non-destructive testing" (NDT) refers to a variety of procedures used to examine things, materials, or systems without endangering their continued usefulness. In short, NDT makes it possible to inspect or measure without risking damage. Currently, NDT techniques are regarded as effective tools for evaluating the durability and strength of existing concrete structures. Because they are dependable and efficient, these techniques are becoming more and more popular. When compared to the traditional practice of periodic concrete sampling for material analysis, the importance of conducting tests on-site has been acknowledged, and this tendency is growing.NDT has advanced into a more complex field in the twenty-first century, moving from simple imaging sensors to complex methodologies like thermography and DIC.

2.1.1 Concrete hydration monitoring using imaging sensors:

Concrete is a homogeneous mixture of locally available diversified materials such as cement, aggregate, sand and water along with compositions of gypsum and admixtures. The hydraulic adhesives like cements react with water in order to create materials with strong cohesive and binding qualities as well as high mechanical resistance (Double DD*et al. 1978).* Cement needs the right moisture levels to hydrate successfully and achieve the quality it is designed. In order to retain an acceptable water content in the concrete mixture throughout the process of hydration, effective curing becomes crucial. Inadequate curing can result in pores developing in the concrete, which eventually lowers the quality of the material and impacts hydration as well. Monitoring the process of curing after the concrete has been poured is essential to ensuring the highest possible level of concrete quality and preventing irreversible flaws (Parrott LJ*et al. 1990*).

The chemical composition, mechanical strength, and core structures of concrete materials are only a few examples of crucial characteristics that cannot be seen with the naked eye (Qin L*et al. 2008*). The ability of the human eye to perceive certain material qualities is limited. The visible band of the electromagnetic spectrum (EMR), that spans wavelengths from 380 nm (violet) to 740 nm (red), is the only range to which it is capable of responding. Other wavelengths, like ultraviolet (UV) and infrared (IR), offer vital information regarding materials beyond this range of wavelengths (Gehlen CD*et al. 2009*). By measuring the absorption and transmission of light at various wavelengths, imaging techniques like ultraviolet-visible (UV-Vis) spectroscopy can assist in determining the chemical makeup of a substance (Akash MS*et al. 2020).* This method is frequently employed in materials research to examine the electrical composition and structure of materials. To evaluate the thermal characteristics and heat distribution of materials, thermal imaging and infrared spectroscopy has been used (Mollah MY*et al. 2000*). Researchers and scientists can better grasp the characteristics of materials that are invisible to the human eye by utilizing cutting-edge imaging technologies.

Evaluating the relationship between hydration kinetics and concrete performance is made possible by the capacity of Near Infrared Spectroscopy (NIRS) to measure water consumption and hydration development in cementing systems (Gastaldi D*et al. 2010*). It enables scientists to assess the efficacy of various cement formulations, curing circumstances, and additives, resulting in improved concrete characteristics and increased structural durability.The use of NIRImaging which is also a complementary technique in cement moisture studies is discussed in relatively little detail in the scientific literature (Saremi SG*et al. 2020*). Studies of CSH (Calcium Silicate Hydrate), a crucial component of hydrated cement, have been pursued. In order to better understand the CSH phase and its spectroscopic behavior, NIR imaging has been used in conjunction with mid and far-infrared spectroscopy. This crucial hydrated phase's composition and structure can be better understood by analyzing the impact of the calcium-silica ratio on the spectral characteristics of CSH. Although NIRS is not yet used as frequently in concrete hydration investigations as other analytical methods, the available research reveals its promise and efficacy in examining particular phases of cement hydration (Azenha M*et al. 2021*).The use of NIR imaging for understanding the intricate and dynamic processes of cement hydration may increase as technology develops and researchers look into new applications, resulting in improvements in cement studies.

2.1.2 Strength estimation methods

Concrete is well-known for its high durability at a low cost, as well as its sustainability, due to the fact that it is a locally and easily available raw material. The quality of the raw materials used in the preparation of concrete is highly responsible in determining its durability. Concrete's mechanical properties should be rigorously tested during the early construction phase to ensure its durability (Akpinar P *et al. 2017*). Monitoring resemble continuous collection of data for quality assurance of concrete to ensure the service life of structure. Each structural member is designed for characteristic strength of concrete and the same is monitored for strength achievements during construction. Monitoring of concrete strength during the construction phase lets the engineers to plan remedial measures based on the severity of problem (Farrag S *et al. 2016*). Strength gain is predominant at the initial 7days of hardening process and it is required to evaluate its strength only during that

particular initial span as 75% of strength attains in that period. Evaluation of concrete strength involves loading and crushing of cubes, which also in turn results in generating more debris and consuming the 4% of the overall project cost. The concrete debris is hard to handle and disposal of materials actually end up in landfills, where vegetation growth is a major concern at such particular locations. Correlating the in-situ structural strength in terms of lab cured specimen strength always varies due to the differential climatic conditions (Ramachandra B *et al. 2018*). Testing the concrete in-situ yields exact information of the concrete components in real-time without impairing the object from further usage of structure (Bagavathiappan S *et al. 2013*). There are various NDT investigation methods are predominantly used in concrete structures to obtain the information of the object without destroying the object (Milovanović B *et al. 2016*). These NDT methods reduce concrete debris while also ensuring the viability of locally available raw materials. The real issue is the application of NDT methods with technically skilled labour on every construction site. Due to a lack of skilled labour in the laboratory and construction site, the contractors are forced to use age-old casting and crushing methods.

NDT methods are basically classified into two categories based on data collection, point wise and whole field wise (Hellier CJ *et al. 2013*). Point wise method instinctively concentrates on particular point or location where there is a point of conflict or to investigate the hidden defect in the concrete structure. Whole field wise method delivers the total information of whole area of interest in a single test run. Depending upon the application, NDT technique is sub classified into contact and non-contact methods (Huke P *et al. 2013*). Contact NDT falls under point wise testing and noncontact falls under whole field wise testing. There are well established contact NDT's for concrete strength evaluation such as:

- Ultrasonic testing: This technique evaluates the interior state of the concrete by using high-frequency sound waves to find voids, cracks, or delaminations (Del Rıo LM *et al. 2004*).
- Ground Penetrating Radar (GPR): GPR uses electromagnetic waves to scan the subsurface of the concrete, locating rebar, spotting cavities, and evaluating general health (Hugenschmidt J *et al. 2008*).

- Impact-Echo Testing: Using this method, stress vibrations are created in the concrete and their reverberations are analysed to find interior flaws (Pessiki SP *et al. 1988*).
- Electrical Resistivity Test: This technique determines concrete's resistivity to electricity, which can reveal details about the material's permeability and moisture content (Layssi H *et al. 2015*).
- Rebound Hammer Test: In this test, the strength of the concrete is evaluated by monitoring how quickly a hitting hammer bounces back from the concrete's surface (Kolaiti E *et al. 1993*).
- Concrete Maturity Method (CMM): CMM works on the principal that the temperature exerted during hydro-chemical reaction of concrete is directly proportional to the strength gain of concrete. The thermal sensors keep track of the interior thermal history of the concrete and link it to the strength gain of it (Carino NJ *et al. 2001*).

All the above mentioned evaluation techniques are contact methods, they can extract the information only through physical communications. Expect CMM all other techniques are employed on the hardened concrete and CMM is adopted for evaluating the hardening concrete (Valdes MD*et al. 2013*). Furthermore based on the adaptability and efficiency of the tool and NDT method, it is divided as surface, sub-surface and volumetric testing methods (Dua G *et al. 2020*). In most cases, the durability of an entire structure is certified based on a few sampling points of NDT setups, which do not test all structural elements.

Concrete Maturity Method:

Concrete maturity method (CMM) is a contact and point-wise NDT method, which is employed to investigate the strength maturity of concrete by recording internal temperatures of it (ASTM C. 1074 *1998*). CMM is a well established and accepted technique for determining how concrete develops and gains strength as it ages in the building industry. The theory behind the CMM holds that the strength of concrete is closely correlated with its level of maturity and the temperature history it endures during curing(Carino NJ *et al. 2001)*. Construction engineers can decide the best timing for a variety of tasks, including formwork removal, post-tensioning, and loading by using the CMM. Instead than depending on conventional time-based curing timetables, this method enables them to make judgements

according on the concrete's real strength attainment. The concrete maturity technique is a useful tool for streamlining construction timelines, assuring quality control, and improving the effectiveness of the placement and curing procedures for concrete.

It offers a trustworthy and non-destructive way to evaluate the strength of concrete in real time, helping to successfully and economically complete building projects. To investigate the temperature history of concrete at periodic intervals thermocouples embedded with a data acquisition platform are inserted inside at core point of concrete specimen as temperature liberated will be high at that point (Abed MA *et al. 2021*). The setup cannot be removed after the experiment as the sensors are placed inside the concrete and casted, it makes sensors unfit for reuse (Domski J *et al. 2015*). There have been several hypothesised maturity functions that have acquired acceptance are mentioned below.

1) Three Parameter Equation (TPE): The Freiesleben Hansen and Pedersen Equation, also referred as the Three Parameter Equation, is an empirical equation used to forecast how concrete's compressive strength would change over time as shown in eqn.1 (Hansen PF & Pedersen EJ *1977*). It is frequently used to calculate the strength gain for fresh concrete.The equation is expressed as:

$$f(t) = a \times t^b \times \ln(ct + 1) \qquad \text{eqn.1}$$

where, $f(t)$ is the predicted compressive strength of concrete at age t, a, b, and c are empirical parameters determined based on the specific characteristics of the concrete mix and the curing conditions.

2) The Nurse-Saul function: this is the age old technique proposed in 1951, According to (ASTM C 1074-11) the strength estimation is achieved by Time-Temperature factor method that is also called as Nurse-Saul method as shown in eqn.2 (Soutsos M *et al. 2018*).The equation is expressed as:

$$M = \sum(T - T_0)\Delta t \qquad \text{eqn.2}$$

where M(t) = maturity indices (°F-hours), T = average external temperature (°F) at Δt, T0 = datum temperature (14°F) andΔt = time interval (hours).

3) The Rastrup function: A practical way to account for the combined impact of time and temperature on strength development is to use the comparable age concept as shown in as shown in eqn.3. Rastrup first proposed it in accordance with a physical chemistry axiom that claimed that if the temperature at which the reaction is occurring rises by 10°C, the rate of reaction doubles (Rastrup E *1955*).The equation is expressed as:

$$f(t) = f_0 + (f_1 - f_0) \times \left(1 - \frac{e^{-kt}}{e^{-kt_0}}\right) \quad \text{eqn.3}$$

where, $f(t)$ is the estimated compressive strength of concrete at age t, f_0 is the intercept parameter, representing the initial concrete strength at age t=0 (Usually taken as the 7-day strength), f_1 is the asymptote parameter, as the ultimate compressive strength of concrete, k is an empirical parameter related to the concrete's strength gain rate, $f_0$is the reference age, typically taken as 7 days.

4) The Weaver and Sadgrove function: The Weaver and Sadgrove approach is an empirical equation used for determining the compressive strength of concrete at multiple ages based on strength observations. This approach is especially effective when predicting concrete strength before traditional testing samples have achieved their target age (Lachemi M *et al. 2007*).The equation is expressed as:

$$f(t) = k \times \left(\frac{t}{x}\right)^m \quad \text{eqn.4}$$

where, $f(t)$ is the estimated compressive strength of concrete at age t, k is a constant that depends on the specific concrete mix and curing conditions, x is a reference age, typically taken as 28 days, which is a common standard age for testing concrete strength, m is an empirical parameter determined based on the characteristics of the concrete mix and its early-age strength development.

5) Svante Arrhenius, a Swedish scientist, developed the Arrhenius equation in the late nineteenth century. It is based on the idea that temperature influences the balance of

energy of molecules, and that higher temperatures offer more kinetic energy to molecules that react, resulting in a faster rate of reaction. In this situation, the apparent activation energy indicates the amount of energy required for the chemical processes associated with cement hydration to occur. The curing reactions speed up as the temperature rises, resulting in a faster rate of concrete strength gain (Laidler KJ *1984*). The equation is expressed as:

$$k = A \times e^{-\frac{E_a}{RT}} \qquad \text{eqn.5}$$

where, k is the rate constant of the reaction or the rate of change of a property with temperature, A is the pre-exponential factor or the frequency factor, representing the reaction's rate at an infinite temperature, Ea is the activation energy, which is the energy barrier that molecules must overcome for the reaction to occur, R is the universal gas constant (approximately 8.314 j/(mol•K)), T is the absolute temperature in Kelvin (K).

Infrared Thermography principles:

Infrared thermography research dates back over 200 years. It is understood from literature that thermography is evolved in the 19th century through the experiments on sunlight radiation (Vavilov V *et al. 2010,* Wisniewski M *et al.2003,* Meola C *et al. 2017*). It evolved from thermopile to infrared radiation capturing lens through thermogram. The concepts and technologies that eventually led to contemporary infrared imaging devices were developed at that time with major help from scientists and inventors. In fact, KálmánTihanyi, a Hungarian engineer and physicist, created the first effective method for obtaining thermal images from a camera in 1929. He is frequently given credit for developing the first electronic television camera that was infrared-sensitive, which he referred to as the "thermal camera" or "infrared-sensitive camera" (HAKA AT *2020*). The development and widespread use of thermal imaging systems occurred throughout the subsequent decades as a result of technological developments and growing knowledge of infrared radiation. Thermal cameras gained popularity in the second half of the 20th century and into the 21st century, finding use in a wide range of applications.

Infrared thermography (IRT) is a process of acquiring thermal images of specimens and performing image processing to obtain the surface temperature it. IRT works on the principal that every object in the universe other than blackbody radiates some InfraRed (IR) energy as a function of their surface temperature (Maser KR *et al. 1990*). Radiative heat transfer involves the transfer of heat in the form of electromagnetic waves (infrared radiation) between objects at different temperatures. The heat flux is determined by the Stefan-Boltzmann law and depends on the temperature and emissivity of the objects (Chandler RC *et al. 2009*). Sensor receives a heat flux L_{tot} (in $W/m2$), which is a combination of several radiative heat fluxes, that is:

$$L_{tot} = \tau_a \varepsilon_\delta L_\delta + \tau_a (1 - \varepsilon_\delta) L_b + (1 - \tau_a) L_a \qquad \text{eqn.6}$$

where,τ_a is the transmissivity of the midcourse between the concrete and the thermal camera,ε_δ is the emissivity of the concrete surface,$L_\delta$is the longwave radiation from the concrete surface (in $W/m2$), $L_b$is the longwave radiation behind the concrete (in $W/m2$), L_a is the longwave radiation from the air (in $W/m2$). The longwave radiation L (in $W/m2$) is a portion of the infrared radiation between 7 and 14 μm, which is expressed from the surface temperature of an object T(in Kelvin) as:

$$L = \sigma T^4 \qquad \text{eqn.7}$$

where,σ is the Stefan-Boltzmann constant (= $5.67.10^{-8}$ $W/m^2\text{-}K^4$),

According to Eqs.(6), (7), the surface temperature of the target surface $T_s = \sqrt[4]{L_s/\sigma}$(in Kelvin) depends on various variables (Tran QH *et al. 2017*), $\sigma$is the emissivity of objects, $L_s$is the longwave radiation emitted by the object.

Emissivity is the key parameter in IRT to calculate the surface temperature of each object. Every pixel in thermal image obtained through thermal imager is unique with variated temperatures and each pixel acts as a temperature node (Gusella V *et al. 2020*). Thermal emissivity of concrete is recognized as 0.93 (Starnes MA *et al. 2002*). Infrared bandwidth

comprises from 0.75μm to 1000μm wavelength region in EMR, which can observed by specific Charged Coupled Device (CCD) (Mohr G *et al. 2020*). Concrete thermal emissions can be captured by the sensors which can able to recognize the 4μm to 13μm wavelength region in Near Infrared (NIR) band of EMR (Starnes MA *et al. 2002*).

By specifying the emissivity of surfaces over a range of temperatures, an IR thermal imager is a tool used to record and visualise thermal patterns. It works by directing the emitted infrared (IR) light through a lens onto a detector. The digital visual display that is produced from the electrical signal produced in response to the IR radiation then translates the various colours or shades of grey that represent the various temperatures of the targeted surface. These thermographic images can be analysed with specialised software, which can even measure temperature fluctuations (Akpinar P *et al. 2017*). Temperatures may additionally be determined if the surface's emissivity within the visible spectrum of the IR sensor is known. With the use of this technology, we can "perceive" any object's temperature at the surface, which represents the total amount of heat transferred from the object's inside to its surface. Typically, the apparatus looks like an IR camera, about the size of a standard video camcorder.

Infrared Thermography is one among the well-established NDT techniques that is predominantly used to investigate both volumetric and non-contact methods of investigation (Fahmy M *et al. 2010*). Currently thermography concepts are implemented in multiple applications in civil engineering like detecting subsurface delamination in bridge decks (Mohr G *et al. 2020*), moisture and chemical effect detection in brick masonry facade as well as thermal energy dissipation of it (Vijay PV *et al. 2019*). These concepts are also used in fresh concretes to monitor the temperature for preserving the heat flux in clod climatic condition and hot environments, taking into account the heat of hydration produced by the chemical reaction of Tricalcium aluminate (C3A) with water in concrete (Starnes MA *et al. 2002*).

2.1.3 Crack Identification

Structures that have cracks run a serious danger of failing to perform safely. Repeated loading cycles can create material fatigue, which can start cracks that spread and finally cause damage to the structure. To avoid serious incidents and to preserve the structural integrity and durability, early fracture identification and localisation are crucial. Numerous analytical, numerical, and experimental studies have been conducted as a result.IRTcan be employed to detect cracks by identifying thermal anomalies caused by crack openings (Balaras and Argiriou 2002, Ghosh and karbhari 2011, Bauer *et al.* 2018, Ramzan*et al*. 2021). DIC is also used to identify the cracks in the structure and measures the crack properties using edge detection techniques.

2.1.4 Digital Image Correlation (DIC):

The closely linked disciplines of structural Condition monitoring (SCM) and non-destructive evaluation (NDE) are frequently used to evaluate the state of structures without endangering their integrity (Jhajharia*et al.* 2015). These methods use numerous assessment methodologies that enable the assessment of a structure's condition while maintaining its functionality. Utilising SHM and NDE makes it feasible to quickly identify and assess infrastructure deterioration, guaranteeing that the system continually satisfies life safety criteria (Thayer *et al*. 2017). In order to maintain the structural health and safety throughout time, these combined procedures are extremely important. There is a high demand for computerised surveillance equipment in SCM since individual visual assessment methods are subjective and time-consuming (NooriHoshyar*et al*. 2019, Kot*et al.* 2021, Kumar 2021). Devices with contacts are frequently employed to keep an eye on infrastructure parts. It used to be usual practice to gather data from numerous embedded devices inside the intended system. These methods, which combine static and dynamic assessment, have advanced tremendously. In SHM applications, contact-based instruments are frequently used, including transducers, strain gauges, inclinometers, accelerometers, and extensometers (Mousa MA *et al. 2021,* Niezrecki C *et al 2018*). Fibre optic sensors, on the other hand, have become respectable substitutes for conventional sensors because of their adaptability, scalability, and immunity to electromagnetic interference (EMI) (Du C *et al 2020*).

Based on the usability it appears that some contact sensors frequently lack the required robustness to be permanently installed on specific structural components for ongoing assessments throughout the infrastructure's service life, particularly when defects are more likely to occur. Despite these difficulties, technological developments have produced a wide range of NDT methods that are suitable for many engineering applications. SHM and NDT have both made use of techniques like radiography, radioactive computer tomography, radar, IRT, ultrasonic arrays, acoustic imaging systems, and AE, each with its own advantages and disadvantages (Rehman SK *et al 2016*). This information is then used to analyse their movement over various time periods or phases. In civil engineering applications, vision-based methods have shown to be effective and efficient for non-contact analysis, enabling the extraction of structural deformation, full-field displacement, geometry profiles, and strain.

DIC is a vision-based approach that precisely measures image variances in both 2D and 3D using image recognition and projection software (Roux *et al.* 2009). DIC has become popular in many scientific and engineering domains, is especially useful for analysing full-field displacement and strain, fracture development, structural deflections and progression in building systems.By photographing the targeted system at several intervals, DIC can be used efficiently for routine or long-term observation (Sutton *et al.* 2009, Pan 2013). Following that, the photos are analysed using specialised software to gauge deformations over time. To improve accuracy and efficiency, various vision-based algorithms such as edge detection, thresholding, segmentation, and filter-based approaches are used (Hild and Roux 2012).One notable benefit of DIC is the fact that it doesn't always require specialised lighting, and in some circumstances, it may operate without any particular surface preparation as long as the target current layer has appropriate photographic granularity. The method keeps tracking the relative position of each point having unique shape applied on the specimen during deformation.

Speckle pattern:

The speckle pattern serves as a unique visual marker on the surface of the object. The speckle pattern is created by applying a random, high-contrast texture to the surface of the

object. This pattern consists of small, randomly distributed speckles that form a distinct and unique texture. The high contrast between the speckles and the background provides clear and identifiable features that DIC algorithms can track with high precision (Chen G*et al.* 2021).

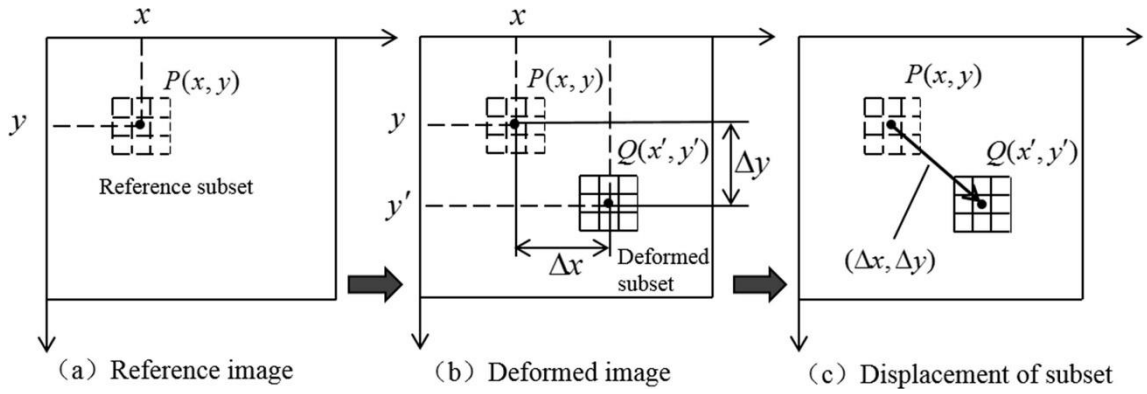

Fig 2.1Tracking of point movement by DIC method.

As shown in Fig. 2.1, to track the movement of a point (P) in the reference image during the deformation, consider the correlation between the reference subset surrounding the point of interest, $P(x, y)$, and the deformed subset surrounding the point, $Q(x', y')$, in the deformed image ($x' = x + \Delta x$, $y' = y + \Delta y$). The reference subset have the same area (S) but different locations by the displacements of $(\Delta x, \Delta y)$, hence their correlation are the functions of $(\Delta x, \Delta y)$:

$$C(\Delta x, \Delta y) = \frac{\iint I(x,y)\, J(x+\Delta x, y+\Delta y)\, dx\, dy}{\sqrt{\iint I^2(x,y) dx\, dy}\sqrt{\iint J^2(x+\Delta x, y+\Delta y) dx\, dy}} \qquad \text{eqn. 8}$$

DIC is more affordable and simpler to use beyond of the lab than other conventional NDT and particular visual techniques like radioactive computerised tomography as given in eqn.8. It can be put up more quickly and is compatible with typical outdoor settings (wang*et al.* 2020, Mousa*et al.* 2021). Additionally, DIC provides improved quantifiability and precision, making it a better option for precise measurements. It makes use of conventional electronic imagery that can be easily incorporated into civil construction techniques to enable accurate assessments of component systems.

Edge Detection

Edge detection is a critical stage in the image analysis workflow in DIC, with the goal of locating and highlighting the edges or boundaries of objects or features inside the pictures(Mohan and Poobal 2008, Shao *et al.* 2013). In DIC, edge detection is crucial because it aids in precisely locating the displacement and distortion of the relevant features. In order to calculate the displacement and strain of the item being analyzed, DIC compares two images, typically referred to as the reference image and the distorted image. In order to track the movement of these edges or contours in the distorted image, edge recognition techniques are performed to both images to find their notable edges or contours.Depending on the particular needs of the application and the features of the images, different edge detection methods can be applied in DIC. Sobel operator, canny edge detector, Roberts cross operator and Prewitt operator are the methods for edge detection that are frequently used.

Thresholding

Thresholding processing is often followed by edge detection algorithms in DIC, to identify and track the features of interest.To transform a grayscale image into a binary image, thresholding is a crucial image processing technique (Cinar*et al.* 2017, Hoang 2018). A threshold value is specified as part of the process, and all pixel values over it are given one binary value (usually 1 or white), while pixel values below it are given the other binary value (often 0 or black). There are many thresholding techniques available like global thresholding, Otsu's method,adaptive thresholding and hysteresis thresholding (Fujita Y*et al, 2011*).The technique selected can have an impact on the precision and dependability of the DIC results. The features are clearly represented in the binary pictures acquired through thresholding, which makes it simpler for the DIC algorithm to track their movement and determine the displacement and deformation fields.

Segmentation

An image processing method called segmentation is used to locate and isolate particular areas or features of interest within an image. Segmentation is the process of dividing an image into useful sections according to particular standards, such as intensity, texture, colour, or boundaries (Sharma N*et al 2012*). The analysis is more accurate and effective thanks to segmenting the image, which allows DIC algorithms to concentrate on tracking the movement and deformation of particular parts (Patil and Jain 2014, Al-Tarawneh 2012). The quality of the input images, the segmentation method selected, and the complexity of the features being analysed are some of the variables that affect how well DIC segmentation works.

Filter-based approach

In the DIC, filter-based methods are frequently used as preprocessing stages before running the correlation analysis. It is an image processing technology used to increase the images' sharpness and the precision of distortion and deformation.These filters enhance image quality, minimise noise, and draw attention to key features, which makes it simpler for the DIC algorithm to precisely monitor displacement and deformation (Khoo SW*et al, 2016*). The filter based approaches commonly used in DIC are Gaussian smoothing, median filtering, Sobel filter,Laplacian filter and anisotropic diffusion (Fischl and Schwartz 1997, Atabany and Degennar 2008, Coady*et al.* 2019). To remove noise, improve edges, and smooth image gradients, these methods subject the images to a variety of filters or convolution kernels. Filter-based techniques are particularly helpful in DIC because they enhance the reliability and robustness of the correlation process.

DIC Analysis Software

There are a variety of DIC software solutions available, both open source and commercial. Open source software solutions are suited to user demands and minimise expenses, but

commercial software solutions are not user friendly, cannot be customised to user needs, and are costly to use.

Open source software

1. Ncorr is a 2D subset based open source and freely available DIC software developed and implemented in MATLAB used to determine displacements and strains from set of speckle images.
2. DICe is open source DIC analysis software. It is easy to use and has three options (local mode, global mode and tracking mode DIC) provided in Graphical User Interface (GUI) for determining strains and displacements.
3. Py2DIC, pyxel and pydic are open source DIC software implemented in python to compute strains and displacements.

Commercial software

1. GOM is correlate software used for DIC analysis and 3D motion analysis.(Smrkić MF et al., 2017)
2. Vic-2D system uses optimized correlation algorithms to determine displacements and strain.(Rubino et al., 2019)

According to the literature, it is considered to use Ncorr software for its fast processing and customize options(Blabber et al., 2015). It is an MATLAB based image processing software and can be easily executed (Suryanto et al., 2018)

2.2 UAV in construction industry

Over the past few years, the construction sector has undergone a notable evolution driven by advancements in technology. Within this landscape of innovations, drones have surfaced as revolutionary tools, fundamentally reshaping the methodologies behind the inception, implementation, and upkeep of construction ventures. Since the advent of UAV, which is mainly used for advanced surveying operations is mushroomed in the construction industry to examine right from the preparation of site to completion of project. Outfitted with advanced sensors, cameras, and GPS (global positioning system) systems, drones provide unmatched capacities for capturing up-to-the-minute information, producing precise

orthomosaic, and facilitating remote inspections. (Anwar *et al.* 2018, Martinez *et al.* 2020, Jacob-Loyola *et al.* 2021). UAV being compact airframes can manage through the narrow portions of building and few inaccessible locations like bridge deck bottoms for inspection. UAV embedded with positioning system is an added advantage to navigate and guide the quadrotors to precisely position at the object of interest. The real innovation will not come from the aircraft itself, but from the sensors equipped on it and the image analysis algorithms. UAV optical imagery is georeferenced and mosaic is generated as a single map for surveying, and excavation quantification, heritage structure modelling and structural modelling applications (Zhu et al. 2019, Franceschini et al. 2019, Manajitprasert et al. 2019, Lobo Torres et al. 2020). It is an economical, precise and real time monitoring equipment for site engineers and take appropriate decisions according to the situation. It helps the team of engineers to maintain the quality of materials and regulate the wastage in site.

2.2.1 UAV photogrammetry

Using airborne photographs, a method known as photogrammetry is used in drone surveys to ascertain the geometric and spatial characteristics of items inside a defined area. The main goal of photogrammetry is to convert two-dimensional data into cartographic information, which offers important new perspectives on the area under investigation. The objects in the survey region must be recorded in a sufficient number of photos in order for the data to be accurately reconstructed. This extensive coverage guarantees that the structure of the objects may be efficiently extracted. Consecutive photos are overlapped to accomplish. This overlap can be used by photogrammetry to collect different viewpoints of the same objects, improving the precision and quality of the final projection of the image. Detailed Three Dimensional (3-D) models and maps can be easily created using the information gleaned from the overlapping photos, allowing for accurate measurements and analysis. This technology has substantially improved the capabilities of aerial surveys and has emerged as a key instrument in a number of sectors, including land surveying, building, agriculture, and environmental monitoring.

Overlapping parameters

A remote-controlled aircraft's (drone's) flight requires an accurate altitude computation that takes into account a number of variables. These variables include the scale of the photograph, the camera focal length, and the "correlation" parameter, which controls how much of the land is covered by photographs. Each image must have a common region with the one before it in order to accomplish good image correlation and guarantee flawless mosaic. The UAV must keep an absolute flight altitude and a constant speed throughout the mission in order to fulfil these requirements. Due to identical pathways and a constant proportion of correlation between succeeding photographs, the drone is able to take pictures at regular intervals. The longitudinal overlap between images must be more than 80% in order to achieve the best results in aerial surveys and mapping (Gini R*et al.* 2013, de Lima RS*et al.* 2021). This means that during the flight path, a significant percentage of each image should overlap with the prior and subsequent photographs. Similarly, the transverse overlap, which occurs when two images are side by side and share a common region, should be more than 60% (Mora-Felix *et al.* 2020).By ensuring these overlapping areas, the acquired imagery could potentially be used to create precise and high-resolution 3D models, maps, and orthophotos. Drone surveys may give thorough and complete visual data with such meticulous planning and adherence to overlap specifications, supporting many applications in industries like land surveying, building, and urban planning.

Ground sampling Distance (GSD):

Data in digital images is represented in the form of matrix of pixels arranged in rows and columns. An image's size is determined by the total number of pixels, and the higher the number of pixels, the higher the resolution of the image.The distance between two adjacent pixel centres on the ground is referred to as the ground sampling distance (GSD)(Terrance Booth *et al.* 2005). A lower spatial resolution is indicated by a larger GSD score, which reduces the amount of apparent detail in the image. The UAV altitude has an impact on the GSD; the higher it is, the greater the GSD will increase (Barba *et al.* 2019).Due to differences

in terrain height and shifts in the camera angle during photography, photos from the same project may have varied GSD values even when maintaining a consistent flight altitude. The 3D point cloud, camera positions, and average GSD are utilised to produce an orthomosaic, which is a geometrically corrected image(Peng *et al.* 2019). In drone flights and photogrammetry, scale is a key factor. It is possible to find out either before or after the flight. When the desired scale is known but the flying height is unavailable, it is possible to establish the ideal height at which the drone should take pictures. The drone's ideal flight height can be found by applying the proper computation between the focal distance and the necessary scale, ensuring that the acquired photos fit the needed scale and resolution requirements for the particular project(Felipe *et al.* 2012). This information is essential for obtaining precise and thorough findings in a variety of applications, including mapping, surveying, and other remote sensing operations. GNSS is also used for automatic positioning of the UAV at the imaging paths and positions throughout the survey.

Global Navigation satellite system

The strong reliance of existing UAVtechnology on Global Navigation Satellite System(GNSS) coverage is a serious restriction.The autopilot uses GNSS module data while in flight to close navigational loops and guarantee precise location. This reliance on GNSS reception, however, presents problems in a number of situations, especially in regions with scant GNSS coverage (Kutsenko*et al.* 2017, Sheridan *et al.* 2020, Zeybek*et al.* 2021). Canyons, both natural and man-made, where the sky is obscured by buildings, create such difficult situations. The quality of the GNSS constellation geometry in these regions is suboptimal, and multipath effects might introduce errors into the position fix, potentially causing crashes or, in the worst case, rendering it unable to compute a trustworthy position fix. This restriction limits the use of UAV-based mapping in urgent situations requiring evaluation, safety checks, and renovation planning. Mountain highways, suspension bridges, and dams are a few examples of such situations.Exceptional GNSS carrier-phase recordings are necessary to attain high precision in photogrammetry despite the fact that GNSS-independent navigation systems are available and trustworthy in a variety of environmental situations. The most popular method for orienting images in UAVs, aerial triangulation (AT)

or indirect sensor orientation (ISO) entirely depends on image metadata (Benassi*et al.* 2017, Verykoku*et al.* 2018,Jurjevic*et al.* 2020,). However, the development of a substantial network of ground control points (GCPs) is required to guarantee global orientation (GGO) and 3D pointing accuracy. Establishing GCPs using traditional topographic techniques based on total stations becomes time-consuming and expensive without GNSS coverage. Further complicating the procedure is the topology of such difficult settings, which may render some sections inaccessible and unusable for operators.In order to increase the applicability of UAV-based mapping to a larger range of environments and ensure safe and reliable data gathering for varied applications, it is imperative to address these constraints in GNSS-dependent UAV technology. UAV mapping missions can be made morecapableand safer by creating reliable GNSS-independent navigation systems and alternate techniques for setting up ground control sites in difficult terrain.

2.2.2 Photogrammetry in various applications of construction

Digital image processing (DIP) is essentialto create virtual models and extract valuable data from UAV images (Kim *et al.* 2015, Lee *et al.* 2018). A good future trend for DIPis suggested by elements like the falling costs of computer hardware and the accessibility of image digitising tools on the market, along with potential new technologies. The primary objective of image processing is to improve image quality and draw attention to certain details. In photogrammetry, 2D photographs are converted into 3D models that may be scaled and used to calculate distances between objects (Bernardini F*et al. 2002*). Architects and archaeologists have benefited immensely from the rapid development of drones in recent years because photogrammetry image processing has been simplified (Dasari S*et al. 2021*). There are few UAV image processing software's currently available, each version have unique capabilities in processing the aerial images. The Table.1 lists the open source and commercial versions of the UAV image processing software that are currently available and used by the researchers in construction site monitoring. It is also detailed with the application it is used for and the primary objective of the study conducted in the construction site. This software's are designed in automated and semi-automated approach with unique workflows and process.

Table 2.1 Open source and commercial versions of UAV data processing software's

Application	Objective	Software	Authors
Construction progress evaluation	3D modelling	3DF Zephyr	Anwar N *et al. 2018*
Construction progress mapping	Periodically change mapping	AgisoftPhotoscan	Kaamin M *et al. 2017*
Construction progress evaluation	Periodically change mapping	Pix4D Mapper	Qu Te *et al. 2017*
Map generation	Site mapping	Open MVG and Open CV	Moulon P *et al. 2017*
Map generation	Road mapping	Micmac	Duarte L *et al. 2017*
Map generation	Surveying	Z-glif	Menci L*et al. 2007*
Construction mapping	3D modelling	Photo Modeler Scanner	Ahmed Memon Z *et al. 2007*
Map generation	Ortho-photo for measurement validation in site	Aerial Photo Survey (Menci software)	Soares G *et al. 2018*
Building reconstruction	3D modelling	ERDAS IMAGINE UAV Workflow	Becker M *et al. 2017*
Map generation	Disaster mapping	Precision Hawk	Duglas P*et al. 2017*
Map generation	3D modelling	Drone Deploy	Hinge L*et al. 2019*

According to the comparison study conducted by the (Yeum CM*et al. 2017)* on the above mentioned software's it is understood that PIX4D Mapper having the most automated process and simple user interface for processing the aerial images and generating Orthorectified map(Mendes T*et al. 2015*). AgisoftPhotoscan Scanner is performing better in generating the 3D models of the and complete reconstruction in the point cloud missing regions.

The importance of Unmanned Aerial Vehicle Image Correlation

While Digital Image Correlation (DIC) offers numerous advantages and capabilities for measuring displacement and deformation in various applications, there are several reasons why it might not be widely adopted in the field bridge monitoring due to the fixed platform conditions. In actual engineering applications, the majority of bridges cross valleys and rivers, which presents difficulties for the placement of cameras. Due to the UAVs considerable flexibility and capacity for carrying high-resolution cameras for measurement, it may be able to overcome the deployment constraints associated with stationary DIC measurements. The data acquisition platforms like digital cameras and terrestrial laser scanners are fixed on tripods that remain immovable facing perpendicular (90+-7) to the object in a particular location (Sudarsanan N *et al., 2019*). The data obtained from different angles of the target object produces oblique images that abruptly end up yielding inaccurate displacements results (Dutton M *et al. 2014*, Santos AH *et al., 2016*). In spite of its impressive accuracy and unique capabilities for investigating the structural strains under dynamic phenomena, DIC is limited to only a few applications in SHM due to a fixed platform (Blaber J *et al. 2015*). The immovable platform and acquisition of near perpendicular images are not permitting the DIC to be performed on inaccessible locations of a bridge (Suryanto B *et al. 2017*). In the process of obtaining near perpendicular images, inspectors use snooper trucks or other elevated platforms that are aligned to the structural members which also require extra effort, time and money. There have been a few ongoing research on DIC deformation evaluation and comparison studies on structures using UAV, but they are limited to laboratory conditions. The practical applicability of drone DIC in structural health monitoring applications is still a critical topic of research (Jalinoos F *et al. 2020*, Reagan D *et al. 2018*).

The majority of remote sensing inspections are done through imaging sensors, different kinds of imaging sensors can perceive different kinds of information. Red Green Blue (RGB) or visible spectrum imaging sensor is employed for damage quantification (Cusson D *et al. 2011*). Similarly, multispectral imaging sensors for damage assessment (Valença J *et al. 2013*), hyperspectral imaging sensors for concrete properties (Shaban A *et al. 2013*), Light Detection and Ranging (LiDAR) sensors or Laser scanning for determining the crack depth (Schnebele E *et al., 2015*) and Near InfraRed (NIR) or Thermal imaging sensors for identifying the moisture ingress and delamination of bridge deck (ASTM D 4788 - 03, *1997*). These techniques are classified depending upon the type of data acquisition platform at varying altitudes and imaging sensors employed.

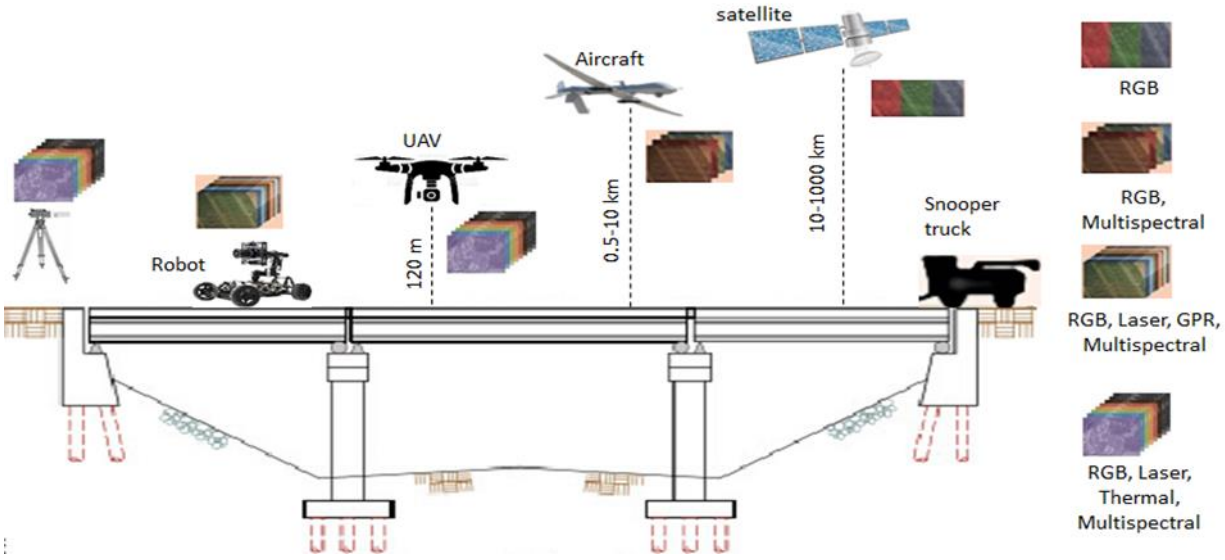

Fig 2.2Remote sensing inspection techniques based on the operational altitudes and data sets produced.

The level of accuracy relies on the operational altitude of sensors and the resolution of imaging data. The data acquisition platforms as shown in Fig 2.2 are categorised based on high accuracy and low accuracy. Inspectors and engineers chose the data acquisition platform based on the type of monitoring, budget allocated and time span.

High accuracy:

a) Terrestrial Cameras: terrestrial cameras are mounted on a tripod and they have the capability to continuously acquire the data for longer periods. Different sensors like visible range (RGB), Laser, Thermal and Multispectral can be mounted on the same data acquisition platform. Terrestrial cameras and laser scanners to produce 3D models through point clouds can be operated even in varied climatic conditions (Vaghefi K *et al 2012*).

b) Robot: Robotics can be operated directly on top of the bridge deck to produce high resolution data sets using sensors like RGB, Laser, Ground Penetrating Radar (GPR) and multispectral. GPR has a unique capability in exploring the internal core condition of the RCC bridge deck to inspect the further serviceability of the structure (*Kaur P et al. 2015*).

c) Unmanned Aerial Vehicle (UAV): UAV/Drone operational altitude is low and restricted to height of 400ft (120m) as per the guidelines issued by the Director General of

Civil Aviation (DGCA), so it can be operated very near to the target object. UAV can acquire high resolution digital, multispectral and thermal imaging datasets along with laser point cloud data to inspect the bridge (Khan F *et al. 2015*).

Low accuracy:

a) Unmanned/ Manned aircraft: Aircraft flying range is above 1km to 10km and flies at supersonic speeds. The data acquired at specified speed and altitude generates coarse resolution images of the structure that can actually be used for preparing a rough estimate of a damaged structure during natural calamity. Only high resolution visible range RGB and Multispectral imaging data acquired through aircraft is considered for damage assessment of a bridge.

b) Satellite: Satellites are operated at higher altitudes of 10-1000km and the revisit time on a particular location is more than 5days, which may not be available at desired dates. Data sets obtained are of coarser resolution and may contain cloud cover that makes the bridge monitoring a hard task (Graettinger A *et al. 2014*).

All remote sensing acquisition systems are well designed to assess the condition above the bridge deck. Although there are certain advantages and disadvantages to each data acquisition system, UAV monitoring systems stand out as it can be operated even below the bridge deck and also at inaccessible locations. UAVs provide many benefits for DIC applications, especially in distant or difficult-to-reach locations where they can quickly access and take high-resolution perpendicular pictures of structures from various heights and angles.

Chapter 3

Scope of Investigation and Objectives

3.1 Critical Appraisal

Advances in computing powers have transformed several sectors, including the building industry. Drone technology has advanced significantly and achieved broad usage in the construction sector during the last decade.Automation and self-diagnosis have become critical instruments for dealing with problems quickly and efficiently. There is a rising interest in the construction industry in studying and developing novel techniques and systems for monitoring material characteristics both before and after construction. The sophisticated technologies in terms of UAV and imaging sensors have paved a new paths to explore in automating the monitoring process. The remote sensing arrangement would also allow

inspectors to remotely access high quality temporal as well as spatial imagery to inspect and actively suggest the engineers.

The process of analysing and comprehending the data generates innovation, not data collecting. Optical imaging sensors can be used with other multispectral sensors to provide a thorough picture of the structure. Multispectral sensors collect data at several wavelengths, allowing for the identification of certain features or attributes of materials that are not apparent to the naked eye. This method enables for the early detection of possible problems such as material flaws, structural deformations, or weaknesses, resulting in more informed decision-making and prompt interventions. There are still many unexplored regions that the usage of multispectral sensors can optimize the monitoring process. Once such area where multispectral IR thermography can be used is early age strength estimation method.

The usage of drones for image data collection can be automated through the advanced setups from flight planning to data transfer protocols for monitoring construction activities. However, when it comes to monitoring the early age strength of concrete using CMM, properly installed thermocouples are critical for accurate data collection, and skilled inspectors are needed to ensure the sensors are correctly placed and maintained throughout the curing process. Due to the scarcity of skilled workers, it can be challenging for the engineers and contractors to make the process automate, as there is limited research on remote sensing and photogrammetric methods in non-destructive testing. This research is intended to design in laboratory and implement in construction site using simple and robust protocols for monitoring the early age construction activities and age-old structures. Developing simple and effective methodologies that combine drone technology with non-destructive testing techniques like CMM could lead to significant advancements in construction quality control and efficiency.

3.2 Research Gap

The UAV in construction site monitoring is been used as a tool for visual documentation technique. In building projects, the post-processing ortho-mosaic created from UAV-acquired photos is a vital source of information. It depicts the building site in great detail and accuracy, allowing for visual inspection and documentation. However, in many circumstances, the ortho-mosaic is not investigated farther than its visual depiction. Very limited literature is available on checking the ortho-mosaic for the measurements to quantify the structural items and generate bill accordingly.In this work, the authors went a step further by assessing the dimensional accuracy of each structural part in the building project using a high-resolution ortho-mosaic. This is an important consideration, particularly in columns and beams, where dimensional accuracy is critical to guaranteeing structural integrity and safety. Accurate dimensions are critical for minimising eccentric loading circumstances, which, if not controlled appropriately, can result in shear failures and impaired structural integrity.The authors were able to discover any deformities or inconsistencies that may have occurred during the construction process by comparing the ortho-mosaic to the specified standards. This useful information can throw light on possible concerns caused by incorrect shuttering or scaffolding shape, which can have a considerable influence on the final dimensions of the structural parts.

Along with investigating the freshly moulded structural dimensions, curing is also one such activity that need to be monitored continuously for 28days of casting. Monitoring the curing process of freshly cast structural parts is crucial for guaranteeing optimum hydration and strength development of the concrete. However, there is a scarcity of literature on the use of Near Infrared (NIR) imaging sensors for curing monitoring in building projects.Images in the near-infrared band, which is sensitive to water concentration, can be captured by NIR imaging sensors. The authors can compute the structure's water indexing and follow the curing process by collecting NIR photographs of newly formed concrete at different intervals over the 28-day curing period.The water indexing calculated from the NIR pictures offers useful information on the moisture distribution inside the concrete over time. Monitoring the curing process using NIR imaging can assist detect regions of low hydration or possible curing difficulties. Construction teams may optimise their curing practises with more thorough data on curing process, resulting in more consistent and reliable concrete performance.

The CMM evaluation procedures include thermocouple installation inside the concrete at certain depth. The thermocouple installed in the concrete is embedded to the Data Acquisition (DAQ) aremore susceptible to the in-situ working conditions. The single use sensitive sensors are more vulnerable to tampering of connectors in the harsh site conditions of passing equipment and materials. The steel formworks and scaffolding also interfere with EMI of the wireless thermocouple sensors.There is a large gap in real time digital documenting and monitoring of the concrete structure with present available NDT techniques. Despite the fact that temperature is a key element in CMM evaluation, there is no literature on the use of IRT to assess concrete strength. it is also observed that a non-contact and volumetric NDT evaluation technique like thermography is more feasible and rapid over the other methods when it comes to large sampling areas. There is a need of simple and robust NDT technique that can be operated easily for monitoring the concrete strength.The novelty of this research is developing aRSNDT method to estimate the strength of concrete by investigating the exothermal emissions at early ages of concreting.

The aim of this research is to automate the monitoring process by employing a multi-sensory UAV that can acquire the multiple spectral images to during and post construction of concrete structures. The usage of UAV mounted with optical and NIR sensor to monitor both progress and curing in the construction site at early stages of concreting and study the aged structural condition. Thermal imaging is thought of as an alternate means of measuring temperature; it just has an initial cost and may be used repeatedly. The construction sector hasn't yet experimented with or developed either NIR or Thermal imaging. Prior research was conducted using the fixed mount camera for the visual documentation and deformation SHM experiments using the DIC. The inspectors' ability to capture a perpendicular, precise image of a bridge deck and beams is limited by the permanent mount. DIC system mounted on a UAV is the need of hour to ascertain the structural condition.The study findings and approaches can make a substantial contribution to the field of construction quality control and project management, resulting in safer, more efficient, and cost-effective construction practices.

Rapid, risk-free, and cost-effective methods are required to monitor and record bridge damage while minimising disruptions to traffic flow. The creation of a DIC that is movable

and can hover through inaccessible areas to check on the structural integrity and gauge the damage the need for a different acquisition platform in order to get close to perpendicular images and reduce pixel drag in order to enhance the quality of the data and outcomes. DIC placed on a UAV in other name Unmanned Aerial Vehicle Image Correlation (UAVIC) can monitor inaccessible areas of a structure and affordably address the problem of collecting images that are almost perpendicular. Additionally, the remote sensing system will make it easier for the inspectors to get high-resolution.

3.3 Research Objectives

i. To study the efficiency of UAV in RCC structural deformation and damage quantification using Unmanned Aerial Vehicle Image Correlation (UAVIC) and evaluation on in-service bridge.
ii. Monitoring structural construction activities using UAV for visual progress evaluation and dimensional accuracy assessment.
iii. Near Infra-Red imaging for hydration monitoring in a construction site.
iv. Estimation of the strength of concrete at initial stages of construction using thermography and validate it in site.
v. To develop a relationship between the internal and external temperature of concrete using thermocouple and thermography methods on multiple grades and volumes.

3.4 Research Methodology

The project's goal is to apply drone technology to the visualization-based inspection of construction sites. It is suggested that this investigation be carried out using advanced imaging infrared band sensors in conjunction with UAV technology. The overall methodology of the study is given in the Fig 3.1. UAV mounted with Optical and NIR sensors are flown on the construction site to evaluate the progress, curing requirements and strength aspects. The optical mounted UAV is also used for the condition monitoring of the structure.

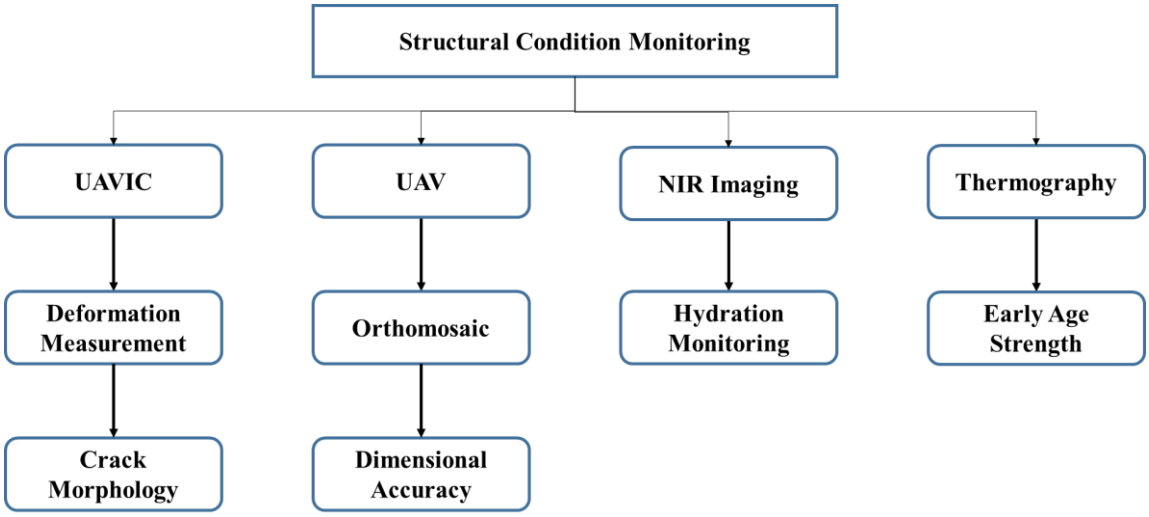

Fig 3.1Overall methodology of monitoring construction site and structural condition.

Each segment of sensory imaging and processing methodology is described according to the objectives. Initially, the visible rage imaging or optical imaging data acquisition and processing is done periodically as per the pace of construction. The acquired data is processed and stitched for generating the ortho-mosaic of the construction site. A change detection study is conducted to delineate the newly constructed structural elements. The newly constructed structures are checked for curing and strength related aspects. UAV mounted with multispectral sensor system is driven to that specified location of new elements and images are acquired. The NIR images are processed and morphological operations are applied to map the curing index of the structural element. Similarly, thermal images of those newly constructed elements are acquired and processed for temperature. The temperature observations are used to predict and monitoring strength using CMM calibration curves. Each objective of work is presented in the subsequent chapters.

Chapter 4

Investigating the UAVIC studies in laboratory and execution on in-service bridge

4.1 Bridge Deformation measurement

Structures madeof RCC are intended to have a certain serviceability life span. RCC is a common material used in high-rise buildings and massive structures like roads, bridges and dams. Repetitive loading and other environmental factors might cause RCC's functionality to degrade. In order to assess damage and keep operating, RCC structures need frequent maintenance and surveillance. According to Federal Highway Administration (FHWA) (1) Inspection Standards, depending on the age of the structure, bridges need to be examined every 2-4 years. Using the wide range of already available NDT techniques,it is easy to examine the service life of ground-level structures. Structures that are above ground level or

more than 5M in height are challenging to assess for serviceability of the structure, which puts engineers and inspectors at danger. Snooper trucks and contact NDT techniques are frequently used in difficult bridge performance evaluation procedures to quantify the service life based on deterioration at crucial zones. It can be challenging to assess infrastructure damage in the wake of natural disasters using conventional techniques like visual inspection and in-contact NDT.

Using high-resolution satellite data sets, the first non-contact damage estimate for buildings and other property is carried out. The ability to monitor a structure connected to data collecting platforms in real-time has been greatly facilitated by the use of in-contact sensors for vibration observations. Due to its great sensitivity, in-contact sensors are easily destroyed by external loads and extreme weather conditions. These sensors have proven to be ineffective at monitoring the entire structure at once, despite being extremely competent of detecting the problem at the implanted spots. The majority of infrastructure failures are attributed to incorrectly identifying and maintaining the damage zone in a structure. Visual inspection, assessment and documentation of repairs are the most common methodology followed by inspectors and engineers. Though it is a quite simple and common process, the machinery involved in inspection makes it more expensive and the occurrence of accidents and manual errors are high. In addition, human vision inspection can perceive limited observations at a time compared to computer vision techniques. Photogrammetry concepts clubbed with computer vision are developed by researchers to identify the critical zones by analysing the digital image for crack properties, spalling and damage in a structure.

Numerous civil engineering applications, such as Structural Health Monitoring (SHM), have been made possible by the recent development of Digital Image Correlation (DIC). By analysing the previous and post-loading digital image, the DIC vision approach is a remote sensing and photogrammetric method that can detect the deformation of an object. The researcher can now choose an image processing method based on the needs of an application thanks to the abundance and diversity of available algorithms. Finding the flaws in a structure and monitoring have become simple thanks to algorithms like pattern recognition. The DIC approach is a non-contact, quick, cost-effective, and reliable NDT method. DIC can process both 2D and 3D information to obtain measurements of a structure's displacements and

deformations. Digital cameras and terrestrial laser scanners are just two examples of the data collecting platforms that are fastened to tripods that are immovably pointed perpendicular (90+-7) to the item in question. Oblique pictures are created from data collected from various angles of the target object and abruptly end up producing findings for erroneous displacements. DIC is restricted to only a few applications in SHM because to a fixed platform, despite its outstanding precision and unique capabilities for evaluating the structural strains under dynamic phenomena. The DIC cannot be carried out on inaccessible areas of a bridge due to the immovable platform and acquisition of almost perpendicular images. Inspectors utilise snooper trucks or other elevated platforms that are aligned to the camera to obtain almost perpendicular pictures that are aligned to the structural members that also require extra effort, time and money.

4.2 Methodology

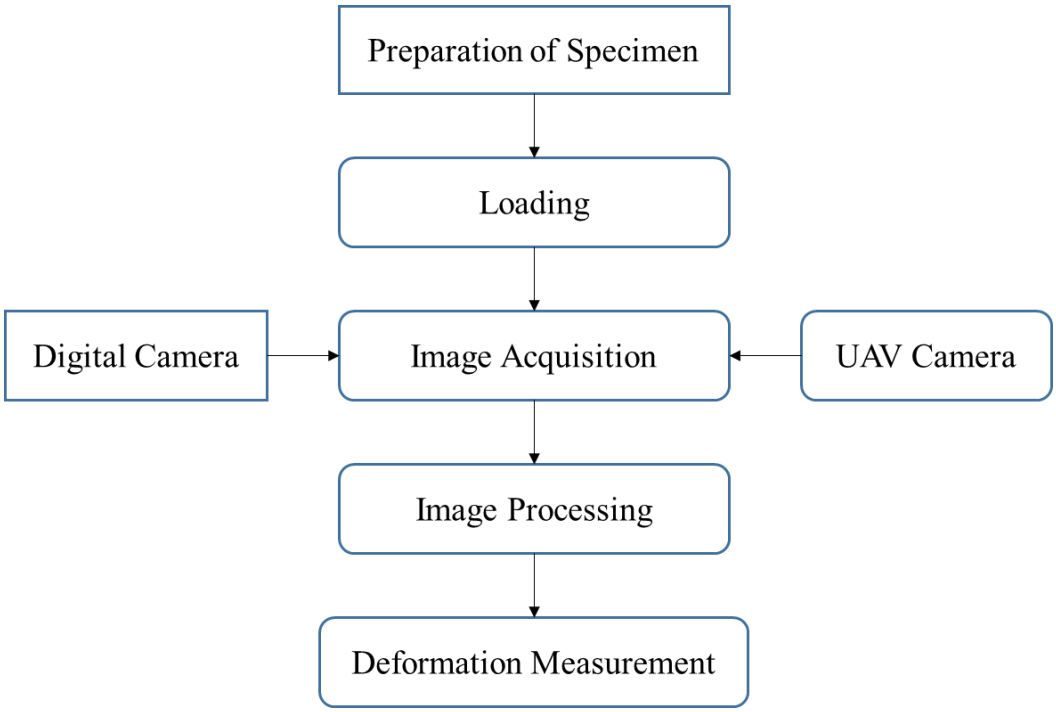

Fig 4.1 Flow chart of UAV DIC for deformation measurement

The flow chart for the study's approach is shown in the previous Fig 4.1. In this chapter, the methodology that includes steps for specimen preparation, image acquisition, and

image processing is thoroughly detailed. The potential image processing techniques for crack identification are also covered in this chapter.

4.3 Specimen Preparation

Three 150*250mm by 1.2M long concrete beams are formed using the M25 mix design proportions as given in table 4.1. The beams consists of four 12mm-diameter bars and eight 8mm-diameter stirrups positioned 150mm apart in the steel. The beams are used for the experimental tests after being fully cured for 21 days. Spraying white paint on the surface of the specimens creates a background for the application of random black paint speckles as shown in Fig 4.2. It is crucial to have a large number of black speckles in a variety of sizes and shapes to get precise results.

Table 4.1M25 concrete mix proportions

Mix Design	Coarse aggregate (kg/m^3)	Fine aggregate (kg/m^3)	Cement(kg/m^3)	W/C (kg/m^3)
M25	1065	753	449	197.5 (0.44)

Fig 4.2Specimens preparation along with random speckle pattern

Loading and DIC Setup

To determine displacements and strains, specimens are put through a three-point bending test. By laying the concrete specimen over the support span on either end of the material, lowering a point load to the middle of the span, and bending the material until it fails while measuring the applied force and displacements, this is referred to as three-point bending as shown in Fig 4.3. It is important to establish the readings and their labelling as stated in the table below in order to match the deformation to the relevant load. Deflection is recorded on the dial gauge for each load increment of 4kN for beam1 and 5kN for other two beams and photos from a digital camera and a drone camera are also acquired at the same time.

Fig 4.3Loading test along with image acquisition using DSLR camera and UAV.

4.4 Image Acquisition

Digital images are taken during load applications at different load level increments to process in DIC.A series of digital images are acquired during load implications at different load levels to process in DIC. Image acquisition duringpre loading condition as shown in Fig.

4.4 and during loading condition as shown in Fig 4.5 is done simultaneously with Digital Single-Lens Reflex(DSLR) camera. Dial Gauge is also placed prior to loading at the bottom center of the beam to measure the deformation occurred due to load implication. Similarly, Images for the rest of the beams are also acquired at specific load levels. The camera images are acquired using Nikon D5600 bearing a CMOS sensor of 24.2MP with a focal length of 18 mm and 1920*1080 resolution and it has 60fps video recording capabilities. The drone image acquisition is achieved by employing DJI Phantom4 Pro V2.0 that is equipped with CMOS 20MP sensor with a focal length of 8.8mm and resolution of 5472*3648 pixels and it has 60fps video recording capabilities. The UAV is a quadcopter with a designed flight time is 30 minutes and a maximum weight of 1,375 grams. Both the cameras are set at 3meters away from the target beam for imaging.

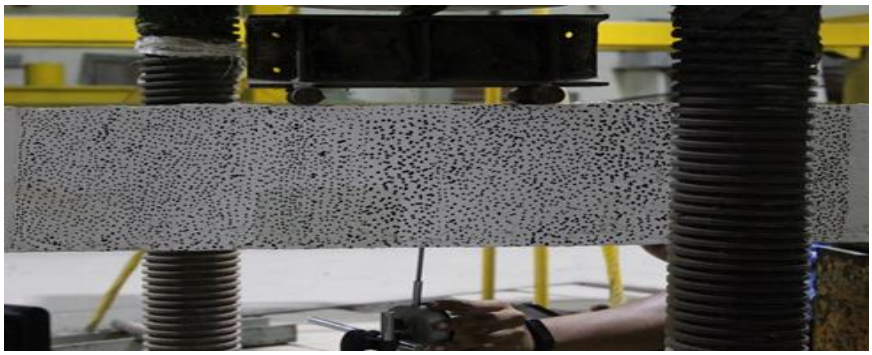

Fig 4.4Image of before application of load using DSLR

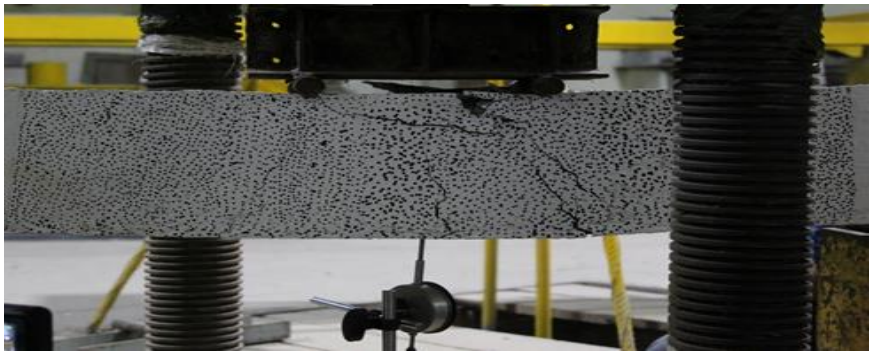

Fig 4.5Image of after application of load using DSLR

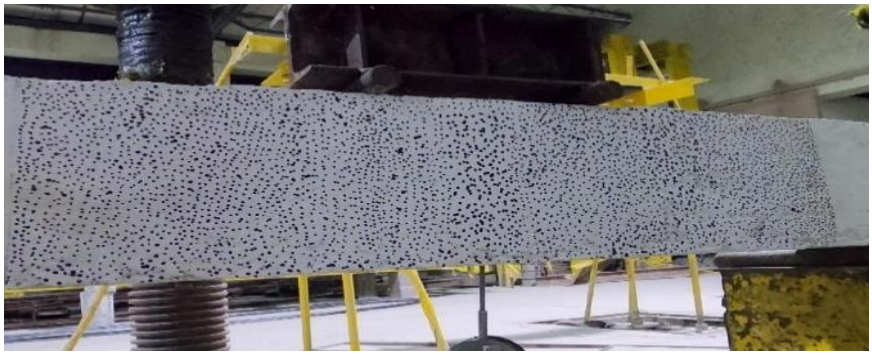

Fig 4.6Image of before application of load using UAV

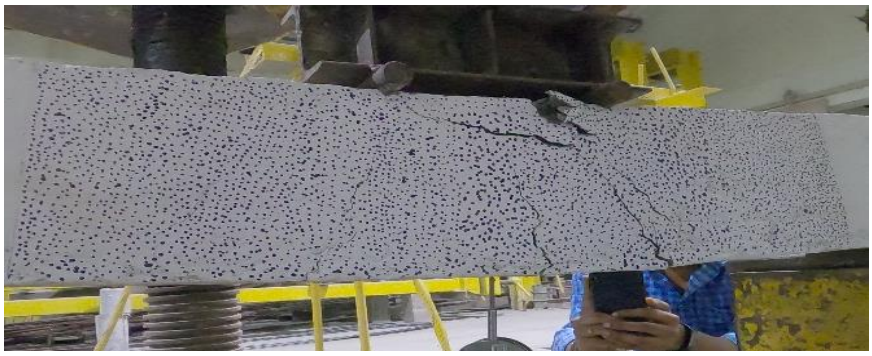

Fig 4.7 Image of after application of load using UAV

Image Pre-processing

The preprocessing of the images are done for camera motion corrections in the UAV acquired pre image as shown in Fig 4.6 and during loading condition image as shown in Fig 4.7. Any minimal camera movement has the ability to directly alter the extrinsic parameters and result in mistakes in the DIC measurements. Consequently, it is essential to adjust camera motion for precise in-field deflection monitoring. The UAV acquired images are rectified with any distortions and change in camera positions using the homography transformation by assigning a Direct Linear Transformation (DLT) projection system.

Homography transformation

A homography transformation across the image planes from the UAV acquired images is established to start the process. A geometric projection known as homography is used to arrange coordinates from one plane to another. In this stage, the homography matrix is

computed using the pixel coordinates of precisely defined points in the images (Chen *et al*. 2021, Zhang *et al*. 2021). An internal MATLAB programmeis used to carry out the homography projection. Pitch, yaw, roll, and translation in three dimensions are the four categories into which the UAV movement can be divided as shown in Fig 4.8.

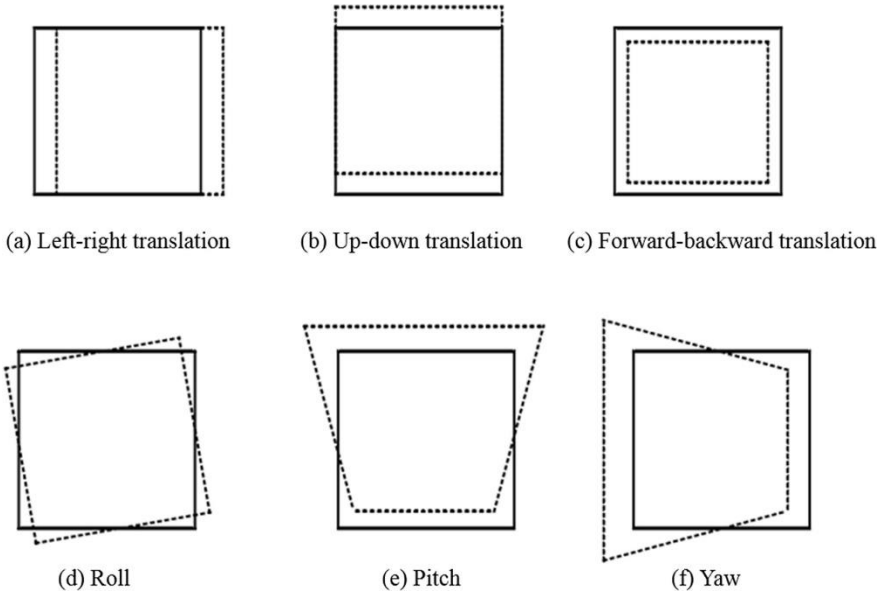

Fig 4.8Image distortions triggered by the UAV motion.

The UAV photos are corrected using the homography transformation matrix to get rid of any perspective flaws or geometric mistakes. Rectification makes ensuring that the images are converted into a similar plane and position, which makes it easier to compare and analyse displacements between images.The pre loading image and the post loading images are assigned to the same plane with automatic and specified control points as shown in Fig 4.9.

x' = f(x; p) given the x as 3*3 matrix it can be written as eqn 9

$$\lambda\begin{bmatrix} u^1 \\ v^1 \\ 1 \end{bmatrix} = \begin{bmatrix} h_{11} & h_{12} & h_{13} \\ h_{21} & h_{22} & h_{23} \\ h_{31} & h_{32} & h_{33} \end{bmatrix}\begin{bmatrix} u \\ v \\ 1 \end{bmatrix} \qquad \text{eqn.9}$$

Multiplied out by u' and v' it can be written as eqn 10

$$u' = \frac{h_{11}u + h_{12}v + h_{13}}{h_{31}u + h_{32}v + h_{33}}$$

$$v' = \frac{h_{21}u + h_{22}v + h_{23}}{h_{31}u + h_{32}v + h_{33}} \qquad \text{eqn. 10}$$

Re arranging the terms

$$Let\, h_{33} = 1, \, then$$

$$h_{11}u + h_{12}v + h_{13} - h_{31}uu' - h_{32}vu' = u' \qquad \text{eqn.11}$$

$$h_{21}u + h_{22}v + h_{23} - h_{31}uv' - h_{32}vv' = v'$$

There are eight unknown parameters in the above equation, we need to find four sets of non-collinear points (the reference points tracked by the DIC method) in two image planes to calculate the homography matrix with eight unknowns. The reference points selected should be kept in the same plane as much as possible; the results of this step affect the measurement accuracy. The above equations can be written in a matrix format as:

$$\begin{bmatrix} u_1 & v_1 & 1 & 0 & 0 & 0 & -u_1u_1' & -v_1u_1' \\ 0 & 0 & 0 & u_1 & v_1 & 1 & -u_1u_1' & -v_1u_1' \\ u_2 & u_2 & 1 & 0 & 0 & 0 & -u_2u_2' & -v_2u_2' \\ 0 & 0 & 0 & u_2 & v_2 & 1 & -u_2v_2' & -v_2v_2' \\ u_3 & v_3 & 1 & 0 & 0 & 0 & -u_3u_3' & -v_3u_3' \\ 0 & 0 & 0 & u_3 & v_3 & 1 & -u_3v_3' & -v_3v_3' \\ u_4 & v_4 & 1 & 0 & 0 & 0 & -u_4u_4' & -v_4u_4' \\ 0 & 0 & 0 & u_4 & v_4 & 1 & -u_4v_4' & -v_4v_4' \end{bmatrix} \begin{bmatrix} h_{11} \\ h_{12} \\ h_{13} \\ h_{21} \\ h_{22} \\ h_{23} \\ h_{31} \\ h_{32} \end{bmatrix} = \begin{bmatrix} u_1' \\ v_1' \\ u_2' \\ v_2' \\ u_3' \\ v_3' \\ u_4' \\ v_4' \end{bmatrix}$$

The continuous image sequence is analyzed frame by frame, and the image taken at the first moment is regarded as the reference image, and the images at different moments are projected into the reference image sequentially. A one-to-one homography transformation is established between the reference image and the image to be corrected (i.e., one of the images taken at other moments).

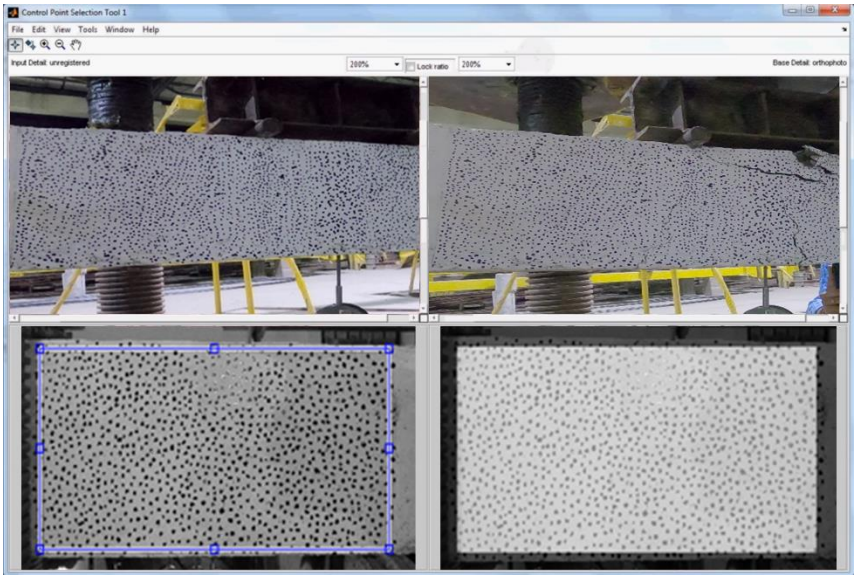

Fig 4.9Application of Homography projection system using MATLAB tool

4.5 DIC Analysis

The displacement and strain fields are obtained using DIC analysis, which is carried out through the application of the correlation algorithms. Ncorr software version 1.2.2 and MATLAB version R2018a are both used in this investigation. The reference image and deformed images as shown above are preprocessed for any translations and distortion corrections. The corrected images are ready for DIC analysis and fed into the image processing software. Reference image, which is the first or initial image captured before the application of load, is posted first. The current image, which is the deformed image as shown in Fig. 4.10is then uploaded and should follow the reference image's format specifications. The reference image is single image used for correlation whereas the deformed images can be multiple. The analysis can be only done in one on one process and cannot parallel process multiple images at a time. The processing time depends on the hardware used and the DIC parameters selected for number of iteration and algorithm used. Certain thresholding parameters also influence the processing and computational efficiencies like subset options and speckle seed radius selection.

Fig 4.10Loading of reference and deformed image in Ncorr

4.5.1 Setting DIC parameters

DIC parameters need to be set up on ROI for displacement measurements in the image processing software. Subset radius is chosen to cover the portion of speckle pattern which should be small and at least covers more than 3 speckles that does not result in noisy displacement data as shown in Fig. 4.11. Subset size is chosen in such a way that it should increase the computational speed and the sizeranges is selected between 10 and 200 and thespacing ranges between 0 and 20.

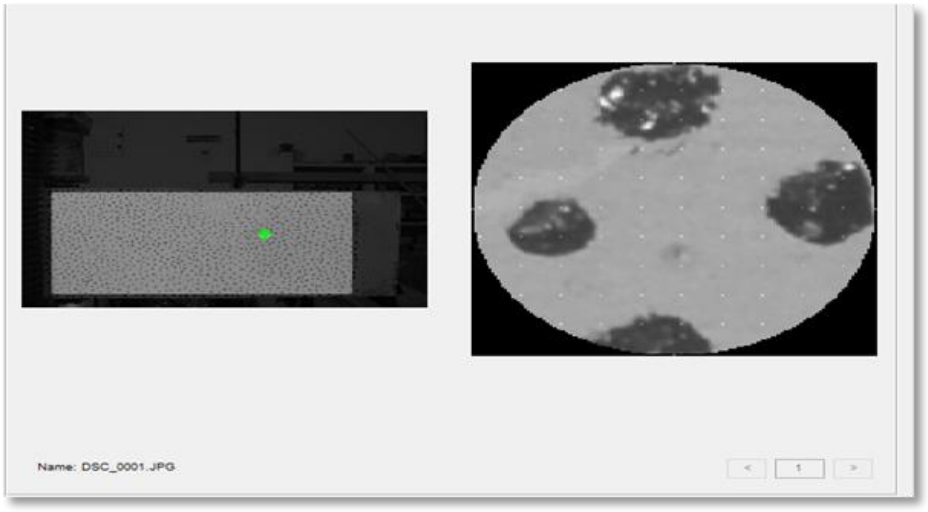

Fig 4.11 Set DICparameters

The multithreading option is used to accelerate the computing process. The more threads there are, the more precise the findings will be. In this study, the best subset size is 80, the subset spacing is 15, and the number of threads is 4. In DIC analysis, subset options are parameter that describes the how large the size of subset and spacing between them. Spacing criteria is meant for reducing computational load. The main aim is to choose smallest subset size that doesn't result in noisy data.Processing the images for deformation measurements need a sophisticated hardware. To enhance the processing speed multi-threading options are used.

4.5.2 Seed placement process

To perform image analysis a contiguous region is selected for processing and seeds are placed for correlation processing. The seed placement process gives initial assessment for DIC analysis from which neighboring pixels are computed for correlation analysis in the series of digital images. DIC analysis for the strain computations are also performed based on the displacements occurring on the beam. The selection of strain radius is similar to that of subset radius which is desired to be the smallest that does not result in noisy strain data. In this study, a strain radius of 10 is selected. The strain anomaly is given on the beam facade based on the load distributionas shown in Fig. 4.12.

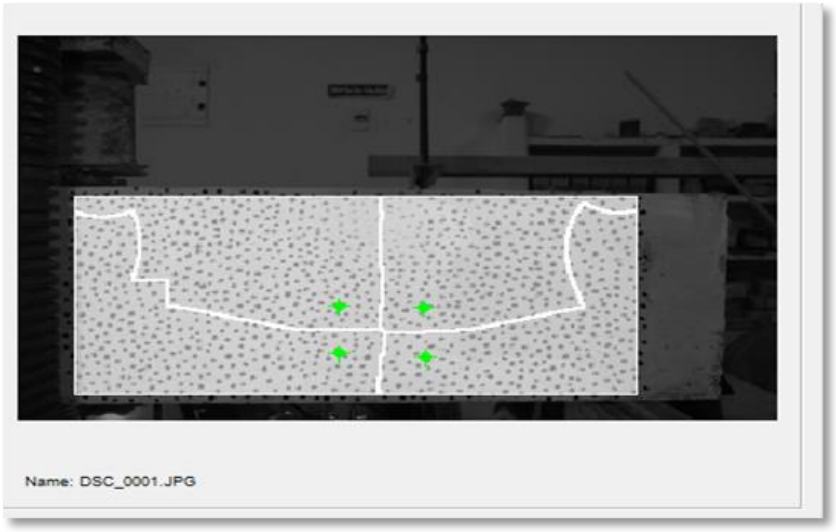

Fig 4.12 Seed setting on selected region

It provides initial guess for DIC analysis and it alsodivides ROI so that each part is analysed in parallel and seeds can be placed in high deformation regions based on the observations. While specifying seed placement the bad data points (points which falls outside the FOV) can be filtered out by reducing correlation coefficient value. The seeds are placed in selected locations where the strains exhibited are more.

Calibration and scaling

The calibration and scaling procedure is completed at this stage. We must give the relevant pixels with unit measures that we desire. It is possible to do this by placing a line at a given position with known dimensions. It is used to translate pixel displacements to real-world units. The true depth of the specimen, 260 and the same is specified at the time of processing for scaling the model. The number of pixels confined in the region of 260mm is divided for obtaining the pixel resolution in the DIC analysis. Displacements are transformed from pixels to millimeters in this study, utilizing a unit measurement of 0.1189mm/pixel.

4.5.3 Strain Calculations:

A continuous region is chosen for processing and seeds are for image analysis. Initial evaluation for DIC analysis is provided by the seed placement method, from which nearby pixels are generated for correlation analysis across a collection of digital images. Based on the displacements happening on the beam, DIC analysis is also carried out for the strain computations. Similar to choosing a subset radius, the strain radius should be chosen to be as small as possible without producing noisy strain data. As illustrated in Fig 4.13 a strain radius of 10 is chosen for this study. Based on the load distribution, the strain anomaly is displayed on the beam facade.

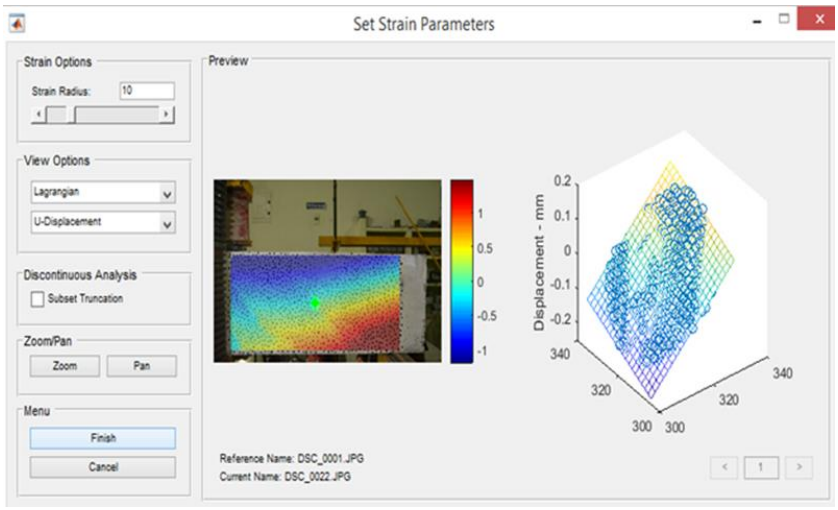

Fig 4.13 Setting strain radius

Displacements investigations:

Results from three point bending tests on RCC beam specimens have been summarized in the software. The image analysis of DSLR and UAV photos of a single beam produced the results listed below. The incident happened at a maximum load of 115kN, according to the records. Following the failure load, the displacement quickly rises while the load falls. The displacement at failure load in the longitudinal direction (U-Displacement) is shown in Fig 4.14 below. This displacement is 5.380 mm, which is positive and implies compression in the distorted picture. 0.0599 mm was found to be the median value. The displacement at failure load in the lateral direction is shown in Fig 4.15 as being -3.563 mm, which is negative and

shows tension. 6.4953 mm has been discovered to be the median value. The supplied beam produces a single deformed image, and each image produces a distinct displacement in accordance with the changing load values. Similarly, the DIC analysis is also conducted for the UAV acquired images. The displacement at failure load in the longitudinal direction (U-Displacement) is 5.410 mm which is positive indicates compression in the deformed image. The median value was found to be 0.0630 mm. The displacement at failure load in the lateral direction (V-Displacement) is -4.113 mm which is negative indicates tension. The median value has found to be -6.992 mm. Displacements of longitudinal direction is only considered from the image analysis for plotting the load over deflection graphs.

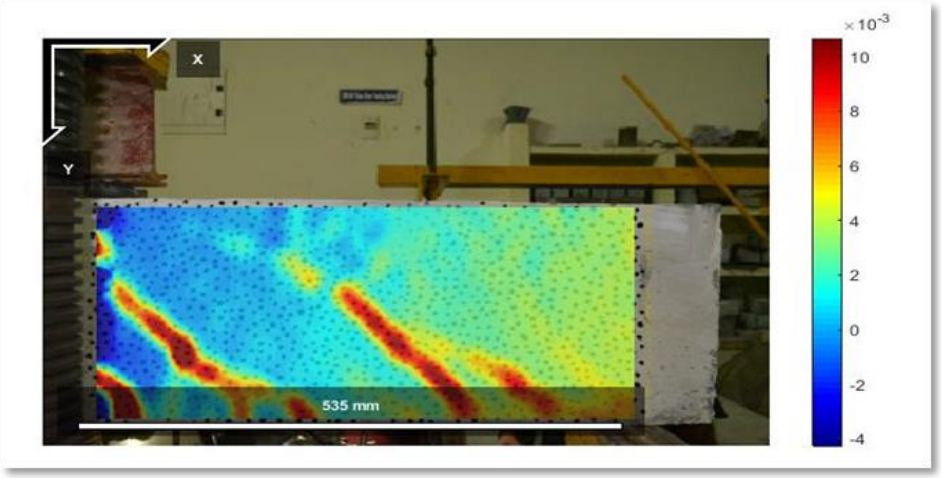

Fig 4.14Displacement in the longitudinal direction for DSLR images

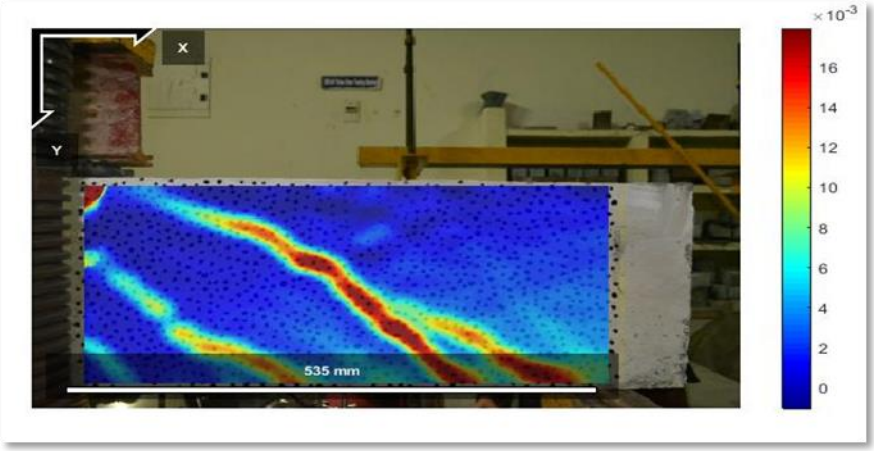

Fig 4.15 Displacement in the lateral direction for DSLR images

4.6 Load- Displacement plots:

Displacements derived from DIC analysis at various load levels are contrasted with experimentally recorded dial gauge values. DSLR image displacement data are obtained independently from UAV image displacement measurements and plotted. With an accuracy of 95%, there is just a slight variance in the investigations between dial gauge and DSLR displacements. In contrast, experiments using an 88% accurate dial gauge to measure UAV displacements show slightly larger differences. Occasionally, a sharp increase in UAVIC findings is seen as a result of the drone's magnetism and vibrations. A load-displacement graph of beam-A with a failure load of 88 kN and a maximum displacement of 4.82 mm is shown in Fig 4.16 (a). Similarly, the beam-2 graph in Fig. 4.16 (b) and beam-3 graph in shown in Fig 4.16 (c). The beam-1 failed early with minimal load whereas the beam-2 and beam-3 indicate failure loads of 110kNand 115 kNand corresponding maximum displacements of 5.36 mm and 6.45 mm, respectively. With a not much difference in experimental values observed in the study using dial gauge, camera DIC and UAVIC have generally produced positive results as given in table 4.2 As the UAVIC results are in compliance with the dial gauge with a variation of 12% it is proposed as an preliminary investigation tool for the in-service bridge.

Table 4.2Load deflection data by dial gauge, camera DIC and UAVIC of three RCC beams

Beam1				Beam2				Beam3			
	Deflection (mm)				Deflection (mm)				Deflection (mm)		
Load KN	Gauge	DIC	UAVIC	Load KN	Gauge	DIC	UAVIC	Load KN	Gauge	DIC	UAVIC
4	0.05	0.07	0.04	5	0.08	0.07	0.08	5	0.09	0.08	0.10
8	0.21	0.21	0.25	10	0.15	0.14	0.18	10	0.31	0.28	0.30
12	0.34	0.32	0.36	15	0.26	0.25	0.30	15	0.48	0.45	0.50
16	0.44	0.45	0.50	20	0.34	0.35	0.39	20	0.67	0.65	0.65
20	0.55	0.53	0.52	25	0.48	0.50	0.48	25	0.81	0.80	0.80
24	0.68	0.65	0.64	30	0.68	0.70	0.70	30	0.96	1.00	1.08
28	0.82	0.84	0.90	35	0.85	0.83	0.90	35	1.09	1.10	1.12
32	0.97	1.00	1.02	40	0.98	1.00	1.03	40	1.26	1.28	1.30
36	1.12	1.10	1.15	45	1.20	1.17	1.21	45	1.48	1.50	1.50
40	1.34	1.35	1.40	50	1.29	1.30	1.34	50	1.72	1.70	1.75
44	1.45	1.42	1.50	55	1.42	1.40	1.40	55	1.87	1.85	1.95

48	1.60	1.64	1.60	60	1.68	1.70	1.75	60	2.02	2.00	2.05
52	1.78	1.82	1.85	65	1.85	1.83	1.90	65	2.26	2.25	2.28
56	1.97	2.00	2.05	70	2.06	2.08	2.10	70	2.48	2.50	2.35
60	2.09	2.14	2.18	75	2.21	2.20	2.20	75	2.71	2.70	2.70
64	2.35	2.40	2.38	80	2.43	2.40	2.40	80	2.95	2.95	3.00
68	2.53	2.56	2.70	85	2.81	2.80	2.83	85	3.32	3.30	3.40
72	2.78	2.80	2.90	90	2.96	3.00	3.00	90	3.61	3.60	3.60
76	3.08	3.14	3.10	95	3.08	3.06	3.10	95	3.96	3.95	3.88
80	3.45	3.50	3.60	100	3.41	3.40	3.44	100	4.44	4.45	4.52
84	3.68	3.74	3.75	105	3.64	3.64	3.65	105	4.83	4.83	4.88
88	3.95	3.98	3.90	110	4.02	4.00	4.10	110	5.12	5.12	5.20
85	4.04	4.05	4.00	105	4.41	4.40	4.50	115	5.38	5.40	5.40
80	4.14	4.18	4.20	100	4.68	4.70	4.72	110	5.69	5.70	5.75
75	4.24	4.28	4.30	95	4.95	4.93	5.00	105	5.98	6.00	6.20
70	4.65	4.70	4.75	90	5.23	5.25	5.30	100	6.41	6.40	6.55

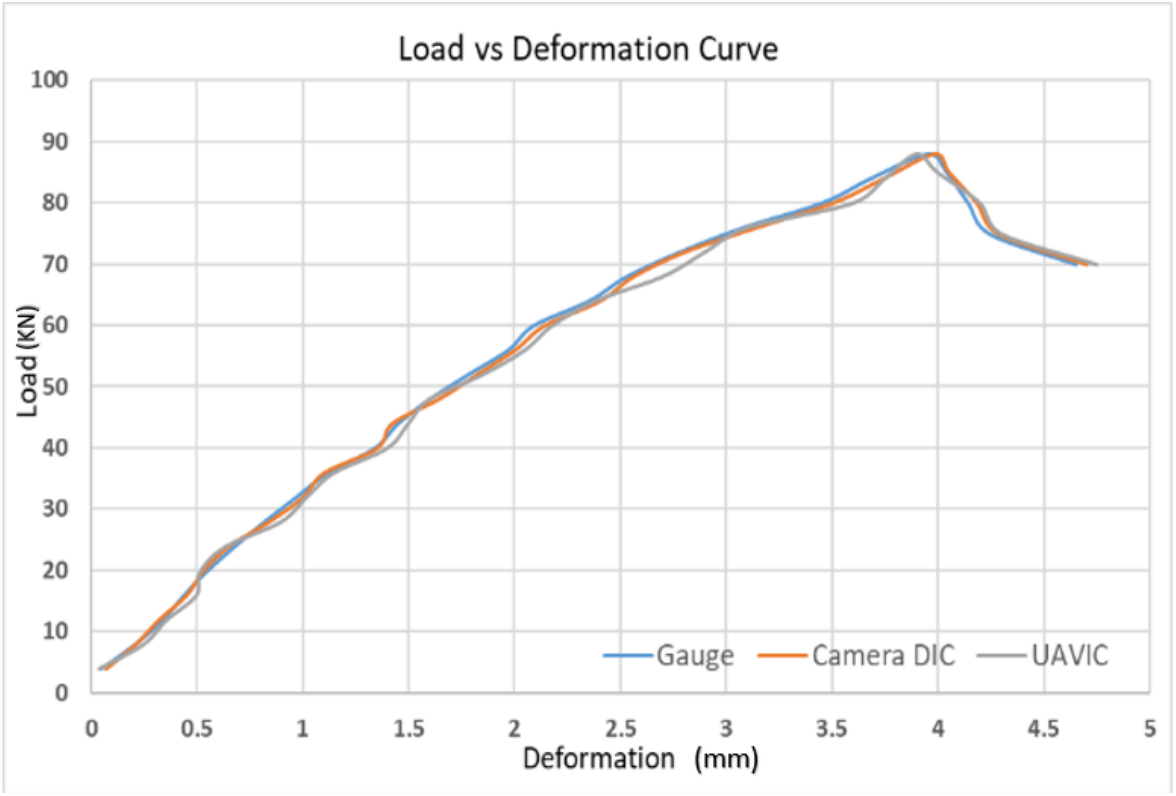

(a)

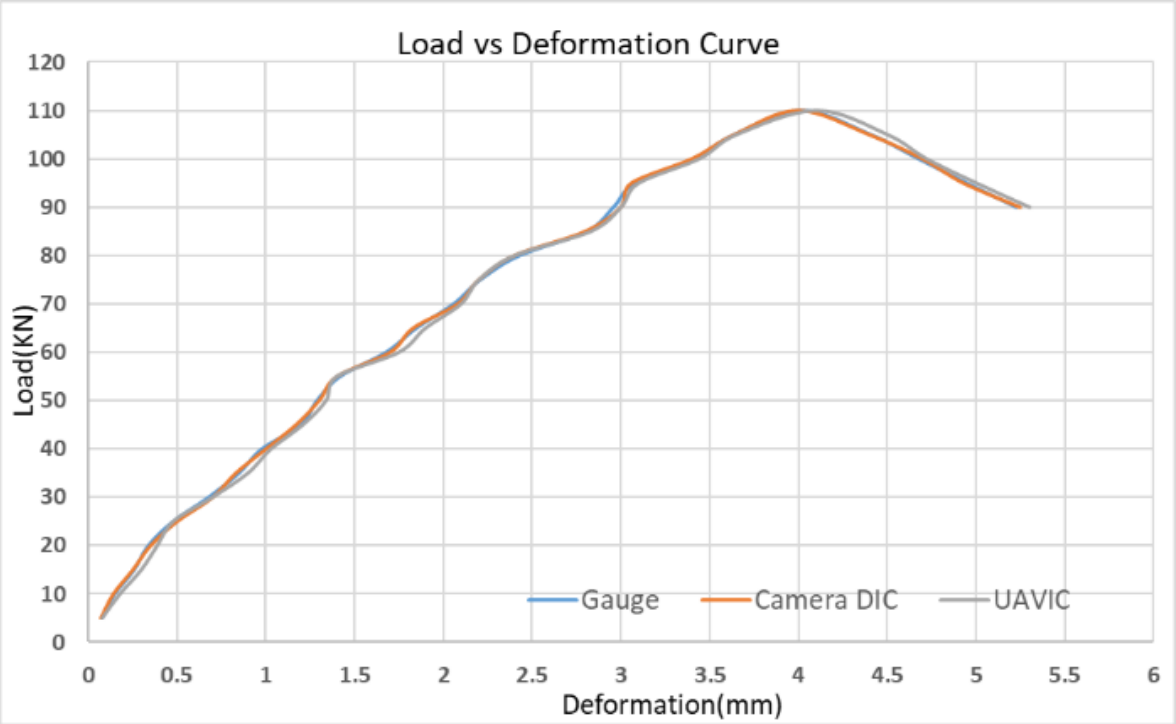

(b)

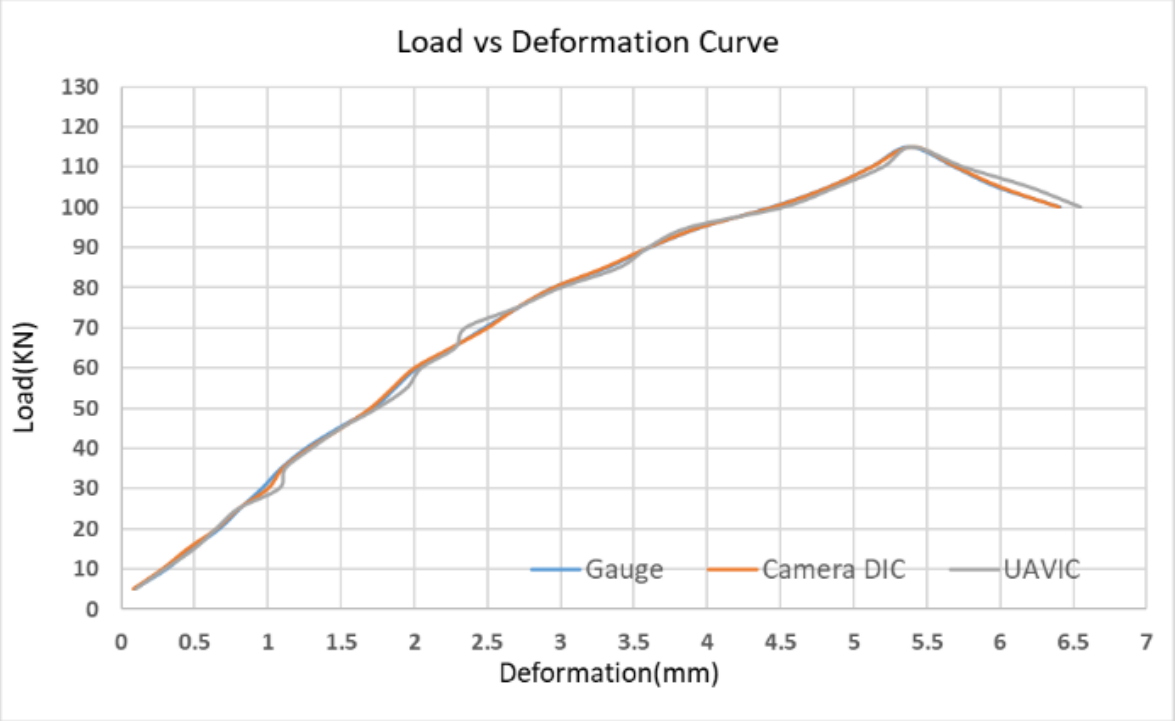

(c)

Fig 4.16Load Displacement plots of RCC Beam1(a), Beam2(b), Beam3(c)

4.7 DAMAGE QUANTIFICATION:

Digital images collected from the concrete specimen are used for automated detection and measurement of cracks as it represents a very small portion of concrete surface. A digital camera is used to capture high resolution images of reinforced concrete beams. Beams labelled RCC tested with increasing displacement levels that correspond to a load step. Structural damages spalled concrete, crack initiation and propagation, crack width measurement and monitoring reinforcing bar buckling were determined by an automated process based on digital imaging and processing.

4.7.1 Crack Identification and Feature Extraction:

When RCC is loaded, it displays minimal elastic characteristics and has a limited bending tendency. When the beam is loaded excessively further, RCC begins to show cracks beyond the elastic limit. Microcracks can develop during shrinkage, creep, heat of hydration, and other construction-related processes. These cracks can lead to structural collapse.

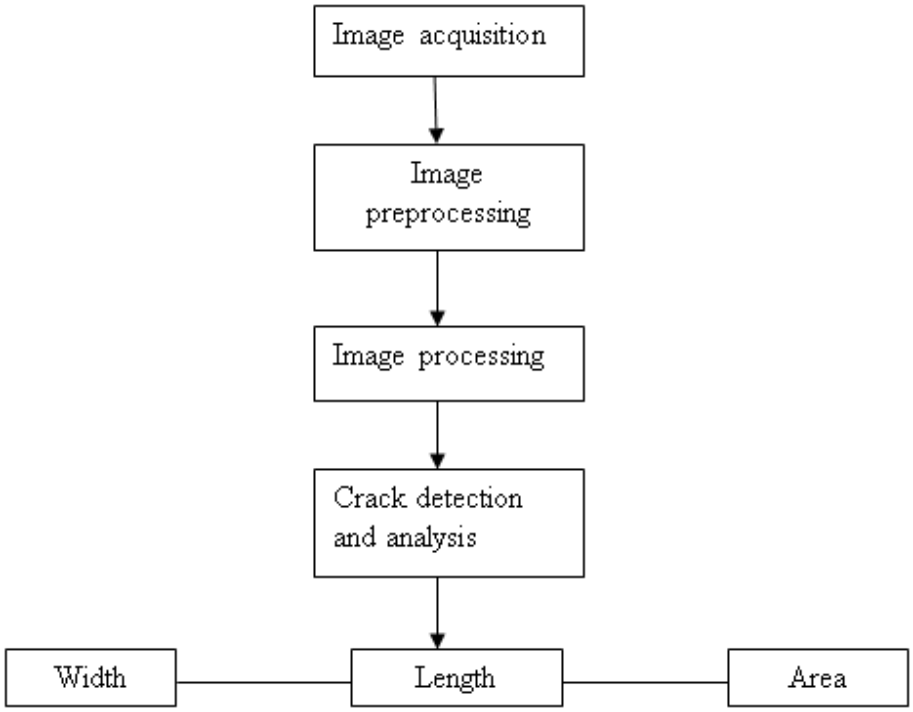

Fig 4.17 Flow chart for proposed crack detection

Advances in image processing by binarizing the image and thresholding it for characterizing the crack through automation is also necessary. The field experimental image acquisition and correlations are required to execute the ongoing studies on cracks. To evaluate the crack detection and evaluation studies the methodology as illustrated in Fig 4.17 is followed. The studies also deal with the noise removal for computational in-efficiency within field operations. The damage of any concrete structure is quantified by the length, width and depth of crack. The identification of this is laborious and time consuming. Automated and reliable image processing techniques are employed to minimize the effort of work force. This method ensures digital mapping of each crack and its propagation. Cracks are ranked based on its width of i.e. width in millimeter between (0.01 - 0.09) ranked as 3, (0.1 – 0.5) ranked as 2, (0.6 – 1.0) ranked as 1. Based on these ranks, hazard quantification is done. This process needs assessment in rank 1 crack as it lies in the danger zone. Table 4.3 discuss the cracks based on the crack hazard zonation based on the width, it also details the repair methods to be followed based on the ranks.

Table 4.3Crack ranking and repair method based on widths

Crack hazard zonation	Crack width(mm)	Repair methods
Rank 1	0.6 - 1.0	Gravity filling method
Rank 2	0.1 - 0.5	Grouting and sealing
Rank 3	0.01 - 0.09	Epoxy injections

The beam facade is subjected to image segmentation in order to determine the crack's width and angle. Cracks have a major axis (length) that is significantly longer than the minor axis (width). By executing segmentation and morphological operations by creating structural elements, the cracks created on the beam are measured for their width and length in the images. Because it represents a relatively small fraction of the concrete surface, digital pictures obtained from the concrete specimen are utilised for automatic detection and quantification of cracks. High quality photos of reinforced concrete beams are captured using a digital camera. RCC-labeled beams were evaluated with escalating displacement levels that corresponded to load steps. An automated technique based on digital imaging and processing was used to evaluate structural damages spalled concrete, crack initiation and propagation, crack width measurement, and monitoring reinforcing bar buckling.

4.7.2 Image processing and pixel length calibration

Image processing uses digital pictures to identify and measure the length and breadth of fractures in beam specimens. Shadows on the specimen surface and overexposure of the picture both require preprocessing. Areas of an image that have been overexposed have extremely bright light in comparison to the rest of the image. It might be challenging to spot crack propagation across overexposed areas in a picture. Shadows that are present on the beam surface should be smoothed for fracture identification after processing for overexposure circumstances. Shadow softening is preferred over shadow removal because, if the shadow is totally removed by picture editing, the parts that lack a shadow will be overexposed.To forecast the fracture length and breadth inside the feature, a calibration factor is produced depending on the amount of pixels. Pixel measurements are multiplied by the calibration factor to yield unit measurement (mm or cm). An item with known length and area is present

inside a picture. picture segmentation is the process of converting an object picture into black and white pixels.

Edge Detection

To identify edges, the picture is converted from RGB to grayscale using rgb2gray. Edge detection techniques in MATLAB require a grayscale picture as input as shown in Fig 4.18. Prewitt edge detection technique is the best among other algorithms for detecting fracture edges and surface flaws, however it only detects a few edges with shading.MATLAB creates black and white pixels as a zero-one matrix. The length and area may then be calculated by adding rows or columns and matrix members.

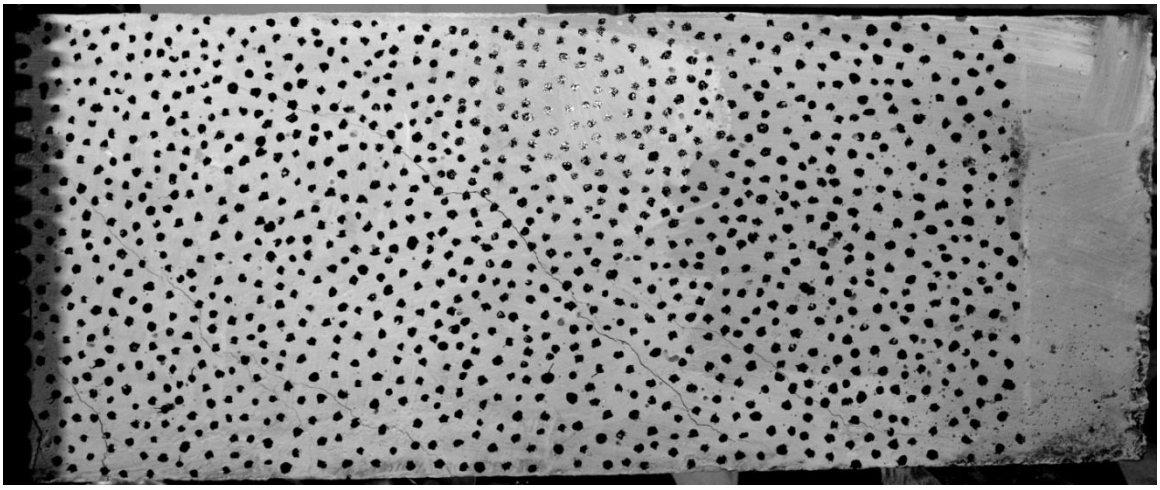

Fig 4.18Input gray scale image

Image segmentation

Image segmentation is the technique of isolating fractures and surface flaws from an image. software is designed based on two points: 1) alignment angle and 2) major-minor axes length ratio are used to separate objects in a picture based on length, breadth, area, and perimeter. The regionprops function in MATLAB is used to assess these two locations. Because many fractures are inclined, the orientation angle is selected as one of the criteria using a MATLAB script that determines the angle between the x-axis and the primary axis of the ellipse. Another script for picture segmentation is based on the main axis length to minor axis length ratio. Cracks will have a substantially longer major axis (length) than a minor axis (width), resulting in a ratio larger than one.

Morphological operations

After edge detection is complete, the picture is altered for image segmentation and measurement. The Morphology tool is used to extract picture components. Morphological techniques are used to remove picture flaws. This technique is carried out using a small matrix known as a structuring element. MATLAB provides access to different morphological procedures that may be used to achieve the following tasks:

1. Bridge: converts black pixels to white when there are two adjacent white pixels.
2. close: based on a matrix of zeros and ones, converts dark pixels to white.
3. Bwareaopen: This procedure eliminates related objects from a black-and-white picture when certain pixels fall below a threshold value.
4. imfill: fills the area of an image using the region's pixel connectivity.
5. imclose: This process dilates the picture after it has been eroded. useful for keeping shape and size when filling in minor gaps in a picture.

4.7.3 Measurement of crack length and width:

Following segmentation, the *regionprops* in MATLAB programme measures the features of each crack. By counting the number of pixels filled by the crack, the *regionprops* function can be used to calculate the crack's area as shown in Fig 4.19. The *regionprops* function can be used to calculate the size of the sole crack, and the crack's area is then stored in an array for later usage. The resultant image contains cracks of unit width that are situated on the centerline of areas found after the image has been further processed using the morphological operator *skel* to remove the boundary pixels without breaking the item independently. By dividing the area of the crack by the length of the centre line, the width of the crack is determined along with crack Id's as given in table 4.4. The length of the centre line is measured using *imdistline* tool in tool box. The user can measure crack length by dragging and resizing the line on the image that connects two endpoints. The crack classification is categorised based on the crack width, a cumulative crack classification is givenin table 4.5.

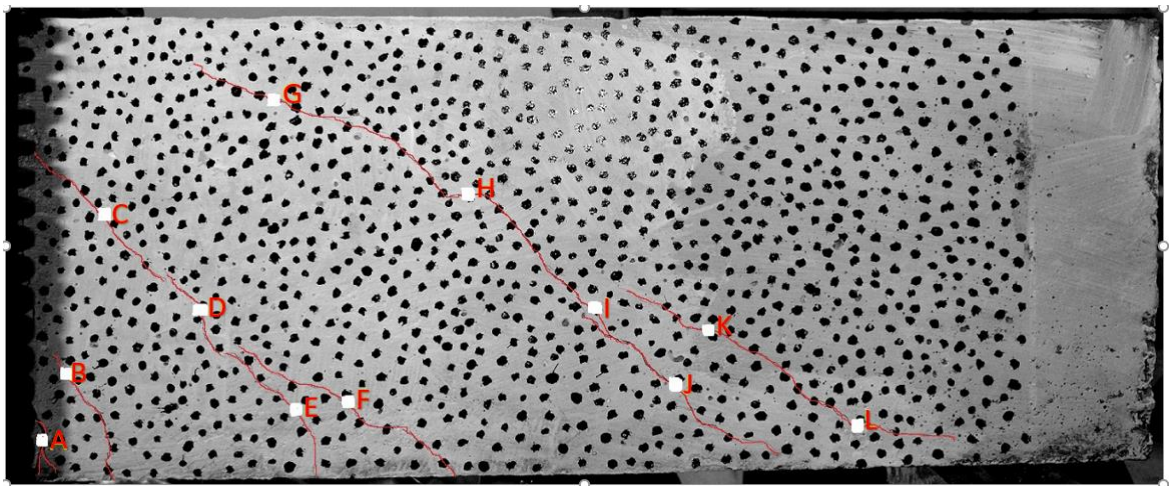

Fig 4.19crack identification and mapping for feature extraction with ID's

Table 4.4RCC Crack width data

Crack Id from Fig 4.19	Crack width measurement (mm)
	RCC
A	0.901
B	0.478
C	0.242

D	0.161
E	0.084
F	0.091
G	0.201
H	0.626
I	0.859
J	0.571
K	0.340
L	0.144

Table 4.5Length and area measurement of crack

Crack width(w) interval	Crack length (mm)	Crack area (mm2)
$0.010 \leq w \leq 0.100$	205	12.4
$0.100 \leq w \leq 0.500$	180	7.68
$0.500 \leq w \leq 1.00$	56	4
$w \geq 1.00$	8	1.2

4.8 UAVIC EVALUATION STUDIES ON IN-SERVICE BRIDGE

The most crucial RCC constructions in the transportation system for tying together difficult places are bridges. Due to its elevation, keeping an eye on the bridges for safety and traffic flow became a monumental undertaking. To investigate the nearby, fully operational RCC Bridge that is available, the suggested and tested UAVIC is deployed. Fig 4.20 shows the procedure for the UAVIC investigation on the bridge. The chosen structure is a 21-year-old Rail Over Bridge (ROB) with a length of 540 metres, a height of 7 metres, and heavy-duty cargo on it. Given that cracks only make up a very small fraction of the concrete's surface, digital images taken from the concrete specimen are used for automatic fracture detection and quantification.

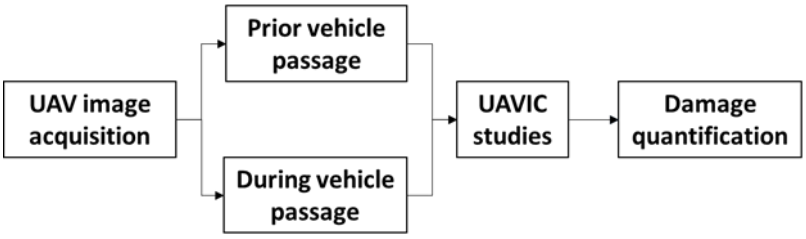

Fig 4.20 Flow chart of UAVIC study on ROB methodology

4.8.1 Bridge image acquisition

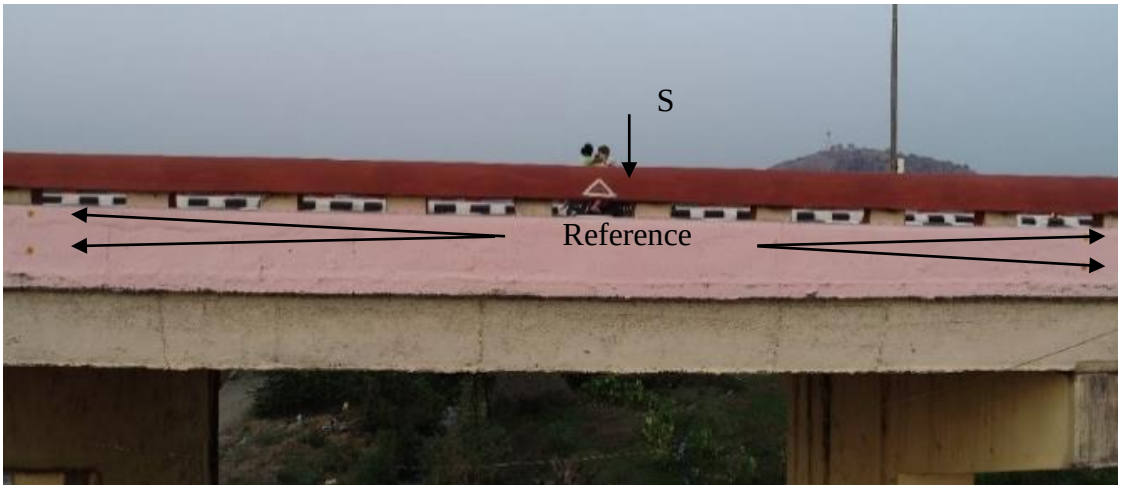

Fig 4.21UAV Images of before vehicle passage (reference image)

Fig 4.22 UAV Images of during vehicle passage (loaded image)

By flying a UAV on the centre span and away from railway power lines, digital photographs of ROB are captured. The bridge's deck span measures 7 metres in height and 11 metres from centre to centre of support. Images of the bridge are taken in bright sunshine during the day to acquire precise information. The surface of the bridge beam's irregularities and other particles served as a speckle pattern for DIC experiments. UAV images prior to vehicle passage facing at the centre of the bridge deck are obtained as illustrated in Fig 4.21. Similar to this, photos of various vehicle types and loading situations are taken at particular points during the passage as shown in Fig 4.22. A triangular scale at the center of the bridge deck is attached for reference length to perform DIC studies on the bridge. The irregularity and other dust particles on the surface of the bridge beam acted as a speckle pattern for conducting DIC studies.

Pre-Processing of UAV images:

The pre-processing is done for every UAV acquired bridge images prior to DIC processing. Homography transformation utilizes the specified fixed points on the bridge for applying ortho-rectification and assigning the projection to the images. The pre-processing is done in MATLAB inclusive image processing software.

4.8.2 UAVIC displacement investigations:

The suggested strategy is examined in the field under low wind conditions. The images are processed for deflection and deformation investigations of the bridge deck. The vehicle during the passage generates an impact load on the deck slab and acts a two-point load on it. Images of prior and during the vehicle loading are given to Ncorr V1.2 software and the above-mentioned processing is done for all the images with different loading conditions. The strains and displacements are recorded from the investigations and results are presented. According to Fig 4.23, image analysis of various vehicle loading circumstances is carried out using the DIC. Table 4.4 displays the examined displacement records.

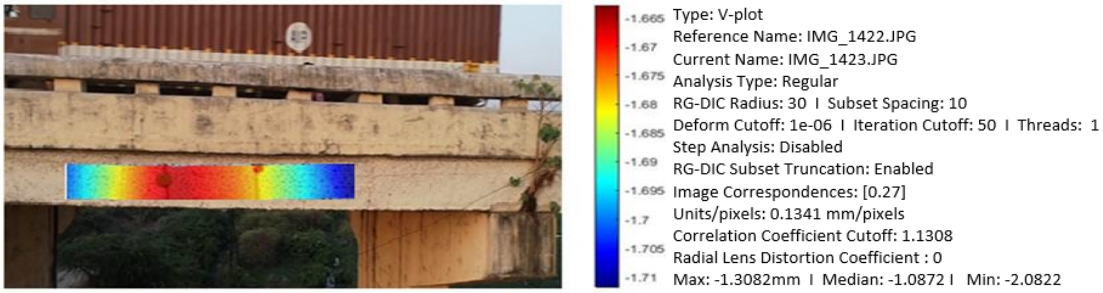

Fig 4.23 Displacement results output of vehicle-5 loading condition obtained from DIC analysis.

Table 4.6 Vehicle load type and displacement values from UAVIC

Vehicle passage	1	2	3	4	5	6	7
Deformation (mm)	2.82	1.47	3.22	3.18	1.30	2.63	0.89

4.8.3 Damage Quantification

By looking at the current structural state of the bridge's components, damage analysis of the beam was performed. By using the UAV, the entire stretch of the bridge is examined for flaws. Important details like the seams between columns and beams, the slab supporting the deck below, the edges of the slab, and the growth of organic matter are all scrutinised. The structural photographs of the damage are analysed for crack width and length studies, and the results are used to determine the extent of the damage. A few of the bridge's damaged sections are alphabetically displayed in Fig 4.24. A) Crack in the joint and damage of beam, B) Crack in the deck of the bridge, C) Damage and crack in the pier, D) Growth of organic matter on beam and E) Crack in the beam and slab joint.

A B C D E

Fig 4.24 Images showing the structural damage investigations done through UAV

4.8.4 Crack detection and parametric analysis on the ROB

The photographs of the bridge elements captured by the UAV are subjected to image analysis comparable to examinations into the properties of beam cracks. The UAVIC studies in the damage quantification put on a show with a few damaged parts. Table 4.5 lists the damaged areas in the designated alphabetical order after crack properties have been examined.

Table 4.7UAVIC captured bridge elements crack properties

Bridge component	Crack Width (mm)	Crack Length (mm)
A) Crack in the joint and damage of beam	1.82	583
B) Crack in the deck of the bridge	2.42	467
C) Damage and crack in the pier	0.96	328
E) Crack in the beam and slab joint	3.28	524

Chapter 5

PROJECT PROGRESS EVALUATION AND DIMENSIONAL ACCURACY ASSESSMENT USING UAV

5.1 Introduction

According to the study conducted based on the Scopus database by the Marta et al. 2021. Over the past ten years, there has been a trend in the volume of publications devoted to the use of UAVs in construction and urban planning. The first three years (2011 to 2014) were marked by low output, with a dearth of reviews and few articles in this field. However, the number of publications significantly increased starting in 2014, tripling from the prior years, and this growth trajectory persisted in the following years. A significant turning point in the advancement and application of UAVs in the fields of construction and urbanization occurred in 2018. In the year 2019 it saw a tremendous increase in interest and study in this field, as evidenced by the fact that the number of papers and reviews more than doubled when

compared to the average of the prior years. This expansion can be ascribed to the growing awareness of the potential and efficacy of UAVs in a range of architectural and urban planning applications. A steady trend in the quantity of publications may be seen from that point onward to the present following the notable growth in 2018. This shows that UAVs are now widely accepted as useful equipment in the field of architecture and urbanism. The continuing increase in publications over the past ten years highlights the UAVs' expanding significance as a transformational tool in construction and urban design. Advancements in design, construction, and sustainable urban development have resulted from their numerous uses, which have created new opportunities for data collecting, analysis, visualisation, and decision-making.

Long before the invention of drones, photogrammetry was utilised for topographic mapping, architecture, and engineering. But the emergence of affordable commercial drone hardware and software has coincided in recent years with the advent of computer vision-driven photogrammetry. The modern systems' automation and ease of use enable experts to incorporate these flying robots intocurrent methods to map vast areas of terrain and create 3D models with high quality. These facts suggest compared to traditional measuring,it is feasible to analyse the environment around us more rapidly and correctly, procedures include hand measurements and ground surveys. The surveys should have the capability of addressing the critical aspects of the construction industry such have obtaining accurate measurement through photogrammetry. Automation of the process by enabling the location based services and fixing the locations for obtaining the aerial imaging data. The processed aerial information enables an extended applications in much detail structural dimension monitoring.

As a part of structural performance, checking the dimensions of structural members should be same as the designed is mandatory. Engineers are not examining as the formwork used is designed for the same dimensions. However, upon consistent usage of same formwork it tends to deform of the prescribed shape and designed size. For eccentricity of loading, the dimensional accuracy of the structural elements is examined using the ortho-mosaic. The methodology of the visual progress evaluation and dimensional accuracy monitoring is given in Fig.15

5.2 Methodology of dimensional accuracy

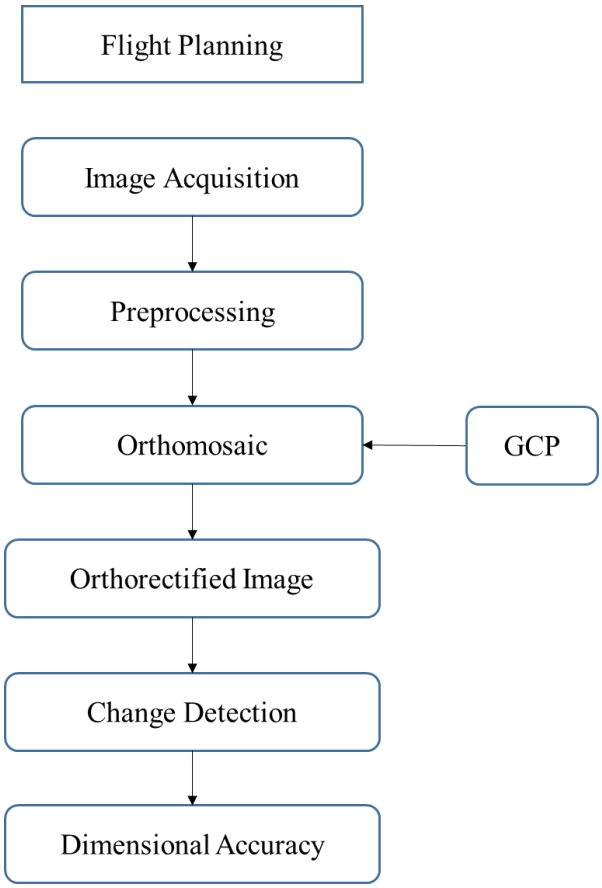

Fig 5.1UAV data processing methodology

There are various phases involved in creating an orthomosaic utilising UAV dataas shown in Fig 5.1. A high-resolution, georeferenced orthomosaicis created by stitching together many overlapping photos. The general steps to make an orthomosaic are as follows:

5.2.1 Flight Planning:

In order to efficiently and successfully gather data for a given goal, the flight route and other characteristics of the drone must be properly planned in UAV surveys. For precise and high-quality results, whether in aerial photography, mapping, or other applications, effective

flight planning is crucial. The major aspects followed while determining a project area is detailed below.

Survey Area

Establish the survey area in terms of coverage of the site and mapping the potential zones that need to be documented. The area selection should be having a buffer zone of 10m more than the required.This helps us in after survey results editing part and overlapping part for having good and legitimate matching points at the edges of the imaging.

Ground Sampling Distance (GSD):

Choose your preferred ground resolution, which describes the amount of information that is recorded in each pixel of the aerial images. The flying altitude of the UAV, camera characteristics, and sensor capabilities all affect ground resolution. In other words the less the flying height the more will be GSD and high flying height will have more coverage with less flying time. The GSD also depends on the power source capability to handle longer flying durations.

Overlap selection:

It is a crucial factor in the collecting of aerial data because it guarantees that there are enough characteristics shared by all of the photos, allowing for precise photogrammetric processing and the production of high-quality outputs.Plan for front overlap (along the path of flight) and side lap (perpendicular to the direction of flight) between succeeding photos. In order to accurately stitch data together and perform mapping, overlap makes sure that there are enough shared characteristics across pictures.The region of interest to ensure that there is

enough overlap between photographs (often between 70 and 80 percent in the front and between 60 and 70 percent in the sides).

Flying altitude:

Based on the survey's goals and needed ground resolution, choose the right flying height. Poorer altitudes give greater information but need longer flights and more data storage whereas higher altitudes cover wider regions but produce poorer ground resolution.

Flying plan:

Pick a flying plan that maximises information gathering and survey area coverage. Typical flying patterns include circular, lawn-mover, and grid patternsas shown in Fig 5.2. The geometry of the region and the intended data output will determine the pattern. The area selection should be able to cover a buffer region more than the required to have an overlapping region.

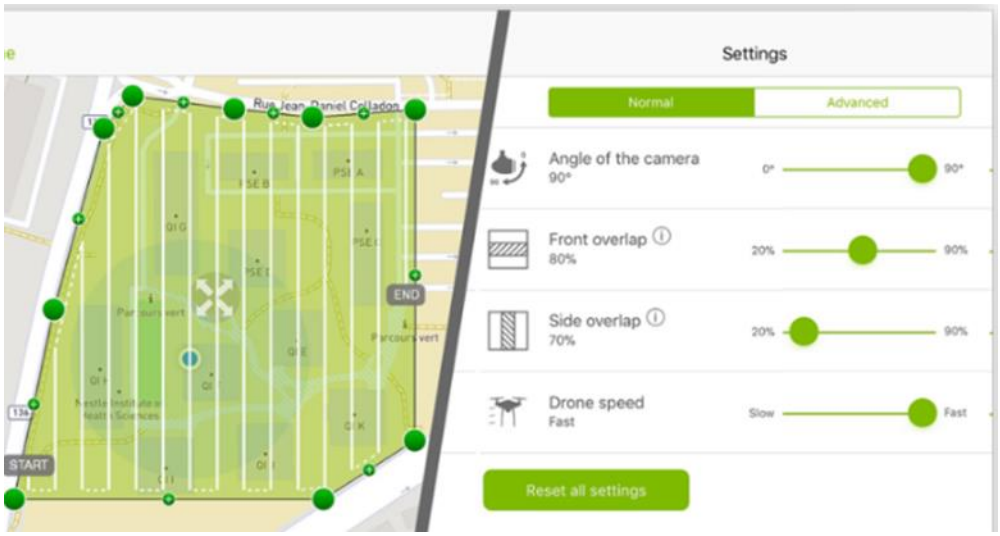

Fig 5.2 Flight planning with specified front and side overlap

Waypoints and Navigation:

UAVs with GPS, an IMU (Inertial Measurement Unit), and other sensors are able to navigate on their own. Waypoints are pre-determined GPS locations that serve as markers on the flight route during autonomous flying. The drone follows the pre-programmed itinerary as it navigates from one waypoint to the next. The limits of the survey region and any particular sites of interest will be included in the waypoints, which will also determine the fly path.

Safety precautions.

The following are the major safety checklist to be followed while data collection for any UAV survey mission.

- Checking the battery health and flight time to cover the selected area and return back to the starting point. Planning a flight plan with reserve battery of at least 30% is advisable.
- Fixing the Return-to-Home (RTH) location point through the console to automatically brings the drone back to its takeoff point if the battery is low, communication is lost, or the operator triggers the command.
- Prioritize flight safety by identifying and maintaining a safe distance from potential hazards, obstacles, or no-fly zones in the survey area.
- Data management for storing the collected images. UAV surveys produce a large quantity of data, so be sure you have enough storage space and a trustworthy way for transferring the data for post-processing.

By carefully taking into account these elements during flight planning, the UAV survey to predefined objectivesand obtain precise and useful data for additional analysis and decision-making. Considering the mentioned conditions the flight planning is designed as detailed in table 5.1 for conducting the study.

Table 5.1Flight-planning parameters of study

UAV flight planning elements	Selected range
Area coverage	0.37 Ha
Ground sampling distance	1.5mm
UAV altitude	12m
End lap	80%
Side lap	70%
Number of strips	13
Number of images	157

5.2.2 Image data acquisition

With the above mentioned preloaded information the UAV hovers through the designated waypoints paths over the entire work site as specified in the image acquisition software. A flight plan is created in such a way that all construction-related operations fit under the category of imagination. The images are acquired at regular intervals of flight path with the associated information of the coordinates, image distortions, orientation errors and image angle. The UAV used in acquiring the data is DJI phantom 4 pro and the technical specifications are given in table 5.2. The UAV collected images are shown in Fig 5.3.

Table 5.2Technical specifications of the UAV (DJI Phantom 4 pro)

Specification	Ranges
Horizontal positioning accuracy (σH_{drone})	1.0 cm + 1 ppm (RMS)
Vertical positioning accuracy (σV_{drone})	1.5 cm + 1 ppm (RMS)
Resolution	20 MP
Image Size	5472×3648
Field of View	84°
Focal Length	8.8 mm
Pixel Size	$2.4\mu m$

GSD @ 10.00 m	≈1.3mm

Fig 5.3Drone image of construction site during foundation and plinth beam stages

5.2.3 Processing of images:

Transfer the UAV's acquired photographs to a computer so they may be processed.To increase image quality and accuracy, correct for lens distortions and sensor flaws.Process the photos and create the orthomosaic using wide range of photogrammetry software available as discussed in table 2.1. In this study, the Pix4D software is used for image processing and orthomosaic preparation. The image processing in desktop consists of three steps, they are:

- Initial processing
- Point cloud and mesh
- DSM, Orthomosaic and index

The collected images are uploaded in to the Pix4Dmapper and the initial processing is carried out. During initial processing the key points in the images are calculated and the matching of key points takes place.According to the compatibility of the data and hardware, picture processing takes time. The methods for cloud processing are also accessible by

uploading the photographs to the cloud. The processing time is reduced, and the product may be downloaded quickly.

Mosaic preparation

An image mosaic is a composite image made up of smaller individual images. The photos will be automatically aligned using shared characteristics, and tie points will be created to match the overlapped regions.The photos will then be seamlessly stitched together to produce an orthomosaic. An orthomosaic map is a distortion-free depiction of a geographic region that may be used to calculate exact distances between points. A good overlapping region provides a better mosaic results that can be utilized in many other ways.

Bundle Block Adjustment

The BBA is a key method in photogrammetry and remote sensing that tries to concurrently adjust the orientation parameters (position and orientation) of numerous overlapping photos in a block (set). The purpose of bundle block adjustment is to obtain precise spatial alignment of the whole picture block.In the overlapping photos, find and match similar characteristics (tie points). These tie points serve as control points for linking the various pictures in the block. Begin by estimating the exterior orientation parameters (EOP) for each picture in the block. The EOP contains the camera's location (X, Y, Z) as well as its orientation (omega, kappa, phi). To refine the initial EOP estimations, use an iterative optimisation technique. The goal of the optimisation is to minimise the disparities between the observed tie points and their anticipated positions on the pictures using the present EOP estimations. The optimisation method is called as bundle adjustment because it modifies the EOP for all pictures in the block at the same time, taking into account their mutual connections via the tie points.

5.2.4 Georeferencing:

The programme precisely positions the orthomosaic on the surface of the Earth by using the GPS coordinates and flight altitude of each image.Georeferencing accuracy can also be increasedby using GCPs. These GCPs are physical markers set on the ground at established locations.The GCP's primary purpose is to assist you in precisely positioning the map in relation to the surroundings and aligning it with it. Depending on the terrain and size of the location, four to ten more people are required to accurately generate an aerial map. A survey and marking of GCPs are done before of the flight. Paint, a checkered square, or any other type of marking is used to designate points on the surface. But make sure the mark stands out from its surroundings and is large enough to be seen in the drone's pictures. Data collection may begin once all GCPs have been identified and tagged, and the drone's flight path is prepared.

10 control points are selected in the study area, out of which 6 points are located on the ground, 3 points are taken by placing the GCP markers on the ground using a painted disk as shown in Fig 5.4. These GCPs are surveyed using a total station and the coordinates are recorded. GCP markers improves the accuracy of the orthomosaic to millimetre level for measuring the structural dimensions.The model's scaling must be done correctly in order to produce an accurate scaled ortho rectified image.

Fig 5.4GCP marker placed on the ground for georeferencing

Editing and quality assurance:

Examine the orthomosaic to look for any mistakes or stitching-related artefacts that could have happened.If required, manually modify the orthomosaic to fix any problems. The automatic flight-planning project featured a differential X-axis of 0.000 metres and a Y-axis of 0.007 metres drift in the UAV.

5.2.5 Ortho-rectified image:

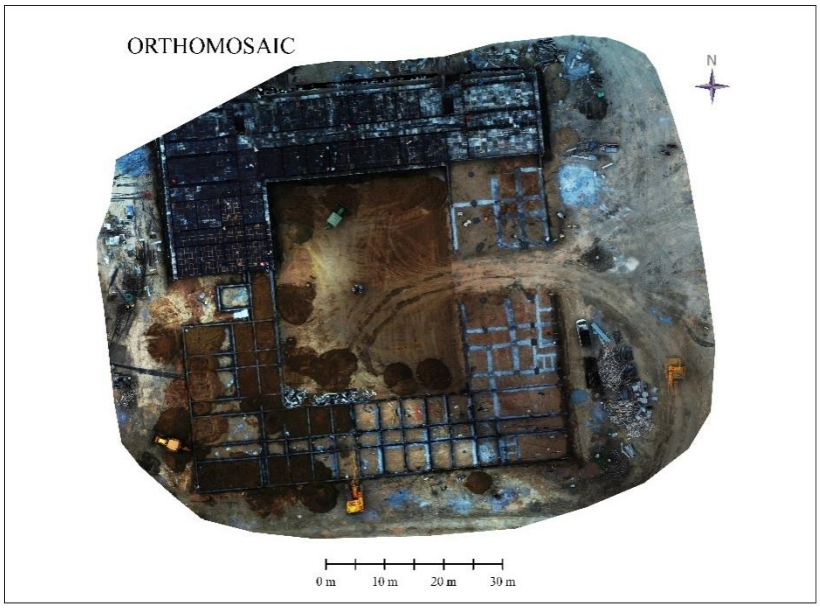

Fig 5.5 Orthomosaic of construction site

After initial processing, such as picture alignment, point cloud generation, and model scaling Fig 5.5 displays the ortho-mosaic created from raw UAV photos. The ortho image is examined for updating newly built elements using change detection algorithm on the previously generated ortho rectified image of the site. The newly built structural components are subjected to a test for dimensional accuracy.

5.2.6 Dimensional accuracy assessment:

For the purpose of evaluating the dimensional accuracy, ortho-mosaic generated by the photos with a 1.5 mm spatial resolution from UAVs are employed. When measurements taken from the ortho-mosaic were compared to real site plans, variations as indicated in Fig 5.6.The staircase beam dimension in the cad drawing differs by 2 mm, and that the diagonal dimension in Fig 5.7 differs by 7 mm when compared to the ortho-mosaic dimensions. Due to the great accuracy that is maintained, UAVs might be useful in monitoring the structural design throughout construction to reduce dimensional inaccuracies.

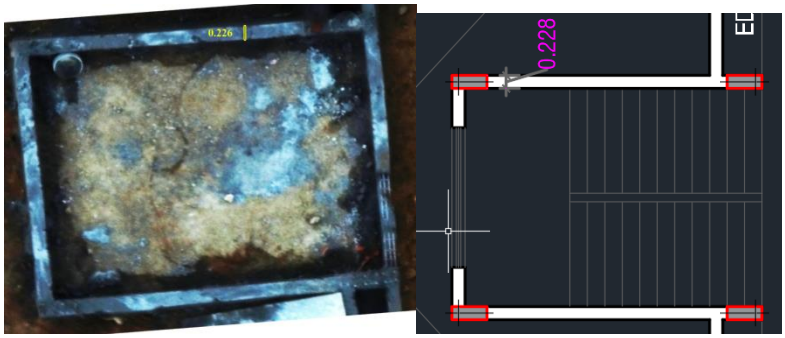

Fig 5.6 Dimensional deviation of beam width

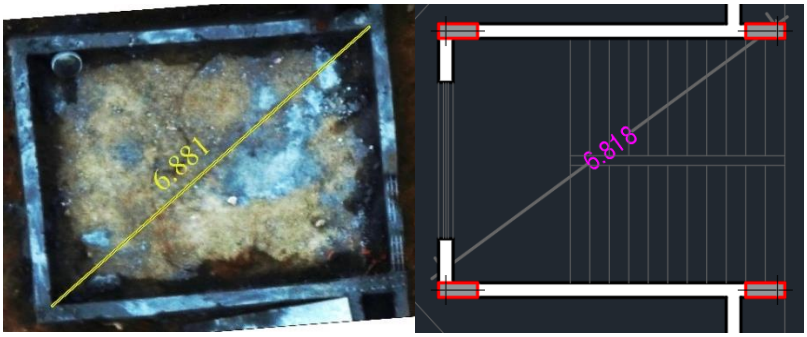

Fig 5.7Dimensional deviation of diagonal length

Chapter 6

Monitoring hydration of concrete using NIR imaging

The quality of concrete components is mostly a result of the curing process. Concrete needs to be treatedfor hydration in order to achieve strength and be durable. Professional curing focuses on the chemical reactions that take place during the hydration, which is connected to the concrete's strength. At this point, a proper hydration is crucial in order to have enough moisture on hand to produce the desired concrete strength. A concrete surface with an inadequate moisture range experiences a drying process linked to the formation of capillary pores, which leads to an imperfect hydration and decreased strength and also results in shrinkage cracks.

6.1 NIR imaging:

Concrete requires curing, which must be regularly monitored throughout the duration of the project. Under construction-related circumstances, it might be difficult to verify or keep track of the proper curing of concrete components. There is a need for procedures that are simple to use, widespread, reproducible, and allow for unambiguous statements. NIR imaging is a promising technique that has already been incorporated into a number of evaluation procedures. It has already been applied to a number of other imaging applications with great success where water plays a significant role. The majority of applications for near-infrared sensors are in the fields of agriculture and water resources. Similarly as moisture is the primary component present on the concrete components, the same principles are utilized to monitor the curing requirements of the construction site.

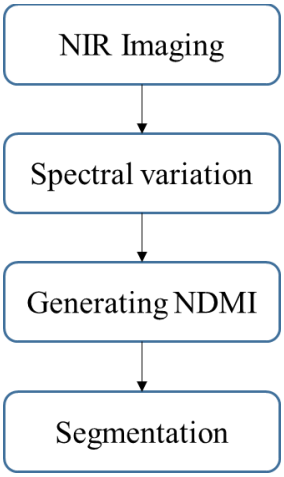

Fig 6.1Curing monitoring methodology

6.1.1 Principle

Curing monitoring using Near-Infrared (NIR) imaging is a non-destructive and non-contact technique used to assess the curing process of materials. Chemical reactions take place during the curing process of some materials, changing their molecular structure as a result. The material's capacity to absorb and reflect light, particularly in the near-infrared region, may be impacted by these modifications.IR imaging gives useful information about

the material's curing status.As per the methodology given in Fig 6.1 the newly constructed superstructure, elements are imaged to determine the moisture index, which aids in identifying the need to remedy any deficiencies in curing. NIR pictures generally encompass the wavelength range of 700 to 1,400 nanometers (nm).

6.1.2 Image acquisition

A light source that emits near-infrared light and a camera with an NIR-sensitive sensor make up a standard NIR imaging system. The curing substance reflects or transmits NIR light, which the camera records.NIR images are taken during the hydration process at pre-determined intervals such as for every two hours. As the curing advances, the external texture of the material in the NIR images transforms. The variation in the moisture content can be easily ascertained by the images as shown in Fig 6.2.

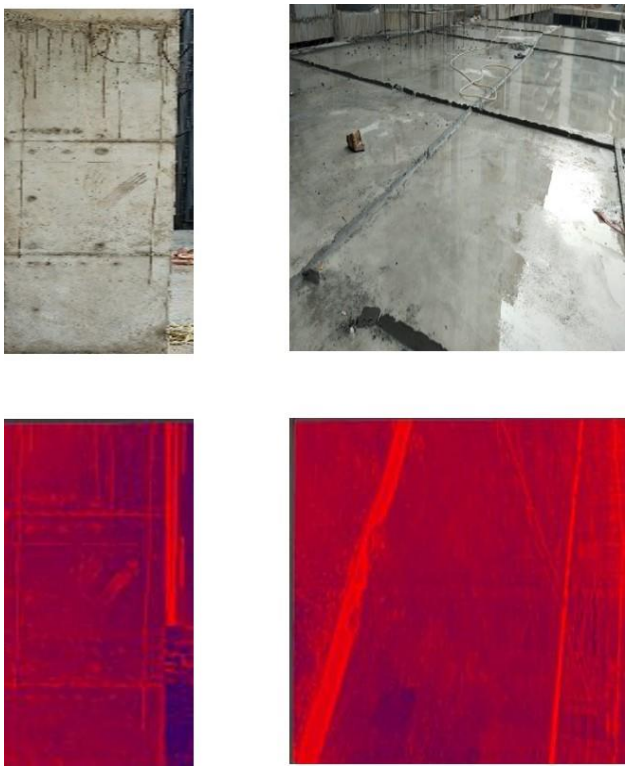

Fig 6.2 Optical and NIR image of column and slab

Spectral variation

To achieve the study's goal, the aquaphotomics approach was used, which is a method of studying water by focusing on its interaction with electromagnetic radiation (EMR). The main goal of this new approach is to better understand water's integrative role in aqueous systems by observing how the water spectrum changes in response to various perturbations. The near infrared (NIR) wavelength region of the EMS, specifically the first overtone of the OH stretching vibrations (1300 - 1600 nm), has been shown to be an excellent window for observation of the water molecular structure, as well as a non-destructive measurement method.Unlike traditional NIR spectroscopy studies, in which the water absorption band is thought to be masking the true information, aquaphotomics views the water spectral pattern as the primary source of information, acting as a sensor or mirror of what is going on in the samples under study. This method of indirect measurement is known as the "water mirror approach." The similar concept is used in analysing the concrete moisture indexing studies. To evaluate the study the thermal imager is set to an emissivity is given as 0.95 an average value of concrete and water i.e., 0.93 and 0.96. The images acquired through thermal imager is analysed through the image processing module as given in the subsequent section.

6.2 Image analysis

NIR imaging sensor offers variation of reflectance throughout a specific wavelength range in the EMS. The obtained NIR pictures are analysed to get crucial curing state information. This may be accomplished through the use of different image processing and data analysis tools.Slab and Column are two distinct factors that are chosen to analyses the curing index. Based on the spectral variance of the NIR bands, the images are displayed. Above displayed image in Fig.6 is a comparison of the visual band image and the NIR image taken before and after the curing process. The NIR images along with visible is obtained to calculate Normalized Difference Moisture Index (NDMI).

$$NDMI = (NIR - RED) / (NIR + RED) \quad \text{eqn.9}$$

The generated image's pixels each contained reflectance data with wavelengths ranging from roughly 800-1300 nm. The spectral signature, which is a continuous representation of the reflectance intensity in the measured wavelength range, was processed individually for each pixel in the image processing software. Image classification is performed on the acquired NDMI calculated image and the color-coding classified map is generated at the end of every curing monitoring survey.

6.3 RESULTS:

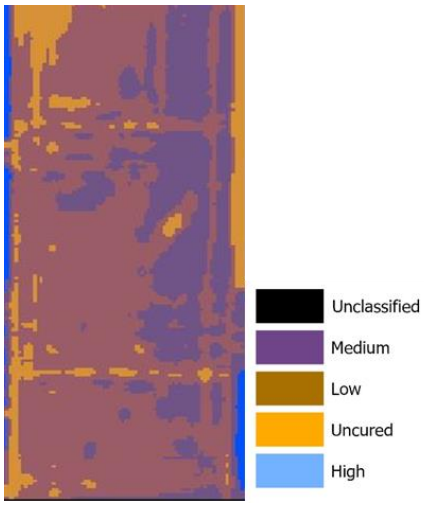

Fig 6.3Column showing the classified curing zones

The acquired NIR image was processed in the image processing software to reveal the partly curing zones of the column. The image is classified based on the curing intensity with NDMI values ranging from 0-1. The value to near to one is categorized as area having more moisture and the value to near to zero is having low moisture content. Based on the nearest neighborhood classification the zones are classified as high, medium, low and uncured as shown in Fig 6.3. Similar to the column image processing the slab is also processed for curing monitoring and the results are put on to the shown in Fig 6.4.

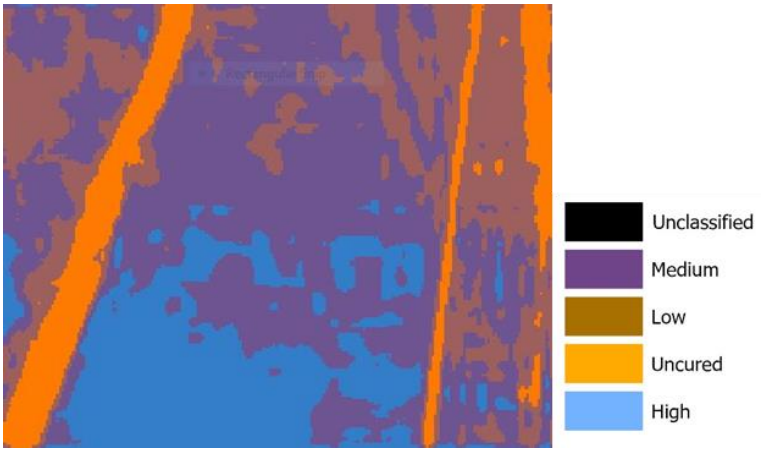

Fig 6.4 Slab showing the classified curing zones

Area of hydration calculation

usclassification1.img

Row	Histogram	Color	
0	0		Unclassified
1	4685		Medium
2	2469		High
3	8466		Low
4	1705		Uncured

usclassification.img

Row	Histogram	Color	
0	0		Unclassified
1	16179		Medium
2	9543		Low
3	3961		Uncured
4	7664		High

A B

Fig 6.5Image classification with hydration level A) column B) slab

The analysed images are given in a tabular format based on the segmented spectral variations and the hydration levelaccordingly. The image of column is acquired from 2m away as the width of the column is known the no of pixels is consisting in the width is measured. The pixel dimension of column from the image analysis is measured as 1.04mm similarly slab is measured as 1.31mm. The slab area is measured as 48.9 square meter and column area is measures as 1.8 square meter. The hydration in the image is divided into 4 zones like highly hydrated, medium, low and uncured as given in Fig 6.5. Similarly the

number of pixels are also classified based on the hydration and the area is also calculated as given in table 6.1.

Table 6.1 Classified area based on hydration

Classification	Column		Slab	
	Pixels	Area	Pixels	Area
High	2469	2567.8	7664	10039.8
Medium	4685	4872.4	16179	21194.5
Low	8466	8804.6	9543	12501.3
Uncured	1705	1773.2	3961	5188.9

Chapter 7

EARLY AGE CONCRETE STRENGTH USING THERMOGRAPHY

7.1 General

Concrete is the most complex and common construction material used in infrastructural development. Due to its complexity evaluation and quantification of its mechanical properties like strength at early hours is required to increase the efficiency of construction. Concrete is easy to mouldduring the early phases and hard to destroy and dissipate after getting hardned. Cement being a crucial raw material in concrete mix designs, the C3A undergoes chemical reaction when comes in contact with water (H2O) (Jiahui P et al. 2006). The ettringite formation in the concrete mix is responsible for high heat of hydration in

the concrete (Wang XY et al. 2017). Concrete core temperature in mass concreting works is high at the initial stages of hardening process that results in evaporating the available capillary water and inducing the volumetric deformations in the specimen (Maruyama I et al. 2014). There are various numerical methods such as CMM are available for predicting the heat of hydration and preparing the remedial measure by inducing the cooling tubes in mass concreting works (Liu D et al. 2021). The hydro-chemical reaction of cement liberates temperature during the hydration process, which instinctively denotes the strength maturity of concrete. Recognizing that the concrete exothermic reaction is directly proportional to the strength attainment of concrete.

The CMM is a well-established Non-Destructive technique for estimating strength by recording the temperature liberated from cement's hydro-chemical reaction in concrete. The hydro-chemical reaction of cement liberates temperature with respective to the volume during the hydration process of concrete. The novelty of this study is investigating the thermal emission using thermography as a substitute of thermocouple for evaluating CMM. As temperature is major parameter in evaluating the CMM it can also be investigated with IRT concepts by recording the surface temperature of the specimen. A RSNDT method is developed to estimate the strength of concrete by investigating the exothermal emissions at early ages of concreting.

7.1.1 CMM Principle

CMM works on the principal that the temperature exerted during hydro-chemical reaction of concrete is directly proportional to the strength gain of concrete. To investigate the temperature history of concrete at periodic intervals thermocouples embedded with a data acquisition platform are inserted inside at core point of concrete specimen, as temperature liberated will be high at that core point. The setup cannot be removed after the experiment as the sensors are placed inside the concrete and casted, it makes sensors unfit for reuse

CMM evaluation procedure:

Determining the on-site strength attainment of concrete involves evaluating the on-site maturity, which is a critical parameter used to assess the strength development of the concrete over time. The technique entails putting temperature sensors in fresh concrete as soon as feasible after it has been placed.Thesensors are linked to maturity instruments or temperature recording devices, which are turned on as soon as possible after concrete laying. When a strength estimate is required, the maturity index from the temperature record is read. The compressive strengths at the thermocouple positions are computed employing the maturity computing methods and the earlier developed strength maturity relationship. The detailed process is described below:

Placement of Temperature Sensors: Temperature sensors (thermocouples) are installed at important spots in the concrete structure immediately after concrete laying as shown in Fig 7.1. These essential areas are determined by exposure circumstances as well as structural needs. The sensors should be strategically placed to correctly capture the temperature profile of the concrete during the curing process (Gorriz *et al.* 2017, Root *et al.* 2020).

Fig 7.1 Thermocouple embedded concrete cube along with temperature displays

Data Collection: Throughout the curing time, the temperature sensors continuously record the temperature of the concrete at precise points as shown in Fig. Data collection normally begins shortly after concrete placement and continues until the target period for strength estimation is achieved.

Calibration of Maturity: The temperature data collected by the sensors is then utilised to calculate the concrete's maturity over time. Maturity is related to strength gain and is a result of the temperature-time history encountered by the concrete during curing.

Estimation of strength: Maturity values are associated with compressive strength data acquired from laboratory tests. A calibration curve or link between concrete strength and maturity is established. This calibration is unique to the project's concrete mix.

Estimation of In-Place Strength: The in-place compressive strength of the concrete can be determined at any moment using the calibration curve and the maturity data collected in the field. This knowledge is invaluable for critical construction operations that rely on obtaining certain concrete strength levels.

7.2 Thermography:

Due to the advancements in sophisticated in remote sensing imaging sensors in the field of a thermal region of the EMS led to investigations of many new applications. These sensorsare very sensitive and well calibrated in such a way that to perceive temperature variations of 0.1˚c. These sophisticated imaging sensors can measure the thermal emissivity of concrete. As per the given literature, the usage of remote sensing sensors coupled with computer vision techniques has delivered superior results in various applications. The capture of images by thermal imaging sensors for the purpose of determining the temperature of a concrete sample by processing and analysing the picture is referred to as thermography.The main benefit of thermography is observations are made without in contact, rapid, without causing any damage, easy to handle than the conventional thermocouples.

7.2.1 Emissivity:

The capacity of a substance to emit heat radiation is described by the fundamental notion of emissivity in physics and thermodynamics. The ratio of a material's radiant energy to the radiant energy emitted by a blackbody (a perfect emitter) at the same temperature is represented by this dimensionless number, which ranges from 0 to 1.A material's emissivity is determined by its surface characteristics, temperature, and spectrum of radiation. At the same a material with a high emissivity radiates more thermal radiation than a blackbody, whereas a material with a relatively low emissivity emits reduced radiation. The emissivity value varies depending on the angle of incidence and polarisation of the light.Emissivity is a significant characteristic in thermography and thermal imaging that is used to transform recorded temperatures to real surface temperatures. Because various materials have varied emissivity values, correct emissivity information is required for exact temperature readings.The emissivity of concrete is preset at 0.93 in most thermal imaging camerasas shown in Fig.

Thermal imager

Fig 7.2 Thermal Imager

Thermal imagers are specialized device that captures and visualizes infrared radiation emitted by objects and surfaces, unless it is a blackbody. Thermal imagers are not high-resolution cameras; the resolution of camera shown in Fig is 520*640 pixels. Each pixel in a

thermal image functions as a temperature node and can represent different temperatures within an image.They can detect and show the distribution of heat or temperature fluctuations in a scene, giving useful information in a variety of applications. The high end thermal imager as shown in Fig 7.2 are embedded with optical camera to obtain the visible spectrum image to understand the location of the thermal image obtained.

7.3 Methodology to evaluate CMM using thermography

To carry out this research, a lab calibration setup is created in order to carry out the experiment and record the results. Fig 7.3 demonstrates the methodology followed to investigate the laboratory thermography tests.

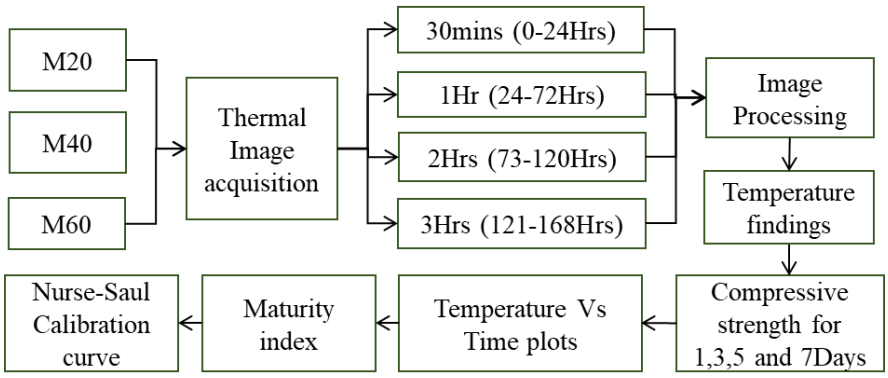

Fig 7.3 Flow chart for laboratory performed thermography tests

7.3.1 Concrete cube casting.

To conduct the study three different mix designs i.e., M20, M40 and M60 are adopted. These were the predominant mix designs used in most of the residential and commercial buildings. Nominal mix proportions as given in Table 7.1 are taken for casting the 15*15cms cubes. 20 cubes for each mix design is casted for conducting the study. Out of 20 cubes, 3 cubes are kept for acquiring the thermal images, 3 cubes for each compressive strength

evaluation at 1, 3, 5, 7 and 28 days are crushed and 3 cubes are kept preserved for validation of calibration curve as shown in Fig 7.4.

Fig 7.4 M20 concrete grade cubes casted for study

Table 7.1concrete mix proportions

Mix Design	Coarse aggregate (kg/m^3)	Fine aggregate (kg/m^3)	Cement(kg/m^3)	W/C (kg/m^3)
M20	1105	740	375	186 (0.49)
M40	1040	646	473	180 (0.38)
M60	10mm- 510 20mm- 750	620	500	166 (0.24)

7.3.2 Thermal Image Acquisition.

To conduct thermography studies Infrared imaging camera is employed. Infrared imaging camera is an active sensor, which is able to image the radiated energy from a body. To perform the experiment TESTO thermal imager is selected for imaging the specimens. To limit the external climatic influence on the concrete specimens for acquiring the thermal images, the specimens are cured in polypropylene box. It restrict the interaction with laboratory conditions for obtaining the thermal images as shown in Fig 7.5. The specimens are left for hydration in water filled polypropylene box with top 10mm left for imaging.The

images are acquired by placing the thermal camera 1 meter away from the area of interest. The lid of the box is closed after every image acquisition procedure is followed.

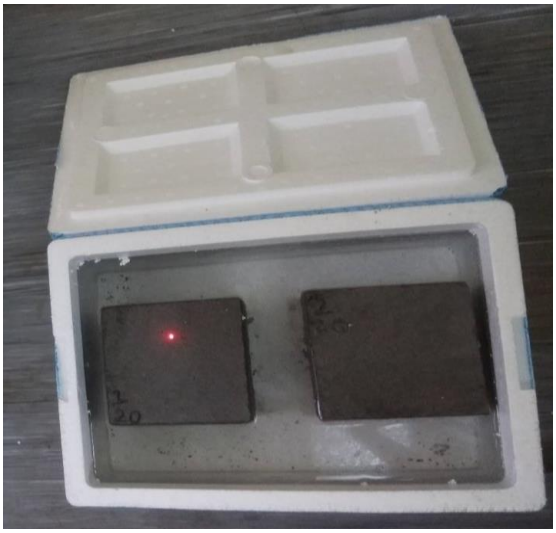

Fig 7.5 Concrete specimens for curing inside a polypropylene box.

Images are acquired only for the first one week (170Hrs) of concreting, as the thermal emissions are high in that phase. Based on the thermal emission in literature survey, it is decided to record the thermal images in time intervals. Due to the rapid hydration process in the first few hours, the imaging time interval is taken is 15mins for 0-24Hrs. Subsequently, the imaging time interval is increased to 30mins (25-72Hrs), 60mins (73-120Hrs), 90(121-170Hrs). With the selected time intervals 2496 thermal images are obtained i.e., 832 images per each mix design. The surface temperature investigations of the concrete specimen are recorded as per the time intervals detailed in table 7.2. The acquired thermal images are analyzed in thermal image processing software for measuring the exact temperature on the surface of the specimen.

Table 7.2No of images obtained per each grade for particular time intervals

S.No	Grade of concrete imaged	Time interval	Time span in Hours	No of images obtained
1	M20, M40 & M60	30mins	0-24	432
2	M20, M40 & M60	60mins	25-72	432
3	M20, M40 & M60	120mins	73-120	216

4	M20, M40 & M60	180mins	121-168	144

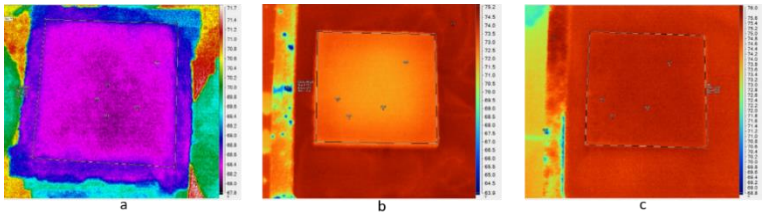

Fig 7.6 M20 Thermal images a) Low temperature b) Medium temperature c) High temperature

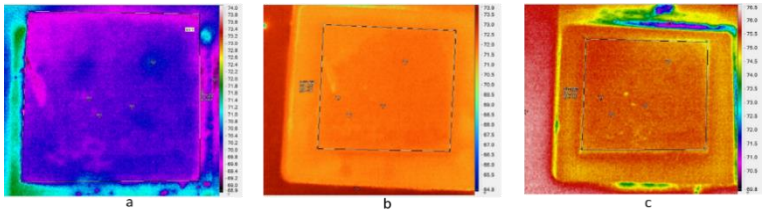

Fig 7.7M40 Thermal images a) Low-temperature b) Medium temperature c) High temperature

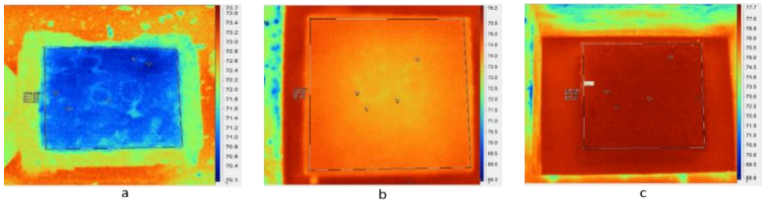

Fig 7.8 M60 Thermal images a) Low-temperature b) Medium temperature c) High temperature

Fig 7.6shows the thermal images of M20 concrete grade the figure has high, medium and low-temperature images. Similarly, Fig 7.7 and Fig 7.8 are also having thermal images of M40 and M60 mix designs at different time periods.

7.3.3 Thermal image processing

The thermal images are processed in proprietary processing software, each supplier have their own file extensions and processing versions. The image processing software's are capable of processing large imaging data sets. Each image is fed into the processing

programme, which is then used to calculate the heat emissions from the concrete cube. As shown in the Fig 7.9, the image processing interface has several information pallets such as thermal image, thermal image markers, temperature scale, normal real image, histogram, and temperature profile. Each pallet has its own relevance in processing and visualising image data. The temperature profile and information of only concrete cube area is required for analysis, to specify that particular portion a rectangular box is drawn over the cubein the image. The average temperature of the cube area is given in histogram pallet denoting maximum, minimum and average temperatures. The pre-defined temperature markers such as high (HS1), low (CSI) and at the center of the image (M1) is set on the image as seen in the thermal image markers pallet.

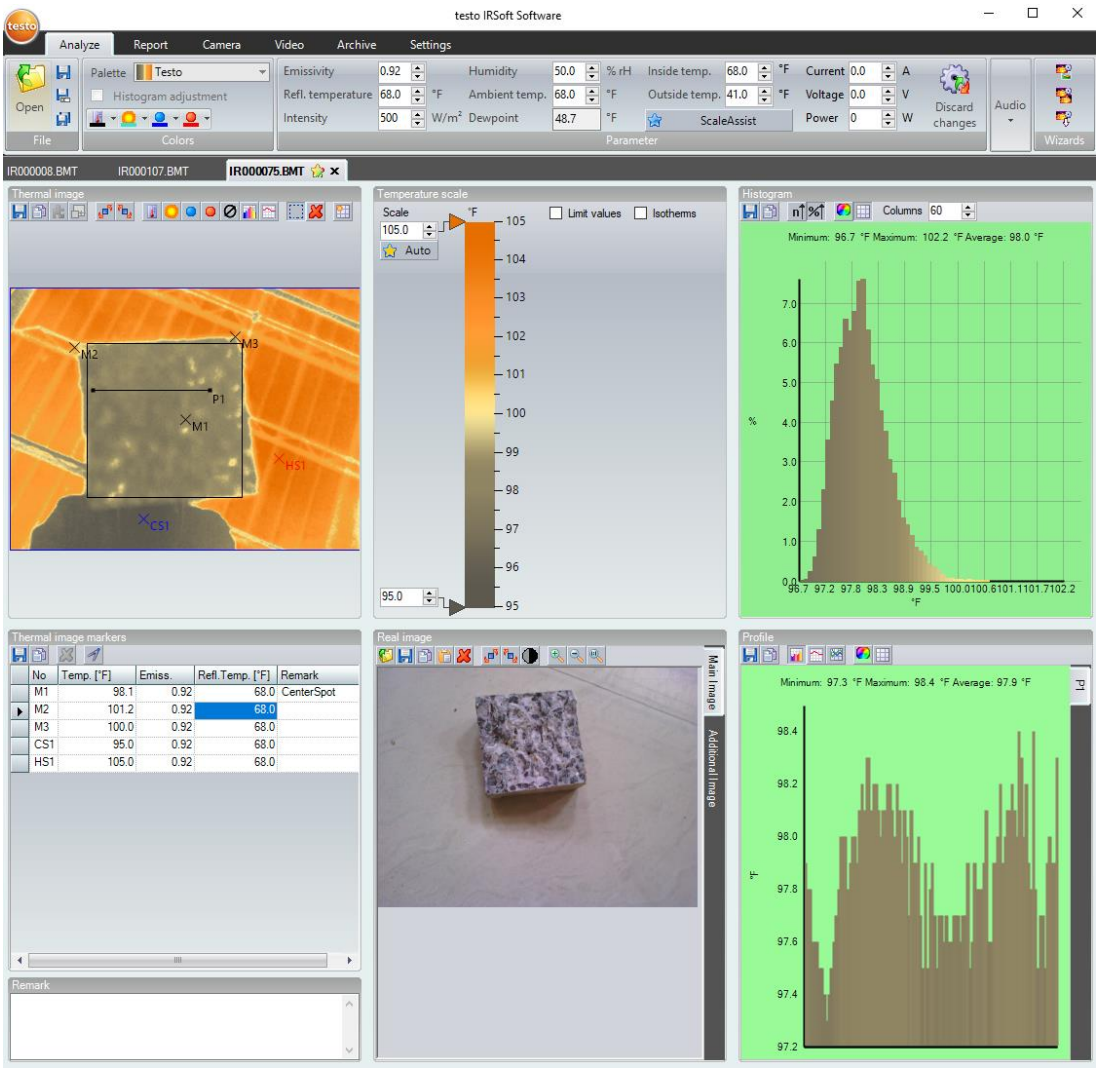

Fig 7.9 Thermal image processing software interface

The external climatic parameters influence the surface temperature of the concrete as in cold climate it tends to decrease the temperature and similarly the temperature increases in the hot climatic region.The climatic parameters like humidity, ambient temperature and dew point in the laboratory conditions also need to be specified in the software. While acquiring the image these climatic parameters need to be obtained with well calibrated thermometer and hygrometer. The measured values need to be given to the software during image processing. All the 1224 thermal images are processed manually and the thermal emissions of concrete cubes are tabulated based on the concrete grades.

7.3.4 Time over temperature plots

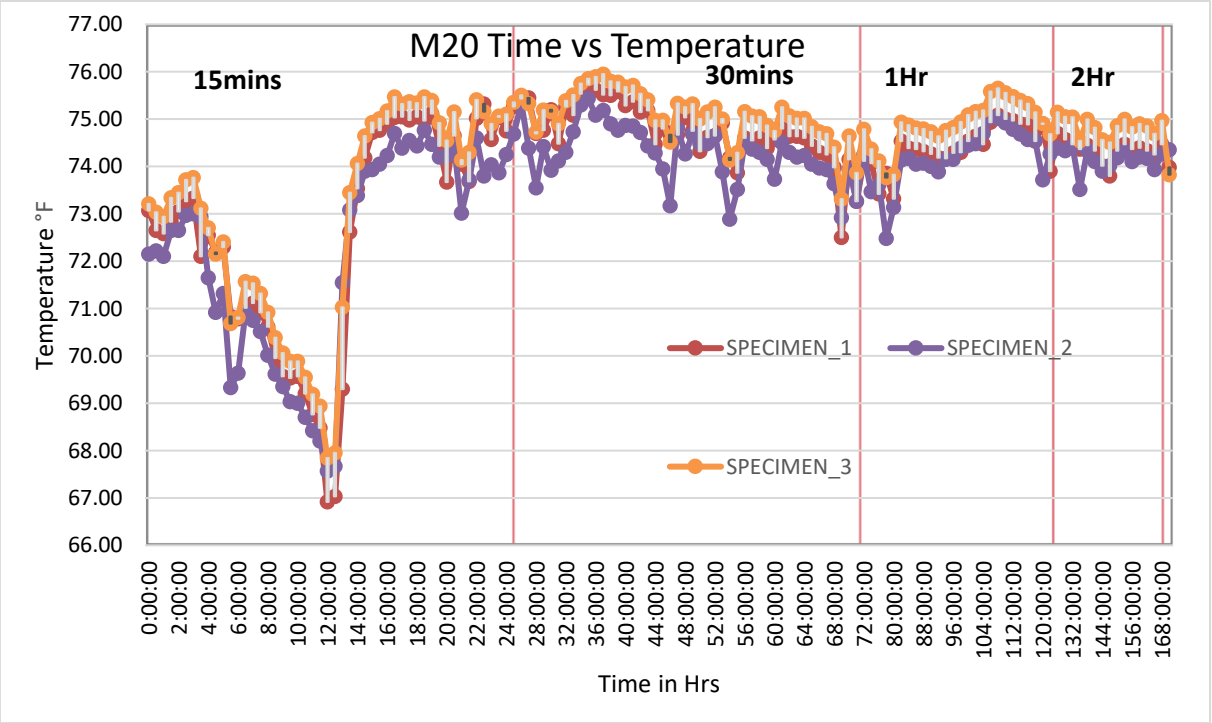

Fig 7.10 Time vs Temperature Plot for M20

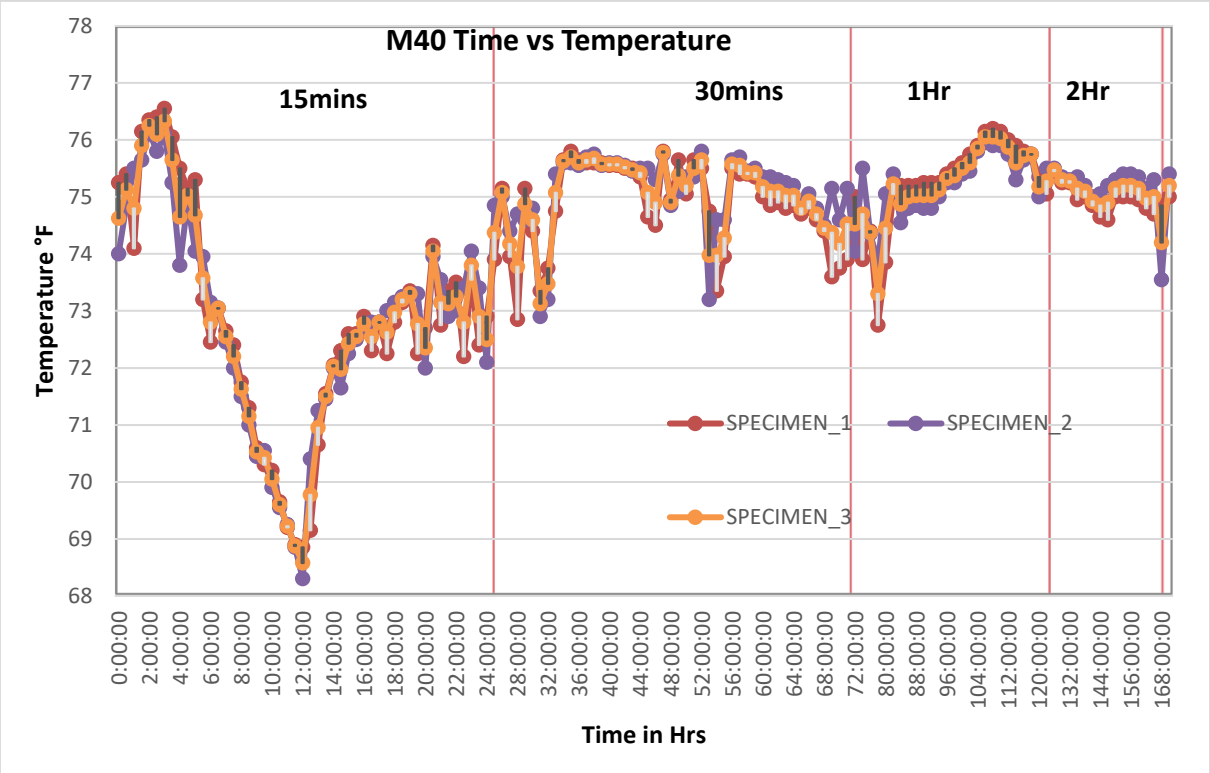

Fig 7.11Time vs Temperature Plot for M40

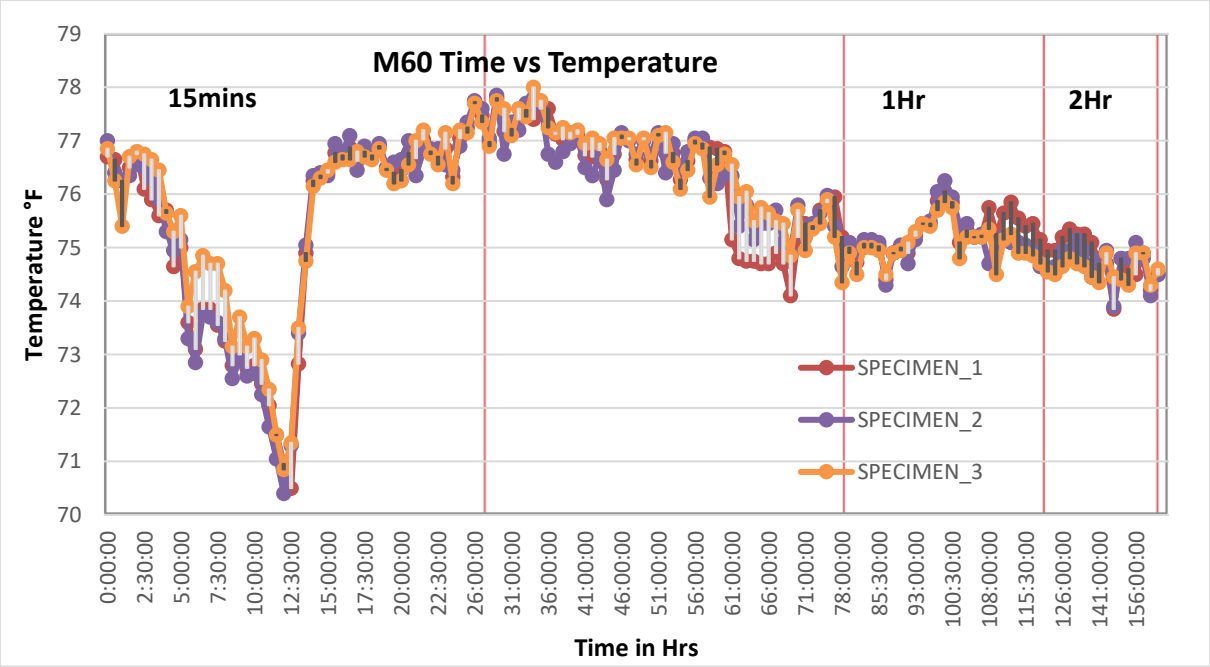

Fig 7.12 Time vs Temperature Plot for M60

Tα is the crucial parameter required for calculating the maturity index which is obtained from the average temperatures of specified time spans i.e., 24hrs, 25-72hrs, 73-120Hrs and 121-168Hrs. The temperature plot of M20 in Fig 7.10 shows that there is a drastic down fall in temperature to 67.3°F at 12:30Hrs. This change is occurred within the initial setting time; it is also understood that the concrete in the initial hours cools down in the hardening process. After 12:30Hrs the temperature increased exponential as specimens are kept in curing tank. When specimens come in contact with water the hydration process increases rapidly and temperature as well also increased upto 76.1°F. Fig 7.11 shows the M40 plot it states that the temperature increased linearly than M20 and attained the maximum temperature to 76.4°F at 31Hrs. In M60 plot as shown in Fig 7.12 the temperature increased as it in M20 and attained the maximum temperature to 78.2°F at 36Hrs.

As per the studies conducted on CMM (Marchon D *et al 2016,*), the maturity of concrete is divided into 4 phases. The initial period, incubation period, acceleration period and stable period as shown in Fig 7.13. The periods aredivided based on chemical reactions behind strength attainment of concrete. The high temperature in all the graphs are observed at acceleration period and similarly low temperature is observed at the incubation period. The temperature is maintained to be stable at the with minimal fluctuations in the stable period.

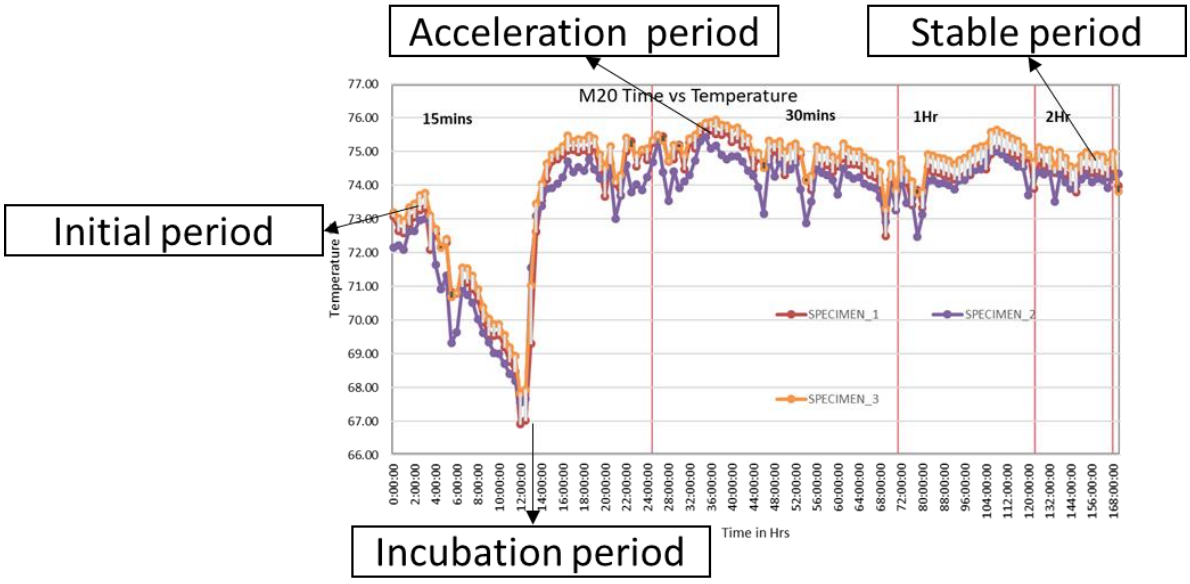

Fig 7.13 Stages of concrete maturity

Initial period

Initial period also called as pre-induction period is the reaction of cement when comes in contact with water. There is an abrupt rise in temperature that occurs very fast (within a few minutes) following the water's contact with the cement. The aluminate phases (C3A and C4AF) are the concrete's main reactive phases during this time. Ettringite, which comes on the outermost layer of the concrete particles, is created when the aluminate and ferrite phases interact with the calcium and sulphate ions. A very thin covering of calcium-silicate-hydrate (C-S-H) will develop during this phase, to a lower extent, since the silicate phases (mostly C3S) also react in extremely tiny fractions relative to their overall volume.

Incubation period

Incubation period in other words also called as induction period or dormant phase. The pace of hydration is noticeably slowed down at this time. According to experiments, this results from the moisture of the aforementioned chemicals on the cement particles, which creates a diffusion barrier that separates the cement and the H_2O that surrounds it. Fresh concrete is carried and installed at this time since it hasn't yet hardened and is still workable. It has been demonstrated that the time of the induction phase varies based on a number of variables (cement type, admixtures, and w/cm). The initial setting time often marks the conclusion of this phase.

Acceleration period

This phase is also called as Strength gain period the concrete begins to strengthen and solidify at this stage. The reaction of the calcium silicates (mostly C3S and to a lesser degree C2S) is the major cause of the heat produced during this phase, which can persist for many hours. The primary reaction product that gives the cement paste strength is "second-stage"

CSH, which is created when the calcium silicate reacts. There may also be a third, smaller heat peak from the reactivated C3A, depending on the cement.

Stable period

As the temperature rises, it stabilises with the surrounding air. Although it will considerably slow down, the hydration process won't halt entirely. If there is enough water and free silicates to hydrate, hydration can last for months, years, or even decades. However, the strength growth will be negligible throughout this time.

7.3.5 Compressive strength

The compressive strength evaluation is required to relate with the temperature based on the age. The compressive strength is used in generating the Nurse-Saul calibrating curve. The specimens of different concrete grades are crushed in UTM at 1, 3, 5 and 7 days for compressive strength evaluation. Three specimens per each grade are evaluated for compressive strength and the average of them are noted and the graph is shown in Fig 7.14.

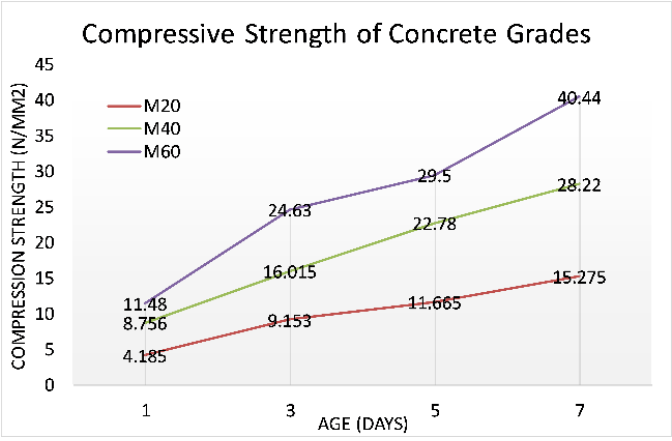

Fig 7.14Compressive strength plot of M20, M40 and M60

7.3.6 Nurse-Saul maturity calibration curve:

An established CMM code ASTM C 1074-11 is followed to derive the maturity calibration curve. The simple and widely used Nurse-saul maturity method is followed to draw the maturity curve as discussed in eqn-2 of section 2.3.1. This equation is simple to calculate. The assumption made is that the initial strength gain varies linearly with temperature, but independent of changes in temperature. It is applicable accurately when curing temperatures does not vary muchwith curing conditions. Generally, the datum temperature (T_0) is the temperature.Where, hydration process cannot occur in concrete, it is assumed to be 10°C (14 °F).To calculate the maturity index, average temperature (Tα) is used which is obtained from the average of surface temperatures for specified hours(Δt). The average of temperature (Tα) for time 0-24Hrs, 24-72Hrs, 72-120Hrs and 120-168Hrs are computed for three concrete grades. The corresponding maturity indices are also calculated by substituting in the eqn-1 and the results are tabulated in table 7.3.

Table 7.3Parameters for computing the maturity index (M (t))

Time in Hrs (Δ t)	24	72	120	168
M20 Temp in °F (Tα)	72.845	75.015	74.805	74.61
M40 Temp in °F (Tα)	73.15	75.37	75.54	75.375
M60 Temp in °F (Tα)	75.33	76.65	75.21	75.77
Datum Temperature in °F (T_0)	14	14	14	14
M20 Maturity Indices in °F-Hrs M (t)	1412.28	4393.08	7296.6	10182.48
M40 Maturity Indices in °F-Hrs M (t)	1419.6	4418.64	7384.8	10311
M60 Maturity Indices in °F-Hrs M (t)	1471.96	4510.68	7345.19	10377.9

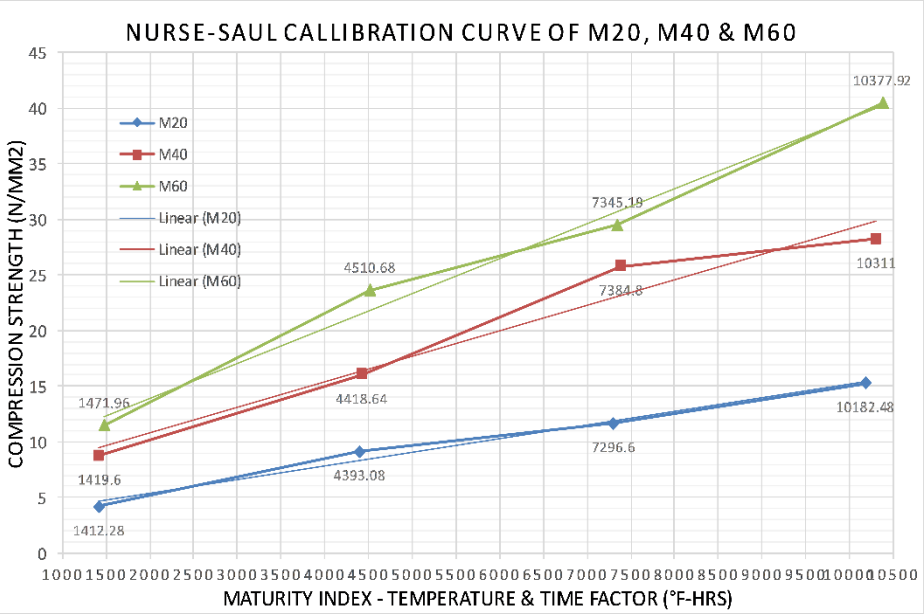

Fig 7.15 Nurse-Saul calibration curve of M20, M40 and M60

To plot the Nurse-Saul calibration curve the calculated maturity indices are plotted on x-axis and corresponding compressive strength of 1, 3, 5 and 7 days on the y-axisas shown in Fig 7.15 Calibration curve is the end product for estimating the concrete strength. Calibration curve is used to estimate the compressive strength of the concrete by simple calculation of maturity indices. The maturity indices is a product of temperature at that particular time.

7.3.7 Validation:

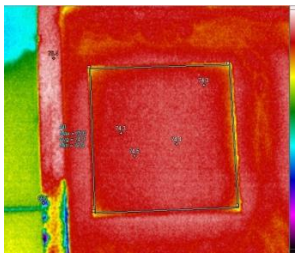

Fig 7.16 M60 Thermal image

The calibration curve is generated by casting the nominal mix concrete cubes at controlled climatic conditions. The setup is validated by estimating the strength of concrete by observing the surface temperature. An M60 concrete specimen is selected and imaged for the time span of 29-42Hrs to estimate the strength as shown in Fig 7.16. For the selected time

spanthe thermal images are processed for average temperature (Tα) and it is observed as 76.8°F. Maturity index (Mt) for the specified average temperature (Tα) is calculated as 3623.65. The estimated compressive strength for the calculated maturity index is 19.2N/mm2.

Chapter 8

DEVELOP A RELATION BETWEEN CORE AND EXOTHERMAL EMISSION OF CONCRETE ON VARIED VOLUMES

8.1 General

The pervious chapter is detailed with evaluation of concrete early age strength using the CMM and thermography technique. The hydro-chemical reaction of cement liberates temperature with respective to the volume during the hydration process of concrete. The volume of concrete affects the temperature liberated from it, the more the volume the high temperature. Mass concrete works like dams, bridges piers and foundation shafts release high

temperatures, where engineers use ice cubes in mixing or employ the cooling tubes inside the concrete. There should be conservative measures to minimize the effect of temperature release. Keeping in a view that the volume of concrete is directly proportional to the temperature release. The elevated surface temperature in high volume concrete is affecting the maturity indices and conveying abnormal results. The objective of this chapter is to study internal temperature and external temperature different volume on each concrete grade and develop a correlation factor between internal and external temperatures.

The present study is intended in the usage of thermography instead of thermocouple setup for evaluating CMM.Internal and external temperature of concrete cubes are monitored simultaneously and continuously by thermocouples and thermography to have a comprehensive temperature history.For performing the study on three different cube dimensions of 7.5cm, 15cm, and 30cms of three different grades such as M20, M40, & M60 are used. This research is conducted for initial 7days of concreting, as hydration process is enormous at initial stage. The external temperatures evaluations are conducted using thermal camera in time intervals of 30mins, 60mins, 120mins and 180mins for 1, 3, 5 and 7 days. This research is conducted for initial 7days of concreting, as hydration process is enormous at initial stage. The external temperatures evaluations are conducted using thermal camera in time intervals of 30mins for 1stday, 60mins for 2nd&3rd, 120mins for 4th&5th day and 180mins for 6th&7th day. The internal temperature liberated from inside is correlated with surface temperature observed for analyzing the thermal dissipation of concrete and correlation factor is derived. The CMM calibration curves are generated based on the temperature emission and corresponding strength of concrete at particular time intervals. The evaluated thermal dissipation of concrete is used for developing hydration models based on grade and volume of concrete.

8.2 Methodology

The study is conducted on concrete cube specimens of different mix designs and quantities. Three nominal mix design of M20, M40 and M60 is adopted and casted with

different cube sizes of 7.5 cm, 15cm and 30cm. As the temperature is the primary parameter in quantifying the heat of hydration, the thermography technique can be used in estimating strength from the surface temperature. The internal and external temperature of concrete cubes is monitored simultaneously and continuously by thermocouples and thermography to have a comprehensive temperature history.Thermal emissions from each specimen is ascertained and accounted for analyzing the hydrochemical reaction to quantify the strength gain by testing the specimen at that particular time. The cubes are insulated from external environmental conditions without any interactions to the external temperature for recording the exact thermal emissions of concrete. The work flow shown in Fig 8.1 is followed to conduct the study.

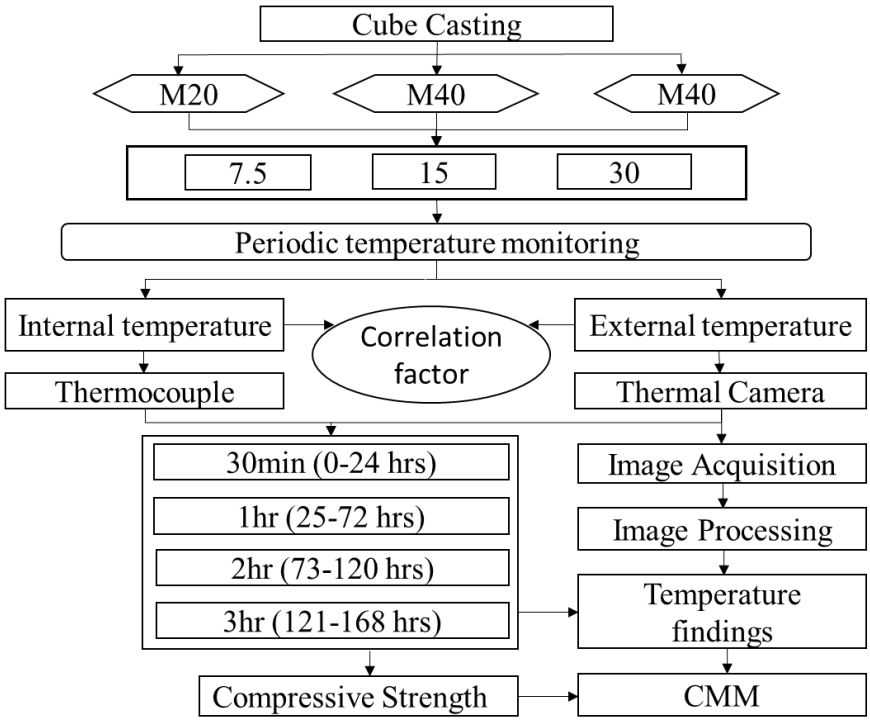

Fig 8.1Workflow of the study

8.2.1 Preparation of Specimens:

To conduct the research three concrete grades like M20, M40 and M60 with three different volumes like 7.5cms, 15cms and 30cms size cubes are castedas shown in Fig 8.2.

The same mix proportions as given in table 7.1 is followed to conduct the study. 6 specimens of 7.5cm and 30cms cubes for each grade and 15 specimens of 15cms cubes are casted as compressive strength is determined by crushing 15cm cubes. After 3 minutes of mixing, the concrete mixture was placed in cube moulds and compacted with the help of a vibrating table. Out of 15 specimens three are kept for recording surface temperature using thermal camera and three for internal temperature recording using thermocouple and rest of the specimens are used to evaluate the compressive strength. The concrete specimens which are kept to measure internal temperature is embedded with thermocouple that are kept exactly at the core center of the specimen. Other concrete specimens are kept for measuring and recording the external surface temperatures using thermal camera. The whole setup is arranged for curing in a thermocol box to isolate the specimens from external temperatures of climate.

Fig 8.27.5cm, 15cm & 30cm concrete specimens

8.2.2 Thermocouple Setup:

The internal temperature of the concrete is monitored by placing the thermocouple inside the concrete at the core. It is ensured that the placement of thermocouples is at center by attaching the thermocouple to a thin rod. The marking on rod as shown in Fig 8.3is made in such a way that it is rested in the center of the cube before casting. It is also displayed that

position of thermocouple in the mould. The spoke is removed immediately after the initial setting time is achieved.

Fig 8.3Thermocouple setup in concrete cube

8.2.3 Thermal Imaging:

The surface of each specimen is cleaned, organized and maintained in a way to capture the surface temperature of the concrete. Specimens are kept in curing with top 10mm left without submerging it in the entire water and leaving the top layer for capturing the thermal emissions of concrete. Thermal images are acquired at every stipulated time interval and thermal emissions are aggressive in the early hours of the hydration process. Concrete curing in thermocol box along with thermal camera used for conducting the study is shown in Fig 8.4. The thermal images obtained are loaded in FLUKE SMART VIEW 4.0 software and processed for investigating the surface temperature of concrete. The investigations are recorded according to the time intervals. Around 3500 thermal images are acquired and processed for conducting the study.

Fig 8.4Thermal image acquisition in isolated curing conditions.

8.3 Experimental Studies:

ASTM C1074-11 standard procedures were ffollowed in the preparation of all specimens. Concrete specimens selected for monitoring the internal and external temperatures are kept in a separate thermocol box with water filled in it for curing. Thermocouple are attached to the data acquisition platform and the internal temperatures are monitored. Simultaneously, thermal images are also acquired at the same time for obtaining the surface temperature. The data collection time intervals are chosen in such a way that even the smallest change in temperature is recorded and analysed. Priority is given for the initial hours of the concrete that is right after water coming in contact with the binding material to initial setting time is achieved (i.e., 0-24Hrs). Internal and external temperature recording is done for every 30mins at the initial stages of hardening process, as enormous heat will be generated due to the hydro chemical rection of concrete. There after the temperature variations is recorded for every 60mins for 2nd and 3rd day of concreting (i.e., 25-72Hrs). similarly, 120mins interval is adopted for 4th and 5th day (i.e., 75-120Hrs) and followed by 180 mins interval for 6th and 7th day (i.e., 120-168Hrs) as the temperature variations in the concrete is gradually decreased. An infrared thermal camera is used to capture the thermal energy emitted by the exothermic reaction of concrete. The acquired thermal images are processed in image processing software to determine the average surface temperature of concrete at that time. There are around 3500 thermal images acquired to conduct this study in a span of 7 days right from the mixing of materials to setting time. All the 3500 images are processed by selecting only the surface of concrete specimen and rest of the imaging part is omitted to have an exact note of concrete temperature as shown in Fig 8.5.

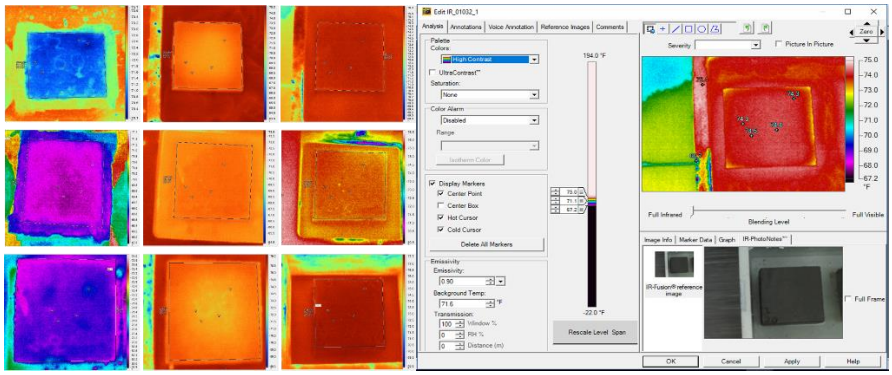

Fig 8.5Different volumes thermal images and its processing

Compressive strength of the specimens is also evaluated at specific time intervals to check the strength maturity of concrete as per the mix designs. Table 8.1 gives the observed compressive strength of lab cured M20 and M40 grade concrete cubes. Three 15cms cubes per mix design is crushed on every 1, 3, 5 and 7days after concreting and respective compressive strength is plotted in Fig 8.6. Along with high heat of hydration, the maximum amount of strength i.e., 65% will be gained in the initial 7days. Compressive strength is accounted to know the strength gain of concrete at that particular time period. These strength recordings also act as a fundamental parameter that serves to develop the maturity curves of concrete to predict the strength gain at early age.

Table 8.1Compressive strength of concrete

Concrete Age (Days)	Compressive Strength (N/mm2)		
	M20 grade	M40 grade	M60 grade
1	3.85	7.56	10.38
3	7.72	16.66	24.44
5	10.82	22.18	33.225
7	14.275	27.22	41.44

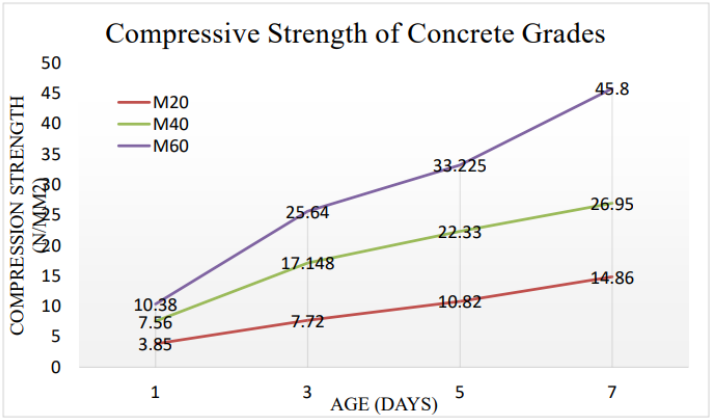

Fig 8.6 Compressive Strength graph of M20 and M40

8.3.1 Internal & External thermal studies

Internal temperature plots

The internal and external thermal emissions of concrete is observed and studied to understand the strength maturity.The thermal recordings are made for 7day and time vs temperature graphs are plotted accordingly. The internal temperatures of the study is obtained similar to the literature (mohamed 2019, jacek).Variations in concrete sizes also exhibited varied thermal emissions and it is also observed that the temperatures are not same in both the internal and external recordings. Different mix designs produce different thermal emissions during the hydration process, which varies with volume. Thermal images acquired at specific time intervals of 30 minutes, 60 minutes, 120 minutes, and 180 minutes are processed and plotted. Fig 8.7 depicts the M20 grade external temperature plot with varying volumes; it is observed that 30cms cube seems to have more variations than other cube volumes. The highest peak temperature in 30cm cube is observed as 126°F and lowest as 102°F at the initial 24Hrs. The external temperatures of M40 grade concrete are depicted in Fig 8.8; it is observed that highest peak as 132°F. and lowest as 102°F for 30cm cube. The external temperature plot of M60 grade with varying volumes is shown in Fig 8.9. Temperatures nearly doubled in a 15cm cube compared to a 7.5cm cube and more than tripled in a 30cm specimen. At high volumes, it is observed from the plots that the temperature patterns of all three grades exhibit

similar pattern crust and thrusts. The temperature drop in M60 is more gradual than in M20. The surface temperature has risen dramatically in all the external temperature graphs after initial setting time ending. The energy dissipations is more from the internal core temperatures as a result external temperatures are soaring high after initial setting time.

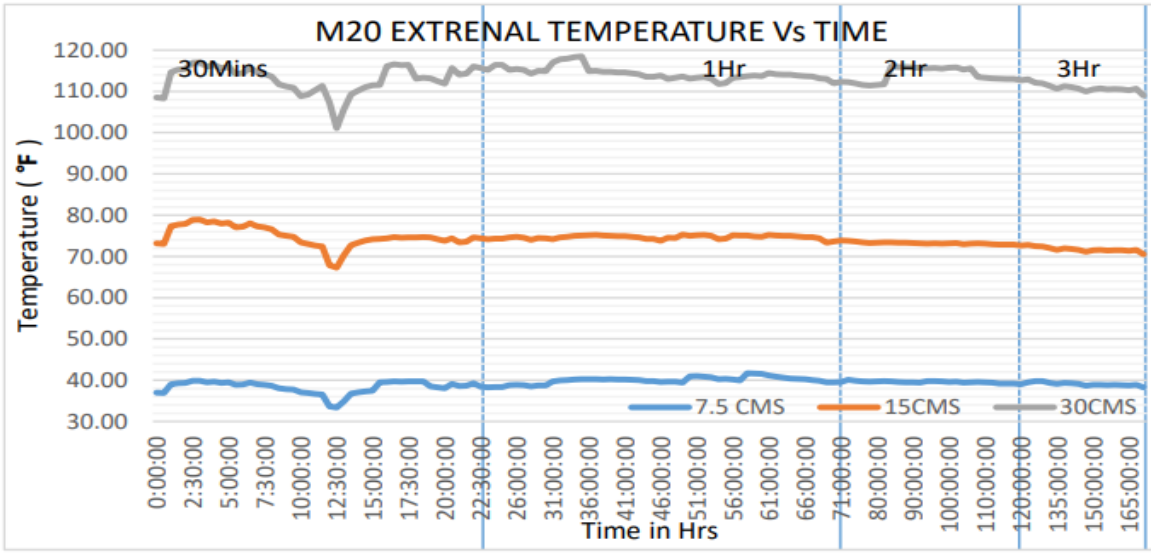

Fig 8.7M20 External Temperature-Time plot of varying sizes

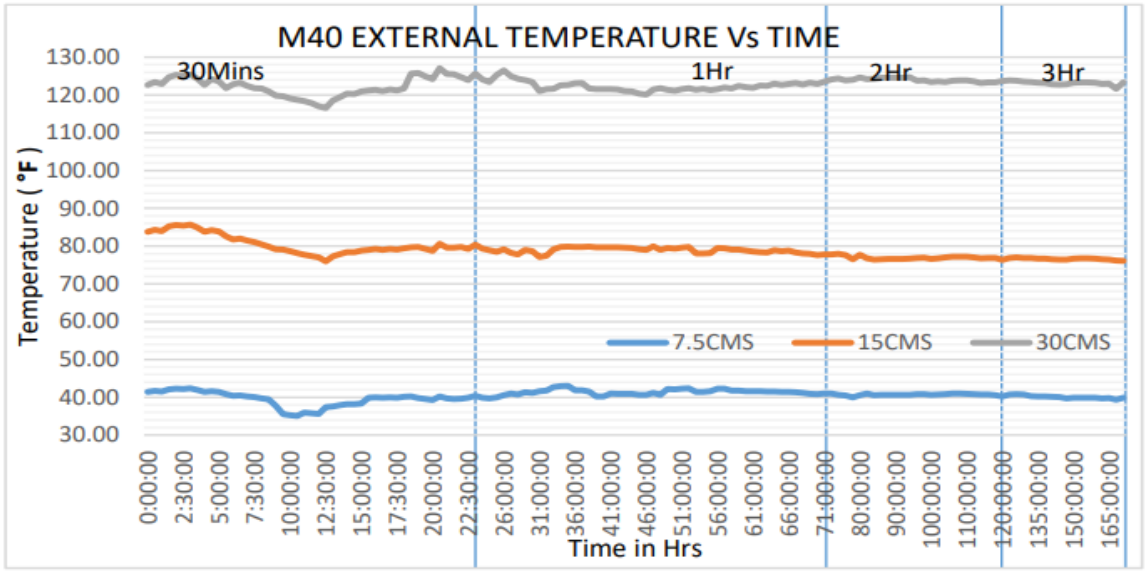

Fig 8.8M40 External Temperature - Time plot of varying sizes

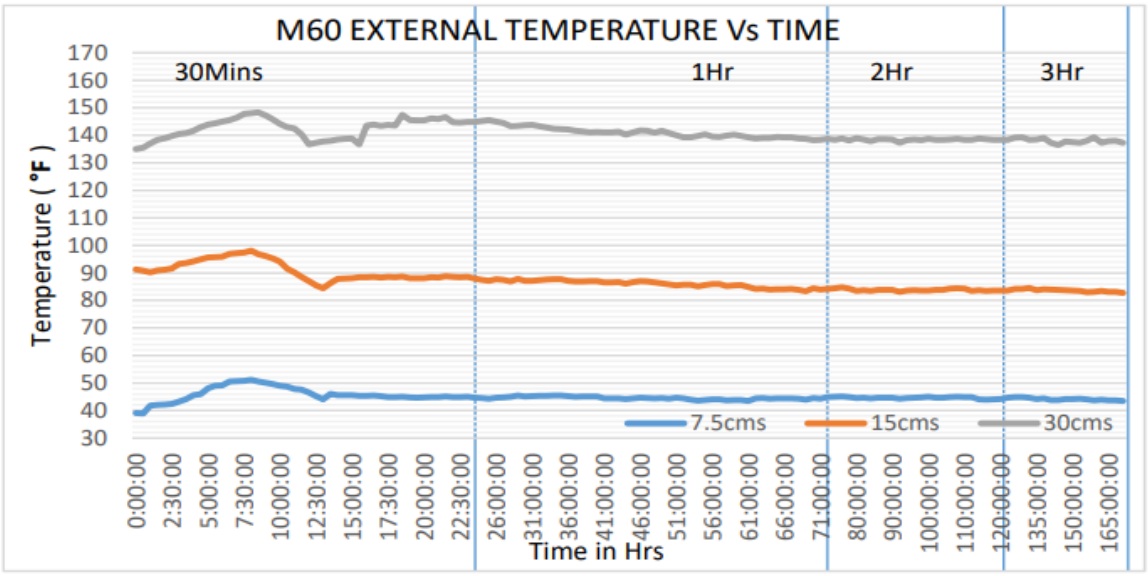

Fig 8.9M60 External Temperature - Time plot of varying sizes

External temperature plots

Fig 8.10 illustrates internal temperatures of M20 grade concrete maximum temperature of 7.5cm cube is observed as 60°F, 15cm cube as 101°F and 30cm cube as 145°F. Increase in internal temperature is observed as per the increase in volume of concrete. Fig 8.11 illustrates the internal temperatures of M40 concrete with varying volumes. M40 grade with 30cms cube has the highest internal temperature at around 170°F at 4:30Hrs, then a gradual decrease in temperature is observed. It is also observed that the temperature drops suddenly to 153°F at 7:30Hrs as the initial setting time end. Similarly, Fig 8.12 illustrates the internal temperatures of M60 grade concrete; temperatures are much higher when compared to M20 and M40 grade concrete. Peak temperature is recorded as 198°F at the middle of the initial setting time and sudden drop of temperature is observed at the end of initial setting time as 178°F.

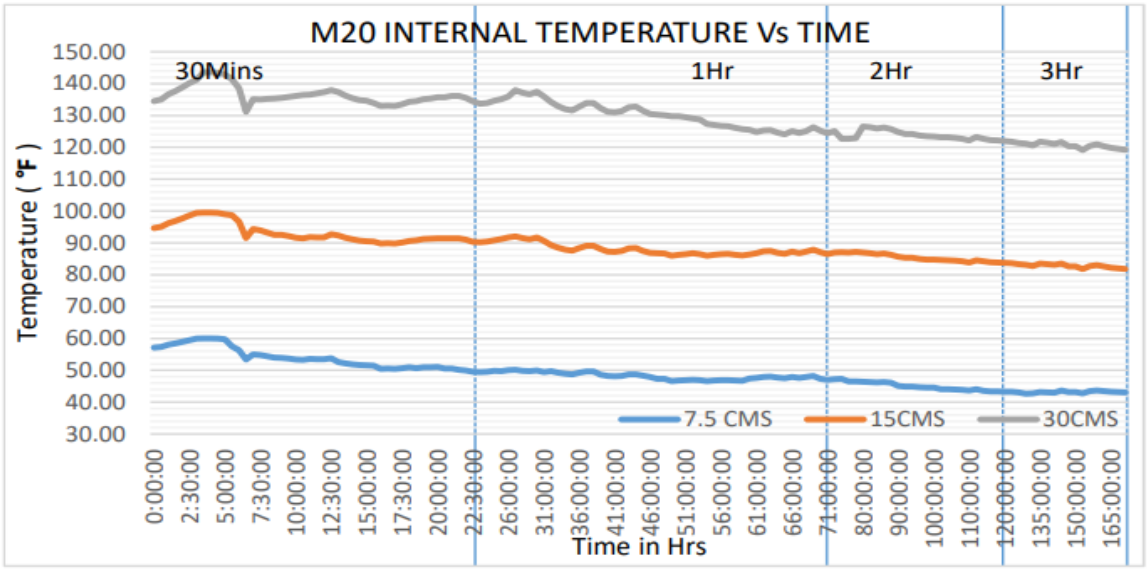

Fig 8.10M20 Internal Temperature-Time plot of varying sizes

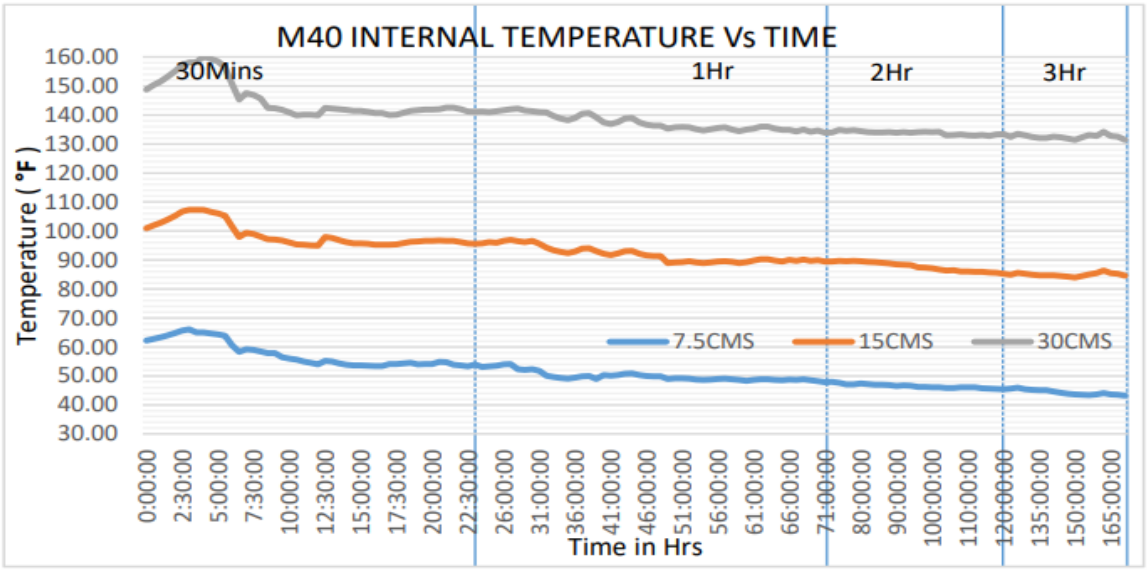

Fig 8.11M40 Internal Temperature-Time plot of varying sizes

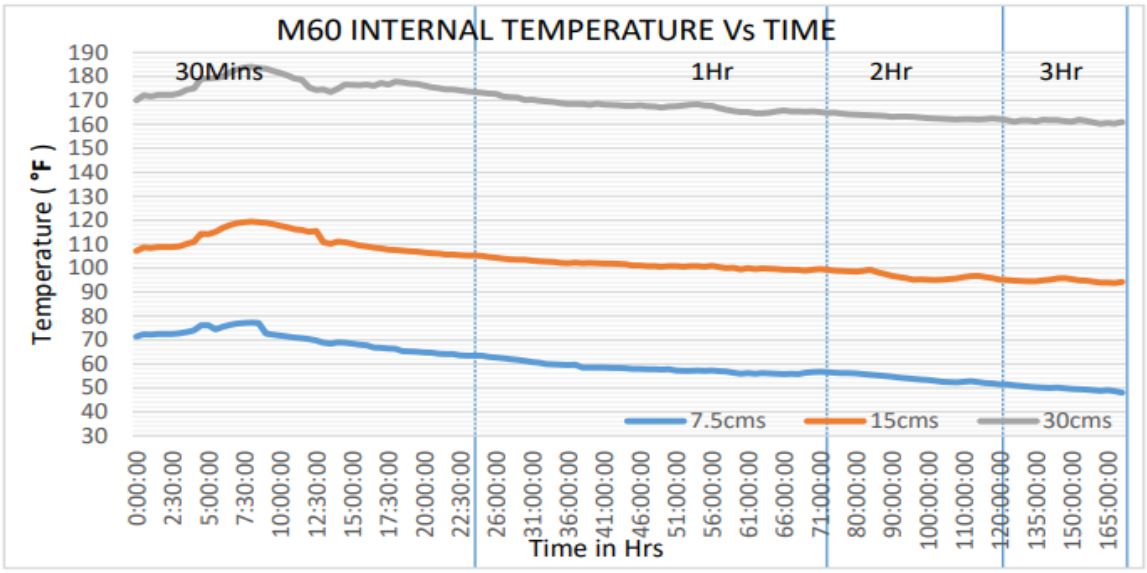

Fig 8.12M60 Internal Temperature-Time plot of varying sizes

8.3.2 Strength Maturity Indices

Maturity indices are the strength estimation indices developed from the well established Nurse-Saul strength estimation method. Temperature being the major parameter in time- temperature strength estimation it is derived from multiplying the external temperature with the given correlation factor in table 8.3. The derived internal temperature as per the time intervals are tabulated for calculating the strength estimation indices by substituting the parameters in Eqn.1. Strength estimation indices are calculated and tabulated in table 8.2

Table 8.2Derived internal temperatures and Nurse-Saul strength estimation indices

Time (hrs)	Internal Temperatures (°F)			Datum temp (°F)	M20 indices	M40 indices	M60 indices
	M20	M40	M60				
24	93.08	98.6	111.15	14	1897.92	2030.4	2331.6
72	87.8	91.62	101.23	14	5313.6	5588.64	6280.56

120	85.3	87.57	96.73	14	8556	8828.4	9927.6
168	82.8	84.94	94.72	14	11558.4	11917.92	13560.96

The calculated strength estimation indices of M20, M40 and M60 are drawn in the form of graph to generate nurse-saul calibration curve. The nurse-saul strength estimation curve of M20, M40 and M60 for initial 7 days of concreting is displayed in Fig 8.13.

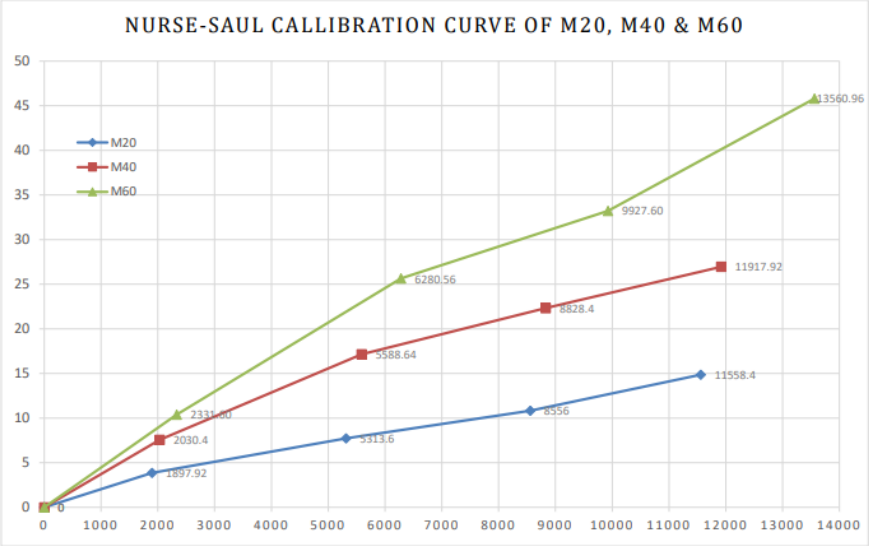

Fig 8.13M20, M40 & M60 grades Nurse-Saul strength estimation calibration curves.

8.3.3 Correlation factor:

A correlation factors are derived from a compressive observations of the external temperature and internal temperature based on time intervals. The external temperatures derived from thermal images can be multiplied with the given correlation factor from table 8.3 to obtain approximate internal temperature of concrete specimens. Initial 24 hours is divided into two time spans as more temperature fluctuations is observed in that period. This correlation factor helps in understanding the thermal behaviors of concrete and quantifying the strength gain. Correlation factors of 7.5cm cube is much lower than the other two cube volumes as energy dissipation is less due to its less surface area of specimen.

Table 8.3correlation factor for external to internal temperature for varied cube sizes

Time (Hrs)	M20			M40			M60		
	7.5cm	15cm	30cm	7.5cm	15cm	30cm	7.5cm	15cm	30cm
0-12	1.47	1.25	1.20	1.53	1.23	1.22	1.59	1.22	1.25
12-24	1.33	1.23	1.19	1.37	1.22	1.20	1.44	1.20	1.23
24-48	1.21	1.19	1.13	1.23	1.18	1.15	1.28	1.17	1.2
48-72	1.16	1.14	1.1	1.18	1.13	1.12	1.22	1.12	1.15
72-120	1.13	1.16	1.08	1.15	1.14	1.09	1.2	1.15	1.12
120-168	1.1	1.15	1.06	1.12	1.1	1.07	1.12	1.13	1.1

Internal to external thermal energy dissipation gradient

It is observed that the concrete core temperature is higher than the external wall temperature and varying with the volumes of the cubes. A specimen of M40 grade 30cm cube is considered for the evaluation of thermal energy dissipation from internal core to the external walls of the cube. The highest internal temperature of 168°F is observed at 5Hrs and highest external temperature of 134°F is observed at 19Hrs as shown in Fig 8.14. The time taken for thermal energy dissipation of the concrete from internal core to reach external wall is 12-15Hrs in 30cm. It also variates according to the volumes and grades of concrete

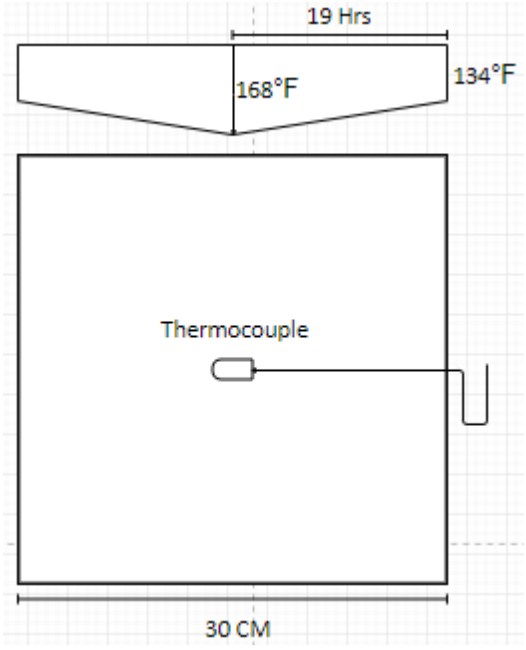

Fig 8.14 Thermal Gradient of M40 grade 30cm cubes

8.4 In-situ strength evaluation of concrete

To evaluate the strength of in-situ post tensioning slabwith mix design of M40 concrete grade is selected in a commercial building. The three locationsare chosen in such a way that they are having different slab thickness of 150mm, 200mm and 300mm to conduct the volumetric analysis. Prior to the concreting a square cut is made on the slab shuttering to open it during the image acquisition as shown in Fig 8.15. A support is placed at below the shuttering cutout portion for easy removal after concreting is finished.

Fig 8.15 cuts made in the slab shuttering

8.4.1 Thermal Image acquisition of slab

The thermal image acquisition is done at the bottom of the slab. The main reason in acquiring the images at bottom is asslab top is covered with curing bunds and water filled in itbecause staying hydrated is essential in strength attainment. The cut out portion of the slab shuttering is removed when thermal images need to be acquired for strength estimation studies. It is covered immediately after the image acquisition is done and supported with a prop. The thermal image acquisition of in-situ concrete is shown in Fig 8.16.Thermal images are acquired post 96hrs of pouring the concrete that is during the acceleration phase.

Fig 8.16 Thermal Image acquisition of concrete

8.4.2 Validation

The thermal images of 150mm, 200mm 300mm slab thickness is analysedfor the surface temperature and the results are put on to show in Fig . The observed surface temperatures are correlated with lab calibrated M40 external temperature graphs.Similarly with the help of correlation factor the internal temperatures is calculated and the results validated on the internal temperature obtained graphs.At the 96th hour the average of 150mm, 200mm and 300mm slab external temperatures at the bottom of the slab is observed as 75.9°F, 95.9°F and 117.6°F respectively. The correlation factor for 150mm and 300mm thick slabs is observed from Table 8.2 as 1.14 and 1.09. The corresponding internal temperatures is calculated as 86.5°F and 128.2°F as and a thick red line is drawn to show the exact derived external temperatures and calculated internal temperatures on the Fig 8.17

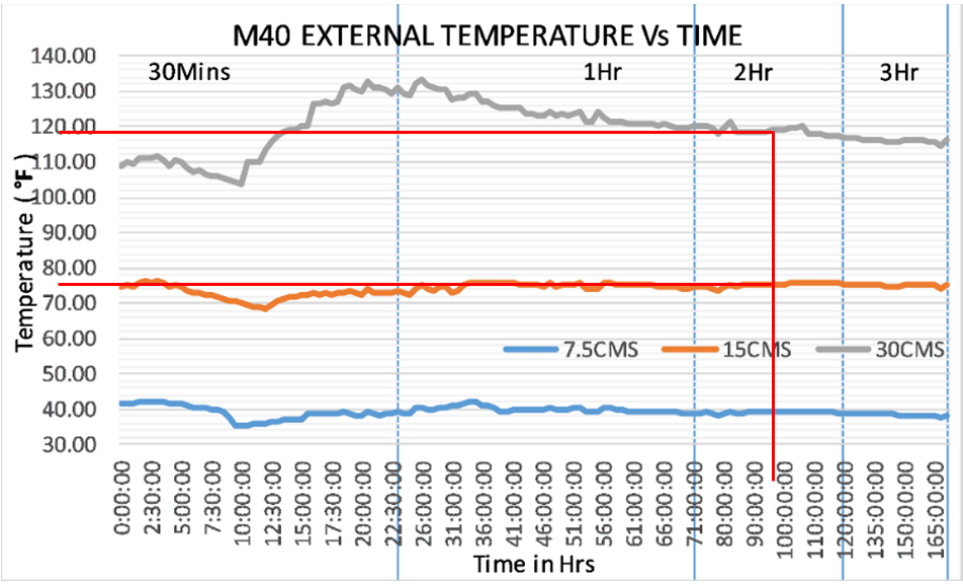

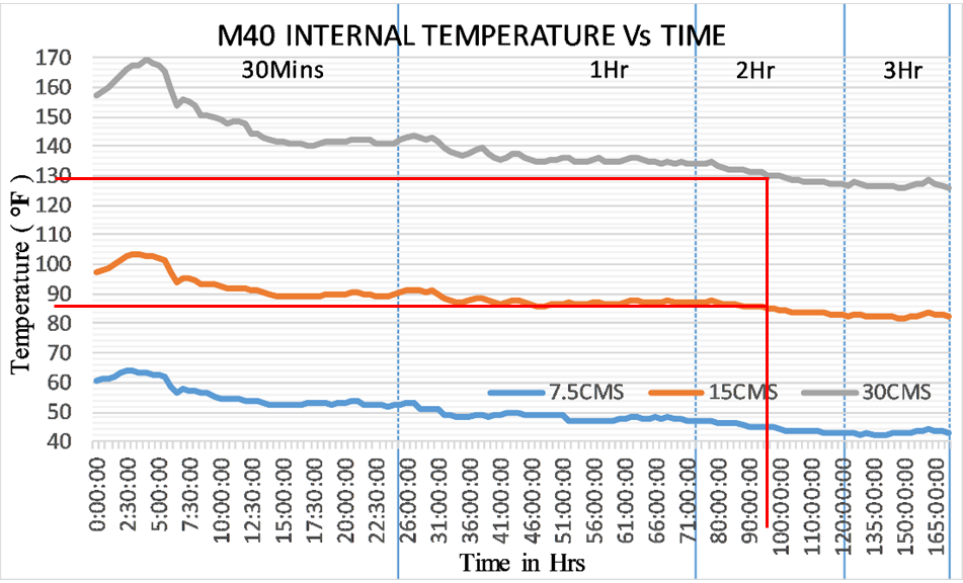

Fig 8.17 The derived and calculated extrenal and internal graphs

Chapter 9

Conclusions

9.1 Brief conclusions:

Through the research, it has been a revealed that the remote sensing imaging sensors have proved its efficiency in analyzing the SCM. In order to monitor and assess the structural diagnosis, the study is being conducted with a keen understanding of multispectral sensors that are restricted to a particular region of the EMR spectrum. Each multispectral sensors haveprovedtheir potential strengths and capabilitiesin analyzing the structure andmechanical properties of concrete. To monitor the condition of structural components, a remote sensing and image-based strength estimation and damage quantification methodology is developed in this study.The imaging methods developed in the study can be operated by any level of skilled person but for processing the images and extracting the information needs skilled and trained labor. Processing the vast image data can be automated with sophisticated artificial

intelligence tools for extracting the information. The remote sensing imaging based NDT methods developed in the study acts as a preliminary evaluation techniques to monitor the dimension, deformation and strength of structural concrete members. Based on the investigation the following conclusions can be drawn in a chapter wise manner.

9.1.1 UAVIC conclusions

From this study, it is understood that RCC beams undergo ductile failure with lateral dis-placements as the steel material has high elasticity of modulus that increases rigidity and moment of inertia so that it can withstand heavy loads and undergo larger deflections before failure.

The load displacement curve declares dial gauge and digital camera DIC and UAVIC investigations results are with a variation of 5% of dial gauge to DIC and 12% for dial gauge to UAVIC. The UAVIC have exhibited 12% more deflection than the dial gauge reading due to the distortion in UAV acquired images.As the UAVIC studies are not having much variation from the dial gauge it can be used as an preliminary deflection monitoring assessment tool at inaccessible locations in RCC structural monitoring

UAVIC investigation shows small spikes in the displacement recordings, it is due to magnetic sensitivity of sensors and vibrations in the UAV. While conducting the study, authors observed a small drift in the UAV due the availability of heavy machinery like Universal Testing Machine (UTM) attractions in the laboratory conditions. In field conditions while monitoring the bridge the wind pressure caused the drift in the drone, gimbal played a major role in locking the view of target point in both the investigations. The homography transformation further helped in minimizing the distortions in the UAV acquired images.

The maximum surface crack width evaluated from DIC analysis is found to be 0.147 mm for RCC beam. Based on the deterioration studies on bridge it is understood that the crack width in the bridge exceeded the permissible limits and it should be treated with fibers

[38,39]. Usage of self-healing concrete in the wide opened cracks also prevents further deterioration[41]. In terms of concrete spalling the severity, level is categorized as 1 and near maintenance is required [40]. The investigated bridge needs immediate and periodic maintenance for enhancing the serviceability of the structure.

For obtaining the better results, bridge-monitoring studies can be restricted to high sunny day with low windy conditions in the field. Rather than quadcopter an octocopter would yield better results for its better stability and improved hovering time at in-situ conditions. The dust on the bridge beam acted as a speckle pat-tern, in exceptional condition permanent speckles like those that printed reflector stickerscan be appliedon the beam to conduct the study.

9.1.2 Dimensional Accuracy Assessment

The UAV facilitates in rapid and real-time monitoring of site thus reporting the condition of structure at element early ages for enhancing the performance during the process of construction. The UAV mounted cameras exhibit better results by accessing the entire workspace in a single flight as given in Fig 5.3. The best part of the technique is application of UAV in visual inspection in the early ages of concrete works in major construction works and dimensional accuracy can be checked for freshly constructed structural elements. Dimensional accuracy can be improved with better scaled and high accuracy 3D models. The analysis of the given sensory data will significantly improve operational intelligence and preventive or predictive maintenance. It is need of the hour to test and refine the proposed method for possible usage in largescale project for automatic image acquisition and orthomosaic generation for checking the quality of construction activities.

9.1.3 Hydration Monitoring

The hydration quality of concrete can be effectively assessed by analysing the concrete material's Near-Infrared (NIR) data. The process of monitoring hydration and deriving statistical insights has been greatly facilitated by the examination of spectral patterns of various classes generated from analysed images. Using image analysis for classification allows for the differentiation of areas within the slab and column areas that show significant changes in hydration levels. These distinctions are based on the curing quality of the concrete. As a result, as evidenced by the observations in the column sections, regions that have not been adequately hydrated tend to experience early drying. This premature drying has a negative impact on the final strength development of the concrete. It keeps a complete track of the hydration and allows the site engineers to effectively plan the hydration of concrete. The color code classification in the image gives a note of stress zones in the concrete elements and further application of curing is followed.

Significant progress has been made in absorption bands, particularly around 1340 and 1400 nm. Notably, the reflectance values corresponding to the water band around 1400 nm show that locations on the slab that have undergone pond curing have the highest recorded. The use of Near-Infrared (NIR) analysis for monitoring concrete curing yields valuable insights into the progression of hydration, the occurrence of premature drying, and its subsequent impact on overall concrete quality.The analysis's effectiveness is heavily reliant on the composition of the concrete's constituent materials and their proportions in the mix, as well as prevailing environmental factors such as light exposure and moisture levels. As a result, when using this methodology, it is critical to implement standardised on-site tests to ensure a reliable evaluation. In this context, it is hoped that ongoing research efforts in this field will contribute to a better understanding of concrete curing assessment.

9.1.4 Thermography based strength estimation method

Non-contact remote sensing method is very helpful in rapid assessment of the fresh concrete strengths. With the investigation, it is evident that the proposed novel method of thermography emerged as a new tool in the area of strength estimation using CMM. Thermography has shown better results in early age strength estimation of concrete same as in

various other applications. The image processing of vast thermal image data is hectic and time taking in this study. Once the comprehensive surface temperature is extracted and calibration curve generated the process of strength estimation is simple Thethermography plays a key role in mapping the heat emissions from the concrete in particular at the initial ages of concreting for strength estimation. Thermography can be used in early age strength estimation of concrete with the constraint that it should be evaluated under controlled environment.

The generated Nurse-Saul calibration curve can be used for nominal mix designs of M20, M40 and M60 specimens, which are cured under controlled climatic conditions. The surface temperatures of concrete cubes started increasing when it is placed for water bath in thermocol box as it reached the acceleration period immediately after the initial setting time is completed. It is also proved that surface temperature dissipation from concrete specimens is varying according to the characteristics strength of concrete. When compared to M20, surface temperature in M40 and M60 is gradually increasing with time. Thermography can be evolved to be modern age preliminary strength estimation tool with further investigation on types of image acquisition methods and varied concrete volumetric exothermal analysis.

9.1.5 Thermography analysis on various volumes and grades ofconcrete

The research is being carried out on nominal mix designs of concrete with no ad-mixture effects on temperature emission. Internal temperatures are higher than external temperatures. Increase in internal and external temperatures are observed from lower grades to higher grades similarly, lower volumes to higher volumes. External peak temperature time spans and internal peak temperature time spans are not the same. The thermal energy emitted from the internal core is high at certain times and is later dissipated through the external surface, causing the temperature of the external surface to rise at later times. The graph shows that internal temperature crusts and thrusts are smoother than external temperature crusts and thrusts. The study's correlation factor can be used as a base parameter for other studies to calculate approximate internal temperature using thermography external temperature. IRT has been shown to be effective in estimating the early age strength of concrete by measuring the surface temperatures of the specimen. Thermography principles have been found to be more

advantageous than thermocouples because each pixel in the image acts as a thermal node for quantifying temperature. According to the findings, the increase in surface temperatures decreases after three days. The authors propose that the IRT method be used in the early stages of concreting because the heat of hydration on the external surface is high at that stage. Acquiring the images at bottom of slab in validation studies is also advantageous as interaction with atmosphere is restricted by closing the opening. The study is proved to be efficient on higher grade of concrete and at higher volumes, when the thermal radiations are high. The IRT early age strength estimation method is rapid, reusable, risk-free, cost-effective, and simple to use. Thermal images obtained can be reviewed by the stake holders at any point of time to increase the transparency of results.

9.2 Limitation of the study

- NIR sensor cannot detect the moisture index if the curing agent is applied on the concrete elements
- The study of thermography is evaluated by assumption that there is regular hydration of concrete
- The study of thermography cannot be performed in high radiated climatic conditions where the exothermal reaction of the concrete is altered
- UAVIC studies cannot be performed in adverse climatic conditions like windy situations where the UAV tend to drift much

9.3 Scope for Future Research

- A 3D model studies can be done by UAV to evaluate the physical properties of a structural element
- As a future scope of study to stabilize the UAVIC images a laser referencing system by placing the lasers at four corners of the target for precise referencing would yield high precision results

- Load consideration of vehicle will give better understanding of the DIC bridge inspection studies
- The thermography study can be extended to different concrete binding material
- The vast thermal imaging data also helps in developing the AI automation tool to process the thermal images and estimate strength of concrete based on the grade and thickness of it
- The experimental studies conducted in a prescribed isolated environment in a laboratory setting provided the opportunity for this study's future scope to consider and develop a relation between the external climatic temperature and concrete radiation

References

1. Abed, M.A. Indirect Evaluation of the compressive strength of recycled aggregate concrete at long ages and after exposure to freezing or elevated temperatures. *Russian Journal of Nondestructive Testing.***2021**, Mar;57(3):195-202.

2. Ahmed M., Z.; Zaimi, M.A.M.; Mustaffar, M. A. Systematic Procedure for Developing the 3D Model to Evaluate the Construction Project Progress. *Constr. Innov.***2007**, *7*, 187–199, doi:10.1108/14714170710738540.

3. Al-Tarawneh, M.S. Lung cancer detection using image processing techniques. *Leonardo electronic journal of practices and technologies,***2012**, 11(21), pp.147-58.

4. Akash, M.S.H.; Rehman, K. Ultraviolet-Visible (UV-VIS) Spectroscopy.; 2019.

5. Akpinar, P.; Khashman, A. Intelligent Classification System for Concrete Compressive Strength. *Procedia Comput. Sci.***2017**, *120*, 712–718, doi:10.1016/j.procs.2017.11.300.

6. Atabany, W.; Degenaar, P. A Robust Edge Enhancement Approach for Low Vision Patients Using Scene Simplification. *2008 Cairo Int. Biomed. Eng. Conf. CIBEC 2008***2008**, 1–4, doi:10.1109/CIBEC.2008.4786060.

7. Azenha, M.; Faria, R.; Figueiras, H. Thermography as a Technique for Monitoring Early Age Temperatures of Hardening Concrete. *Constr. Build. Mater.***2011**, *25*, 4232–4240, doi:10.1016/j.conbuildmat.2011.04.065.

8. Bagavathiappan, S.; Lahiri, B.B.; Saravanan, T.; Philip, J.; Jayakumar, T. Infrared Thermography for Condition Monitoring - A Review. *Infrared Phys. Technol.***2013**, *60*, 35–55, doi:10.1016/j.infrared.2013.03.006.

9. Balaras, C.A.; Argiriou, A.A. Infrared Thermography for Building Diagnostics. *Energy Build.***2002**, doi:10.1016/S0378-7788(01)00105-0.

10. Barba, S.; Barbarella, M.; Di Benedetto, A.; Fiani, M.; Gujski, L.; Limongiello, M. Accuracy Assessment of 3d Photogrammetric Models from an Unmanned Aerial Vehicle. *Drones***2019**, *3*, 1–19, doi:10.3390/drones3040079.

11. Bauer, E.; Milhomem, P.M.; Aidar, L.A.G. Evaluating the Damage Degree of Cracking in Facades Using Infrared Thermography. *J. Civ. Struct. Heal. Monit.***2018**, *8*, 517–528, doi:10.1007/s13349-018-0289-0.

12. Benassi, F.; Dall'Asta, E.; Diotri, F.; Forlani, G.; Cella, U.M. di; Roncella, R.; Santise, M. Testing Accuracy and Repeatability of UAV Blocks Oriented with Gnss-Supported Aerial Triangulation. *Remote Sens.***2017**, *9*, 1–23, doi:10.3390/rs9020172.

13. Bernardini, F.; Rushmeier, H. The 3D Model Acquisition Pipeline. *Comput. Graph. Forum***2002**, *21*, 149–172, doi:10.1111/1467-8659.00574.

14. Blaber, J.; Adair, B.; Antoniou, A. Ncorr: Open-Source 2D Digital Image Correlation Matlab Software. *Exp. Mech.***2015**, *55*, 1105–1122, doi:10.1007/s11340-015-0009-1.

15. Carino, N.J.; Lew, H.S. The Maturity Method: From Theory to Application. In *Structures 2001: A structural engineering odyssey*; 2001; pp. 1–19.

16. Chandler, R.C.; Shull, P.D. Increasing the Surface Emissivity of Aluminum Shapes to Improve Radiant Heat Transfer. *TMS Annu. Meet.***2009**, 713–716.

17. Chen, G.; Liang, Q.; Zhong, W.; Gao, X.; Cui, F. Homography-Based Measurement of Bridge Vibration Using UAV and DIC Method. *Meas. J. Int. Meas. Confed.***2021**, *170*, 108683, doi:10.1016/j.measurement.2020.108683.

18. Cho, S.; Yun, C.-B.; Lynch, J.P.; Zimmerman, A.T.; Spencer, B.F.J.; Nagayama, T. Smart Wireless Sensor Technology for Structural Health Monitoring of Civil Structures. *Steel Struct.***2008**, *8*, 267–275.

19. Cinar, A.F.; Barhli, S.M.; Hollis, D.; Flansbjer, M.; Tomlinson, R.A.; Marrow, T.J.; Mostafavi, M. An Autonomous Surface Discontinuity Detection and Quantification Method by Digital Image Correlation and Phase Congruency. *Opt. Lasers Eng.***2017**, *96*, 94–106.

20. Coady, J.; O'Riordan, A.; Dooly, G.; Newe, T.; Toal, D. An Overview of Popular Digital Image Processing Filtering Operations. *Proc. Int. Conf. Sens. Technol. ICST***2019**, *2019-December*, 1–5, doi:10.1109/ICST46873.2019.9047683.

21 Dasari, S.; Mesapam, S.; Kumarapu, K.; Mandla, V.R. UAV in Development of 3D Heritage Monument Model: A Case Study of Kota Gullu, Warangal, India. *J. Indian Soc. Remote Sens.***2021**, *49*, 1733–1737, doi:10.1007/s12524-020-01250-0.

22. de Lima, R.S.; Lang, M.; Burnside, N.G.; Peciña, M.V.; Arumäe, T.; Laarmann, D.; Ward, R.D.; Vain, A.; Sepp, K. An Evaluation of the Effects of Uas Flight Parameters on Digital Aerial Photogrammetry Processing and Dense-Cloud Production Quality in a Scots Pine Forest. *Remote Sens.***2021**, *13*, 3–5, doi:10.3390/rs13061121.

23. Del Río, L.M.; Jiménez, A.; López, F.; Rosa, F.J.; Rufo, M.M.; Paniagua, J.M. Characterization and Hardening of Concrete with Ultrasonic Testing. *Ultrasonics* 2004, *42*, 527–530.

24. Double, D.D.; Hellawell, A.; Perry, S.J. The hydration of Portland cement. Proceedings of the Royal Society of London. A. *Mathematical and Physical Sciences*, **1978**, 359(1699), pp.435-451.

25. Domski, J.; Katzer, J. An Example of Monitoring of Early-Age Concrete Temperatures in a Massive Concrete Slab. *Sel. Pract. Theor. Asp. Contemp. Mech.***2015**, 94–105.

26. Du, C.; Dutta, S.; Kurup, P.; Yu, T.; Wang, X. A Review of Railway Infrastructure Monitoring Using Fiber Optic Sensors. *Sensors Actuators, A Phys.***2020**, *303*, 111728, doi:10.1016/j.sna.2019.111728.

27. Dua, G.; Arora, V.; Mulaveesala, R. Defect Detection Capabilities of Pulse Compression Based Infrared Non-Destructive Testing and Evaluation. *IEEE Sens.*

*J.***2021**, *21*, 7940–7947, doi:10.1109/JSEN.2020.3046320.

28. Duarte, L.; Teodoro, A.C.; Moutinho, O.; Gonçalves, J.A. Open-Source GIS Application for UAV Photogrammetry Based on MicMac. *Int. J. Remote Sens.***2017**, *38*, 3181–3202, doi:10.1080/01431161.2016.1259685.

29. Duglas, P. METHODS OF SURVIVING IN EMERGENCY SITUATIONS ON BOARD SHIPS. In Proceedings of the ProfMarket: Educatin. Language. Success (ProfMarket: Образование. Язык. Успех); 2017; pp. 193–195.

30. Dutton, M.; Take, W.A.; Hoult, N.A. Curvature Monitoring of Beams Using Digital Image Correlation. *J. Bridg. Eng.***2014**, *19*, 05013001, doi:10.1061/(asce)be.1943-5592.0000538.

31. Elghaish, F.; Matarneh, S.; Talebi, S.; Kagioglou, M.; Hosseini, M.R.; Abrishami, S. Toward Digitalization in the Construction Industry with Immersive and Drones Technologies: A Critical Literature Review. *Smart Sustain. Built Environ.***2021**, *10*, 345–363, doi:10.1108/SASBE-06-2020-0077.

32. Estanqueiro, R.; Tenedório, J.A.; Rebelo, C.; Marques, J.P. Future 3D Urbanism: From UAV Data Modelling to Information Visualization. In *Methods and Applications of Geospatial Technology in Sustainable Urbanism*; IGI Global, 2021; pp. 552–585.

33. Fahmy, M.; Moselhi, O. Automated Detection and Location of Leaks in Water Mains Using Infrared Photography. *J. Perform. Constr. Facil.***2010**, *24*, 242–248, doi:10.1061/(asce)cf.1943-5509.0000094.

34. Farrag, S.; Yehia, S.; Qaddoumi, N. Investigation of Mix-Variation Effect on Defect-Detection Ability Using Infrared Thermography as a Nondestructive Evaluation Technique. *J. Bridg. Eng.***2016**, *21*, 04015055, doi:10.1061/(asce)be.1943-5592.0000779.

35. Felipe-García, B.; Hernández-López, D.; Lerma, J.L. Analysis of the Ground Sample Distance on Large Photogrammetric Surveys. *Appl. Geomatics***2012**, *4*, 231–244, doi:10.1007/s12518-012-0084-2.

36. Franceschini, M.H.D.; Bartholomeus, H.; van Apeldoorn, D.F.; Suomalainen, J.; Kooistra, L. Feasibility of Unmanned Aerial Vehicle Optical Imagery for Early Detection and Severity Assessment of Late Blight in Potato. *Remote Sens.***2019**, *11*,

doi:10.3390/rs11030224.

37. Fujita, Y.; Hamamoto, Y. A Robust Automatic Crack Detection Method from Noisy Concrete Surfaces. *Mach. Vis. Appl.***2011**, *22*, 245–254, doi:10.1007/s00138-009-0244-5.

38. Gastaldi, D.; Canonico, F.; Irico, S.; Pellerej, D.; Paganini, M.C. Near-Infrared Spectroscopy Investigation on the Hydration Degree of a Cement Paste. *J. Mater. Sci.***2010**, *45*, 3169–3174, doi:10.1007/s10853-010-4323-9.

39. Gehlen, C.D.; Wiens, E.; Noll, R.; Wilsch, G.; Reichling, K. Chlorine Detection in Cement with Laser-Induced Breakdown Spectroscopy in the Infrared and Ultraviolet Spectral Range. *Spectrochim. Acta - Part B At. Spectrosc.***2009**, *64*, 1135–1140, doi:10.1016/j.sab.2009.07.021.

40. Gencturk, B.; Hossain, K.; Kapadia, A.; Labib, E.; Mo, Y.L. Use of Digital Image Correlation Technique in Full-Scale Testing of Prestressed Concrete Structures. *Meas. J. Int. Meas. Confed.***2014**, *47*, 505–515, doi:10.1016/j.measurement.2013.09.018.

41. Ghahri Saremi, S.; Goulias, D. Concrete Strength Gain Monitoring with Non-Destructive Methods for Potential Adoption in Quality Assurance. *Constr. Build. Mater.***2020**, *260*, 120464, doi:10.1016/j.conbuildmat.2020.120464.

42. Gholizadeh, S. A Review of Non-Destructive Testing Methods of Composite Materials. *Procedia Struct. Integr.***2016**, *1*, 50–57, doi:10.1016/j.prostr.2016.02.008.

43. Ghosh, K.K.; Karbhari, V.M. Use of Infrared Thermography for Quantitative Non-Destructive Evaluation in FRP Strengthened Bridge Systems. *Mater. Struct. Constr.***2011**, *44*, 169–185, doi:10.1617/s11527-010-9617-5.

44. Gini, R.; Pagliari, D.; Passoni, D.; Pinto, L.; Sona, G.; Dosso, P. Uav Photogrammetry: Block Triangulation Comparisons. *Int. Arch. Photogramm. Remote Sens. Spat. Inf. Sci.***2013**, *XL-1/W2*, 157–162, doi:10.5194/isprsarchives-xl-1-w2-157-2013.

45. Gorriz, B.T.; Paya-Zaforteza, I.; García, P.C.; Maicas, S.S. New fiber optic sensor for monitoring temperatures in concrete structures during fires. *Sensors and Actuators A: Physical*, **2017**, 254, pp.116-125.

46. Graettinger, A.J.; Ramseyer, C.C.E.; Freyne, S.; Prevatt, D.O.; Myers, L.; Dao, T.; Floyd, R.W.; Holliday, L.; Agdas, D.; Haan, F.L.; et al. Tornado Damage Assessment in the Aftermath of the May 20th 2013 Moore Oklahoma Tornado. *Tech. Rep. to Natl. Sci. Found.***2014**, 133.

47. Gusella, V.; Cluni, F.; Liberotti, R. Feasibility of a Thermography Nondestructive Technique for Determining the Quality of Historical Frescoed Masonries: Applications on the Templar Church of San Bevignate. *Appl. Sci.***2021**, *11*, 1–16, doi:10.3390/app11010281.

48. HAKA, A.T. Thermography. Inbetween making and knowing: *Tools in the History of Materials Research.***2020**, (pp. 539-551).

49. Ham, Y.; Han, K.K.; Lin, J.J.; Golparvar-Fard, M. Visual Monitoring of Civil Infrastructure Systems via Camera-Equipped Unmanned Aerial Vehicles (UAVs): A Review of Related Works. *Vis. Eng.***2016**, *4*, 1–8, doi:10.1186/s40327-015-0029-z.

50. Hansen, P.F.; Pedersen, E.J. *Maturity Computer for Controlled Curing and Hardening of Concrete*; 1977;

51. Hayat, S.; Yanmaz, E.; Muzaffar, R. Survey on Unmanned Aerial Vehicle Networks for Civil Applications: A Communications Viewpoint. *IEEE Commun. Surv. Tutorials***2016**, *18*, 2624–2661, doi:10.1109/COMST.2016.2560343.

52. Hellier, C.J. Handbook of nondestructive evaluation. **2013**.*McGraw-Hill Education.*

53. Hild, F.; Roux, S. Digital Image Correlation. *Opt. methods solid Mech. A Full-f. approach***2012**, *367*, 183–228.

54. Hinge, L.; Gundorph, J.; Ujang, U.; Azri, S.; Anton, F.; Rahman, A.A. Comparative Analysis of 3D Photogrammetry Modeling Software Packages for Drones Survey. *Int. Arch. Photogramm. Remote Sens. Spat. Inf. Sci. - ISPRS Arch.***2019**, *42*, 95–100, doi:10.5194/isprs-archives-XLII-4-W12-95-2019.

55. Hoang, N.D. Detection of Surface Crack in Building Structures Using Image Processing Technique with an Improved Otsu Method for Image Thresholding. *Adv. Civ. Eng.***2018**, *2018*, doi:10.1155/2018/3924120.

56. Hoshyar, A.N.; Rashidi, M.; Liyanapathirana, R.; Samali, B. Algorithm Development for the Non-Destructive Testing of Structural Damage. *Appl. Sci.***2019**, *9*, doi:10.3390/app9142810.

57. Hugenschmidt, J.; Loser, R. Detection of Chlorides and Moisture in Concrete Structures with Ground Penetrating Radar. *Mater. Struct. Constr.***2008**, *41*, 785–792, doi:10.1617/s11527-007-9282-5.

58. Huke, P.; Klattenhoff, R.; von Kopylow, C.; Bergmann, R.B. Novel Trends in Optical Non-Destructive Testing Methods. *J. Eur. Opt. Soc.***2013**, *8*, 1–7, doi:10.2971/jeos.2013.13043.

59. Jacob-Loyola, N.; Muñoz-La Rivera, F.; Herrera, R.F.; Atencio, E. Unmanned Aerial Vehicles (Uavs) for Physical Progress Monitoring of Construction. *Sensors***2021**, *21*, doi:10.3390/s21124227.

60. Jalinoos, F.; Amjadian, M.; Agrawal, A.K.; Brooks, C.; Banach, D. Experimental Evaluation of Unmanned Aerial System for Measuring Bridge Movement. *J. Bridg. Eng.***2020**, *25*, 04019132, doi:10.1061/(asce)be.1943-5592.0001508.

61. Jensen, J.R.; Hodgson, M.E.; Garcia-Quijano, M.; Im, J.; Tullis, J.A. A Remote Sensing and GIS-Assisted Spatial Decision Support System for Hazardous Waste Site Monitoring. *Photogramm. Eng. Remote Sensing***2009**, *75*, 169–177, 30.

62. Jhajharia, M.; Mehta, A.; Shukla, A. Structural Health Monitoring using Destructive Non destructive Evaluation. **2015**, doi:10.14358/PERS.75.2.169.

63. Jurjević, L.; Gašparović, M.; Milas, A.S.; Balenović, I. Impact of UAS Image Orientation on Accuracy of Forest Inventory Attributes. *Remote Sens.***2020**, *12*, doi:10.3390/rs12030404.

64. Kaamin, M.; Razali, S.N.M.; Ahmad, N.F.A.; Bukari, S.M.; Ngadiman, N.; Kadir, A.A.; Hamid, N.B. The Application of Micro UAV in Construction Project. *Malaysian Constr. Res. J.***2017**, *2*, 122–129.

65. Kashif Ur Rehman, S.; Ibrahim, Z.; Memon, S.A.; Jameel, M. Nondestructive Test Methods for Concrete Bridges: A Review. *Constr. Build. Mater.***2016**, *107*, 58–86, doi:10.1016/j.conbuildmat.2015.12.011.

66. Kaur, P.; Dana, K.J.; Romero, F.A.; Gucunski, N. Automated GPR Rebar Analysis for Robotic Bridge Deck Evaluation. *IEEE Trans. Cybern.***2016**, *46*, 2265–2276, doi:10.1109/TCYB.2015.2474747.

67. Khan, F.; Ellenberg, A.; Mazzotti, M.; Kontsos, A.; Moon, F.; Pradhan, A.; Bartoli, I. Investigation on Bridge Assessment Using Unmanned Aerial Systems. *Struct. Congr. 2015 - Proc. 2015 Struct. Congr.***2015**, 404–413, doi:10.1061/9780784479117.035.

68. Khoo, S.W.; Karuppanan, S.; Tan, C.S. A Review of Surface Deformation and Strain Measurement Using Two-Dimensional Digital Image Correlation. *Metrol. Meas. Syst.***2016**, *23*, 461–480, doi:10.1515/mms-2016-0028.

69. Kim, H.; Sim, S.H.; Cho, S. Unmanned Aerial Vehicle (UAV)-Powered Concrete Crack Detection Based on Digital Image Processing. *Int. Conf. Adv. Exp. Struct. Eng.***2015**, *2015-August*.

70. Kolaiti, E.; Papadopoulos, Z. Evaluation of Schmidt Rebound Hammer Testing: A Critical Approach. *Bull. Eng. Geol. \& Environ.***1993**, *48*.

71. Kong, Q.; Fan, S.; Mo, Y.L.; Song, G. A Novel Embeddable Spherical Smart Aggregate for Structural Health Monitoring: Part II. Numerical and Experimental Verifications. *Smart Mater. Struct.***2017**, *26*, 95051.

72. Kot, P.; Muradov, M.; Gkantou, M.; Kamaris, G.S.; Hashim, K.; Yeboah, D. Recent Advancements in Non-Destructive Testing Techniques for Structural Health Monitoring. *Appl. Sci.***2021**, *11*, doi:10.3390/app11062750.

73. Kumar, D. Wireless Sensing and Acquisition System for Non Destructive Evaluation and Structural Health Monitoring. *Michigan State University*. **2021.**

74. Kutsenko, O. V.; Ilnytska, S.I.; Kondratyuk, V.M.; Konin, V. V. Unmanned Aerial Vehicle Position Determination in GNSS Landing System. *2017 IEEE 4th Int. Conf. Actual Probl. Unmanned Aer. Veh. Dev. APUAVD 2017 - Proc.***2018**, *2018-January*, 79–83, doi:10.1109/APUAVD.2017.8308781.

75. Kylili, A.; Fokaides, P.A.; Christou, P.; Kalogirou, S.A. Infrared Thermography (IRT) Applications for Building Diagnostics: A Review. *Appl. Energy***2014**, *134*, 531–549, doi:10.1016/j.apenergy.2014.08.005.

76. Lachemi, M.; Hossain, K.M.A.; Anagnostopoulos, C.; Sabouni, A.R. Application of Maturity Method to Slipforming Operations: Performance Validation. *Cem. Concr. Compos.***2007**, *29*, 290–299, doi:10.1016/j.cemconcomp.2006.12.001.

77. Laidler, K.J. The Development of the Arrhenius Equation. *J. Chem. Educ.***1984**, *61*, 494–498, doi:10.1021/ed061p494.

78. Lakshmi Aparna, M.; Chaitanya, G.; Srinivas, K.; Rao, J.A. Fatigue Testing of Continuous GFRP Composites Using Digital Image Correlation (DIC) Technique a Review. *Mater. Today Proc.***2015**, *2*, 3125–3131, doi:10.1016/j.matpr.2015.07.275.

79. Layssi H, Ghods P, Alizadeh AR, Salehi M. Electrical resistivity of concrete. Concrete international. 2015, May 1;37(5):41-6.

80. Lee, J.-H.; Yoon, S.-S.; Kim, I.-H.; Jung, H.-J. Diagnosis of Crack Damage on Structures Based on Image Processing Techniques and R-CNN Using Unmanned Aerial Vehicle (UAV). In Proceedings of the Sensors and Smart Structures Technologies for Civil, Mechanical, and Aerospace Systems 2018; Sohn, H., Ed.; SPIE, 2018; Vol. 10598, p. 1059811.

81. Liu, D.; Zhang, W.; Tang, Y.; Jian, Y. Prediction of Hydration Heat of Mass Concrete Based on the SVR Model. *IEEE Access***2021**, *9*, 62935–62945, doi:10.1109/ACCESS.2021.3075212.

82. Liu, P.; Chen, A.Y.; Huang, Y.N.; Han, J.Y.; Lai, J.S.; Kang, S.C.; Wu, T.H.; Wen, M.C.; Tsai, M.H. A Review of Rotorcraft Unmanned Aerial Vehicle (UAV) Developments and Applications in Civil Engineering. *Smart Struct. Syst.***2014**, *13*, 1065–1094, doi:10.12989/sss.2014.13.6.1065.

83. Lynch, J.P. An Overview of Wireless Structural Health Monitoring for Civil Structures. *Philos. Trans. R. Soc. A Math. Phys. Eng. Sci.***2007**, *365*, 345–372, doi:10.1098/rsta.2006.1932.

84. Mahajan, G. Applications of Drone Technology in Construction Industry: A Study 2012-2021. *Int. J. Eng. Adv. Technol.***2021**, *11*, 224–239, doi:10.35940/ijeat.a3165.1011121.

85. Manajitprasert, S.; Tripathi, N.K.; Arunplod, S. Three-Dimensional (3D) Modeling of Cultural Heritage Site Using UAV Imagery: A Case Study of the Pagodas in Wat Maha

That, Thailand. *Appl. Sci.***2019**, *9*, 1–14, doi:10.3390/app9183640.

86. Martinez, J.G.; Gheisari, M.; Alarcón, L.F. UAV Integration in Current Construction Safety Planning and Monitoring Processes: Case Study of a High-Rise Building Construction Project in Chile. *J. Manag. Eng.***2020**, *36*, doi:10.1061/(asce)me.1943-5479.0000761.

87. Maruyama, I.; Teramoto, A.; Igarashi, G. Strain and Thermal Expansion Coefficients of Various Cement Pastes during Hydration at Early Ages. *Mater. Struct. Constr.***2014**, *47*, 27–37, doi:10.1617/s11527-013-0042-4.

88. Maser R, K.; Roddis, W.M.K. Principles of Thermography and R a D a R. **1991**, *116*, 583–601.

89. McCormick N, Lord J. Digital image correlation. Materials today. 2010, Dec 1;13(12):52-4.

90. Menci, L.; Rinaudo, F. New Trends in Digital Photogrammetry Teaching and Diffusion: The {Z-GLIF} Software. *Proc. XXI Intl CIPA Symp.***2007**, 4 pp.

91. Mendes, T.; Henriques, S.; Catalão, J.; Redweik, P. Photogrammetry with UAV ' S : Quality Assessment of Open -Source Software for Generation of Ortophotos and Digital Surface Models. *n VIII Conf. Nac. Cartogr. e Geod.***2015**, 1–8.

92. Meola, C.; Boccardi, S.; Carlomagno, G.M.; Boffa, N.D.; Ricci, F.; Simeoli, G.; Russo, P. Impact Damaging of Composites through Online Monitoring and Non-Destructive Evaluation with Infrared Thermography. *NDT E Int.***2017**, *85*, 34–42, doi:10.1016/j.ndteint.2016.10.004.

93. Milovanović, B.; Pečur, I.B. Review of Active IR Thermography for Detection and Characterization of Defects in Reinforced Concrete. *J. Imaging***2016**, *2*, 1–27, doi:10.3390/jimaging2020011.

94. Mohamed, A.R.; Hansen, W. Effect of nonlinear temperature gradient on curling stress in concrete pavements. *Transportation Research Record,***1997**, 1568(1), pp.65-71.

95. Mohan, A.; Poobal, S. Crack Detection Using Image Processing: A Critical Review and Analysis. *Alexandria Eng. J.***2018**, *57*, 787–798, doi:10.1016/j.aej.2017.01.020.

96. Moharana, S.; Bhalla, S. Development and Evaluation of an External Reusable Piezo-Based Concrete Hydration-Monitoring Sensor. *J. Intell. Mater. Syst. Struct.***2019**, *30*, 2770–2788, doi:10.1177/1045389X19873414.

97. Mohr, G.; Nowakowski, S.; Altenburg, S.J.; Maierhofer, C.; Hilgenberg, K. Experimental Determination of the Emissivity of Powder Layers and Bulk Material in Laser Powder Bed Fusion Using Infrared Thermography and Thermocouples. *Metals (Basel).***2020**, *10*, 1–36, doi:10.3390/met10111546.

98. Mollah, M.Y.A.; Yu, W.; Schennach, R.; Cocke, D.L. Fourier Transform Infrared Spectroscopic Investigation of the Early Hydration of Portland Cement and the Influence of Sodium Lignosulfonate. *Cem. Concr. Res.***2000**, *30*, 267–273, doi:10.1016/S0008-8846(99)00243-4.

99. Mora-Felix, Z.D.; Sanhouse-Garcia, A.J.; Bustos-Terrones, Y.A.; Loaiza, J.G.; Monjardin-Armenta, S.A.; Rangel-Peraza, J.G. Effect of Photogrammetric RPAS Flight Parameters on Plani-Altimetric Accuracy of DTM. *Open Geosci.***2020**, *12*, 1017–1035, doi:10.1515/geo-2020-0189.

100. Moulon, P.; Monasse, P.; Perrot, R.; Marlet, R. OpenMVG: Open Multiple View Geometry. *Lect. Notes Comput. Sci. (including Subser. Lect. Notes Artif. Intell. Lect. Notes Bioinformatics)***2017**, *10214 LNCS*, 60–74, doi:10.1007/978-3-319-56414-2_5.

101. Mousa, M.A.; Yussof, M.M.; Udi, U.J.; Nazri, F.M.; Kamarudin, M.K.; Parke, G.A.R.; Assi, L.N.; Ghahari, S.A. Application of Digital Image Correlation in Structural Health Monitoring of Bridge Infrastructures: A Review. *Infrastructures***2021**, *6*, doi:10.3390/infrastructures6120176.

102. Najam, F.; Amir Izhar, M.; Anwar, N.; Ahmed Najam, F. Construction Monitoring and Reporting Using Drones and Unmanned Aerial Vehicles (UAVs) 50 PUBLICATIONS 12 CITATIONS SEE PROFILE Construction Monitoring and Reporting Using Drones and Unmanned Aerial Vehicles (UAVs). **2018**, 325–332.

103. Negi, P.; Kromanis, R.; Dorée, A.G.; Wijnberg, K.M. Structural Health Monitoring of Inland Navigation Structures and Ports: A Review on Developments and Challenges. *Struct. Heal. Monit.***2023**, doi:10.1177/14759217231170742.

104. Ngadiman, N.; Kaamin, M.; Nizam, M.A.H.M.; Johar, M.A.H.; Roslin, M.A. Unmanned Aerial Vehicle (Uav) Visual Monitoring in Construction. *Ann. Rom. Soc. Cell Biol.***2021**, *25*, 3097–3104.

105. Omar, T.; Nehdi, M.L. Remote Sensing of Concrete Bridge Decks Using Unmanned Aerial Vehicle Infrared Thermography. *Autom. Constr.***2017**, *83*, 360–371, doi:10.1016/j.autcon.2017.06.024.

106. Palma, P.; Steiger, R. Structural Health Monitoring of Timber Structures – Review of Available Methods and Case Studies. *Constr. Build. Mater.***2020**, *248*, 118528, doi:10.1016/j.conbuildmat.2020.118528.

107. Pan, B. Bias Error Reduction of Digital Image Correlation Using Gaussian Pre-Filtering. *Opt. Lasers Eng.***2013**, *51*, 1161–1167.

108. Patil, B,G.; Jain, S.N. Cancer cells detection using digital image processing methods. *International Journal of Latest Trends in Engineering and Technology*, **2014**, 3(4), pp.45-49.

109. Parrott, L.J.; Geiker, M.; Gutteridge, W.A.; Killoh D. Monitoring Portland cement hydration: comparison of methods. *Cement and concrete research.***1990**, Nov 1;20(6):919-26.

110. Peng, A.S.; Turkmen, A.; Eickhoff, B.; Finta, M.; Gerads, P. Design of a Ground ampling Distance Graphical User Interface for an Unmanned Aerial Vehicle System. *2019 53rd Annu. Conf. Inf. Sci. Syst. CISS 2019***2019**, 1–6, doi:10.1109/CISS.2019.8692786.

111. Pessiki, S.P.; Carino, N.J. Settingtime and Strength of Concrete Using the Impact-Echo Method. *Mater. J.***1988**, *85*, 389–399.

112. Porta, D. 6 . THERMAL NON-DESTRUCTIVE TESTING : SHORT HISTORY , STATE-OF-THE-ART AND TRENDS Vavilov V ., Tomsk Polytechnic University , Tomsk , Russia. **1990**.

113. Qin, L.; Li, Z. Monitoring of Cement Hydration Using Embedded Piezoelectric Transducers. *Smart Mater. Struct.***2008**, *17*, 55005, doi:10.1088/0964-1726/17/5/055005.

114. Qu, T.; Zang, W.; Peng, Z.; Liu, J.; Li, W.; Zhu, Y.; Zhang, B.; Wang, Y. Construction Site Monitoring Using UAV Oblique Photogrammetry and BIM Technologies. *CAADRIA 2017 - 22nd Int. Conf. Comput. Archit. Des. Res. Asia Protoc. Flows Glitches***2017**, 655–662, doi:10.52842/conf.caadria.2017.655.

115. Quanjin, M.; Rejab, M.R.M.; Halim, Q.; Merzuki, M.N.M.; Darus, M.A.H. Experimental Investigation of the Tensile Test Using Digital Image Correlation (DIC) Method. *Mater. Today Proc.***2020**, *27*, 757–763, doi:10.1016/j.matpr.2019.12.072.

116. Ramachandra, B.; Nawathe, P.; Monroe, J.; Han, K.; Ham, Y.; Vatsavai, R.R. Real-Time Energy Audit of Built Environments: Simultaneous Localization and Thermal Mapping. *J. Infrastruct. Syst.***2018**, *24*, 1–9, doi:10.1061/(asce)is.1943-555x.0000431.

117. Ramzan, B.; Malik, M.S.; Martarelli, M.; Ali, H.T.; Yusuf, M.; Ahmad, S.M. Pixel Frequency Based Railroad Surface Flaw Detection Using Active Infrared Thermography for Structural Health Monitoring. *Case Stud. Therm. Eng.***2021**, *27*, 101234, doi:10.1016/j.csite.2021.101234.

118. Rashid, K.; Waqas, R. Compressive Strength Evaluation by Non-Destructive Techniques: An Automated Approach in Construction Industry. *J. Build. Eng.***2017**, *12*, 147–154, doi:10.1016/j.jobe.2017.05.010.

119. Rastrup E. Discussion: Heat of hydration in concrete. *Magazine of Concrete Research.***1955**, Jul;7(20):103-5.

120. Reagan, D.; Sabato, A.; Niezrecki, C. Feasibility of Using Digital Image Correlation for Unmanned Aerial Vehicle Structural Health Monitoring of Bridges. *Struct. Heal. Monit.***2018**, *17*, 1056–1072, doi:10.1177/1475921717735326.

121. Rinaudo, F.; Chiabrando, F.; Lingua, A.; Spanò, A. Archaeological Site Monitoring: Uav Photogrammetry Can Be an Answer. *Int. Arch. Photogramm. Remote Sens. Spat. Inf. Sci.***2012**, *XXXIX-B5*, 583–588, doi:10.5194/isprsarchives-xxxix-b5-583-2012.

122. Root, W.; Bechtold, T.; Pham, T. Textile-Integrated Thermocouples for Temperature Measurement. *Materials (Basel).***2020**, *13*, doi:10.3390/ma13030626.

123. Roux, S.; Réthoré, J.; Hild, F. Digital Image Correlation and Fracture: An Advanced Technique for Estimating Stress Intensity Factors of 2D and 3D Cracks. *J. Phys. D. Appl. Phys.***2009**, *42*, doi:10.1088/0022-3727/42/21/214004.

124. Rubino, V.; Lapusta, N.; Rosakis, A. Laboratory earthquake measurements with the high-speed digital image correlation method and applications to super-shear transition. *InAGU fall meeting abstracts.***2012**, Dec (Vol. 2012, pp. T24A-06).

125. Runkel, I.; Middelmann, W.; Becker, M.; Espinosa, N. 3D Building Reconstruction in a Remote Sensing Workflow.; 2017; p. 6.

126. SANTOS, A.H.A.; PITANGUEIRA, R.L.S.; RIBEIRO, G.O.; CARRASCO, E.V.M. Concrete Modulus of Elasticity Assessment Using Digital Image Correlation. *Rev. IBRACON Estruturas e Mater.***2016**, *9*, 587–594, doi:10.1590/s1983-41952016000400007.

127. Schnebele, E.; Tanyu, B.F.; Cervone, G.; Waters, N. Review of Remote Sensing Methodologies for Pavement Management and Assessment. *Eur. Transp. Res. Rev.***2015**, *7*, doi:10.1007/s12544-015-0156-6.

128. Schreier, H.; Orteu, J.J.; Sutton, M.A. *Image Correlation for Shape, Motion and Deformation Measurements: Basic Concepts, Theory and Applications*; 2009; ISBN 9780387787466.

129. Shaban, A. Determination of Concrete Properties Using Hyperspectral Imaging Technology : A Review. *Sci. J. Civ. Eng. Archit.***2013**, *2013*.

130. Shao, L.; Yan, R.; Li, X.; Liu, Y. From Heuristic Optimization to Dictionary Learning: A Review and Comprehensive Comparison of Image Denoising Algorithms. *IEEE Trans. Cybern.***2013**, *44*, 1001–1013.

131. Sharma, N.; Mishra, M.; Shrivastava, M. Colour Image Segmetation Technique and Issue: An Approach. *Int. J. Sci. Technol. Res.***2012**, *1*, 9–12.

132. Sheridan, I. Drones and Global Navigation Satellite Systems: Current Evidence from Polar Scientists. *R. Soc. Open Sci.***2020**, *7*, doi:10.1098/rsos.191494.

133. Sivakumar, M.; Naga Malleswari, T.Y.J. A Literature Survey of Unmanned Aerial Vehicle Usage for Civil Applications. *J. Aerosp. Technol. Manag.***2021**, *13*, 1–23, doi:10.1590/jatm.v13.1233.

134. Smrkić, M.F.; Košćak, J.; Damjanović, D. Application of 2D digital image correlation for displacement and crack width measurement on RC elements. *Gradjevinar.***2018**, Jan 1;70(9):771-81.

135. Soares, G.; Inocencio, L.; Veronez, M.; da Silveira Jr, L.; Bordin, F.; Marson, F.

Analysis of Positional and Geometric Accuracy of Objects in Survey with Unmanned Aerial Vehicle (UAV).; 2018.

136. Sony, S.; Laventure, S.; Sadhu, A. A Literature Review of Next-Generation Smart Sensing Technology in Structural Health Monitoring. *Struct. Control Heal. Monit.***2019**, *26*, e2321.

137. Soutsos, M.; Kanavaris, F. The Modified Nurse-Saul (MNS) Maturity Function for Improved Strength Estimates at Elevated Curing Temperatures. *Case Stud. Constr. Mater.***2018**, *9*, e00206, doi:10.1016/j.cscm.2018.e00206.

138. Spencer, B.F.; Ruiz-Sandoval, M.E.; Kurata, N. Smart Sensing Technology: Opportunities and Challenges. *Struct. Control Heal. Monit.***2004**, *11*, 349–368, doi:10.1002/stc.48.

139. Starnes, M.A.; Carino, N.J.; Kausel, E.A. Quantitative Infrared Thermography for Quality Control of Concrete Structures Strengthened with FRP Composites. *Am. Concr. Institute, ACI Spec. Publ.***2002**, *SP-209*, 247–268, doi:10.14359/12504.

140. Sudarsanan, N.; Arulrajah, A.; Karpurapu, R.; Amrithalingam, V. Digital Image Correlation Technique for Measurement of Surface Strains in Reinforced Asphalt Concrete Beams under Fatigue Loading. *J. Mater. Civ. Eng.***2019**, *31*, 04019135, doi:10.1061/(asce)mt.1943-5533.0002743.

141. Suryanto, B.; Tambusay, A.; Suprobo, P. Crack Mapping on Shear-Critical Reinforced Concrete Beams Using an Open Source Digital Image Correlation Software. *Civ. Eng. Dimens.***2017**, *19*, 93–98, doi:10.9744/ced.19.2.93-98.

142. Tenedório, J.A.; Estanqueiro, R.; Henriques, C.D. *Methods and Applications of Geospatial Technology in Sustainable Urbanism*; IGI Global, 2021;

143. Terrance Booth, D.; Cox, S.E.; Fifield, C.; Phillips, M.; Williamson, N. Image Analysis Compared with Other Methods for Measuring Ground Cover. *Arid L. Res. Manag.***2005**, *19*, 91–100.

144. Thayer, P. Enabling the Fourth Industrial Revolution (4IR) and the role of NDE and monitoring. *Insight-Non-Destructive Testing and Condition Monitoring,***2017,** 59(9), pp.469-472.

145. Tkáč, M.; Mésároš, P. Utilizing Drone Technology in the Civil Engineering. *Sel. Sci. Pap. Civ. Eng.***2019**, *14*, 27–37.

146. Torres, D.L.; Feitosa, R.Q.; Happ, P.N.; La Rosa, L.E.C.; Junior, J.M.; Martins, J.; Bressan, P.O.; Gonçalves, W.N.; Liesenberg, V. Applying Fully Convolutional Architectures for Semantic Segmentation of a Single Tree Species in Urban Environment on High Resolution UAV Optical Imagery. *Sensors (Switzerland)***2020**, *20*, 1–20, doi:10.3390/s20020563.

147. Tran, Q.H.; Han, D.; Kang, C.; Haldar, A.; Huh, J. Effects of ambient temperature and relative humidity on subsurface defect detection in concrete structures by active thermal imaging. *Sensors*. **2017**, Jul 26;17(8):1718.

148. Vaghefi, K.; Oats, R.C.; Harris, D.K.; Ahlborn, T. (Tess) M.; Brooks, C.N.; Endsley, K.A.; Roussi, C.; Shuchman, R.; Burns, J.W.; Dobson, R. Evaluation of Commercially Available Remote Sensors for Highway Bridge Condition Assessment. *J. Bridg. Eng.***2012**, *17*, 886–895, doi:10.1061/(asce)be.1943-5592.0000303.

149. Valdes, M.D.; Moure, M.J.; Menendez, L.M. Full Autonomous Sensor and Actuator Network for Maturity Estimation in Early Age Concrete Structures. *IECON Proc. (Industrial Electron. Conf.***2013**, 3922–3927, doi:10.1109/IECON.2013.6699762.

150. Valença, J.; Gonçalves, L.M.S.; Júlio, E. Damage Assessment on Concrete Surfaces Using Multi-Spectral Image Analysis. *Constr. Build. Mater.***2013**, *40*, 971–981, doi:10.1016/j.conbuildmat.2012.11.061.

151. Vavilov, V. Thermal non-destructive testing: Short history, state-of-the-art and trends. *InProceedings of the European Conference and Exhibition on Non-Destructive Testing, Tomsk, Russia.***2010,** Aug 1 (p. 6).

152. Verykokou, S.; Ioannidis, C. Oblique Aerial Images: A Review Focusing on Georeferencing Procedures. *Int. J. Remote Sens.***2018**, *39*, 3452–3496, doi:10.1080/01431161.2018.1444294.

153. Vijay, P. V.; Tulasi Gadde, K.; GangaRao, H.V.S. Structural Evaluation and Rehabilitation of Century-Old Masonry and Timber Buildings. *J. Archit. Eng.***2019**, *25*, 05019001, doi:10.1061/(asce)ae.1943-5568.0000350.

154. Wang, B.; Zhong, S.; Lee, T.L.; Fancey, K.S.; Mi, J. Non-Destructive Testing and

Evaluation of Composite Materials/Structures: A State-of-the-Art Review. *Adv. Mech. Eng.***2020**, *12*, 1–28, doi:10.1177/1687814020913761.

155. Wang, X.Y.; Park, K.B. Analysis of the Compressive Strength Development of Concrete Considering the Interactions between Hydration and Drying. *Cem. Concr. Res.***2017**, *102*, 1–15, doi:10.1016/j.cemconres.2017.08.010.

156. Wisniewski, M.; Bassett, C.; Gusta, L. V. An Overview of Cold Hardiness in Woody Plants: Seeing the Forest through the Trees. *HortScience***2003**, *38*, 952–959, doi:10.21273/hortsci.38.5.952.

157. Yeum, C. M.; Anup M.; Shirley J.D.; Mohammad J.; Jongseong C.; Ziyi Z.; Ali L.; Julio A. R. Image-based collection and measurements for construction pay items. **2017.**

158. Zeybek, M. Accuracy Assessment of Direct Georeferencing UAV Images with Onboard Global Navigation Satellite System and Comparison of CORS/RTK Surveying Methods. *Meas. Sci. Technol.***2021**, *32*, 65402.

159. Zhang, J.; Wu, Z.; Chen, G.; Liang, Q. Comparisons of Differential Filtering and Homography Transformation in Modal Parameter Identification from Uav Measurement. *Sensors***2021**, *21*, doi:10.3390/s21165664.

160. Zhao, S.; Kang, F.; Li, J.; Ma, C. Structural Health Monitoring and Inspection of Dams Based on UAV Photogrammetry with Image 3D Reconstruction. *Autom. Constr.***2021**, *130*, 103832, doi:10.1016/j.autcon.2021.103832.

161. Zhu, X.; Hou, Y.; Weng, Q.; Chen, L. Integrating UAV Optical Imagery and LiDAR Data for Assessing the Spatial Relationship between Mangrove and Inundation across a Subtropical Estuarine Wetland. *ISPRS J. Photogramm. Remote Sens.***2019**, *149*, 146–156, doi:10.1016/j.isprsjprs.2019.01.021.

Publications from the Research work

Journals:

1. **Kumarapu, K.,** Shashi, M., Keesara, V.R. UAV in Construction Site Monitoring and Concrete Strength Estimation. J Indian Soc Remote Sens 49, 619–627 (2021). https://doi.org/10.1007/s12524-020-01246-w
2. **Kumarapu, K**., Mesapam S., V. R. et al., RCC Structural deformation and damage quantification using Unmanned Aerial Vehicle Image Correlation technique. Advances in Unmanned Aerial Vehicle (UAV) System, Appl. Sci. 2022, 12(13), 6574. https://doi.org/10.3390/app12136574
3. Dasari, S., Shashi, M., **Kumarapu, K**. et al. UAV in Development of 3D Heritage Monument Model: A Case Study of Kota Gullu, Warangal, India. J Indian Soc Remote Sens 49, 1733–1737 (2021). https://doi.org/10.1007/s12524-020-01250-0
4. **Kumarapu, K**., Shashi, M., Keesara, V.R. A Simple and Robust Non-Destructive Technique for Estimating Strength by Evaluating the Exothermal Reaction of Hydration using Thermography and a Thermocouple on a Variety of Concrete Grades and Volumes. Russian Journal of Non-destructive Testing (2nd review)

Conferences :

1. **Kumarapu, K**., Shashi, M., "Monitoring of curing activity in construction site using UAV" International conference on Urban Geoinformatics, TERI University, New Delhi, 22 nd -23 rd February, 2017.
2. **Kumarapu, K**., Shashi, M, K. Venkata Reddy "Thermal Remote sensing in early Age Concrete Strength Estimation;, ICGCE-2018, International Conference on Geomatics in Civil Engineering, IIT Roorkee, 5-6 April, 2018.
3. **Kumarapu, K**., Shashi, M, K Venkata Reddy "UAV in Construction Site Monitoring and Concrete Strength Estimation", 1st International Conference on Unmanned Aerial System in Geomatics, Greater Noida Extension Centre, Indian Institute of Technology Roorkee, India,06-07 April 2019.
4. **Kumarapu, K**., Shashi M, Venkata Reddy K., "Thermography to evaluate multiple grades and volumes exothermal reaction of concrete hydration", international

Conference on “Challenges of Resilient and Sustainable Infrastructure Development in Emerging Economies”, ASCE India chapter-1, Kolkata, March 02-04, 2020.

5. **Kumarapu, K**., Shashi M, and Venkata Reddy K., “RCC Structural deformation and damage quantification using Unmanned Aerial Vehicle Image Correlation (UAVIC)”., Unmanned Aerial Systems in Geomatics – 2021, 02 – 04 April 2021, IIT Roorkee, India.
6. **Kumarapu, K**., Shashi M, and Venkata Reddy K., “Thermography to Evaluate Stresses Release Through Cracks” International Conference on Developments and Applications of Geomatics (DEVA-2022), 29 - 31 August 2022, NIT Warangal, India